I.R.Iran

ISSN:2423-5547
e-ISSN:2423-7469

Journal of Renewable Energy and Environment

Volume 7, Number 4, Autumn 2020

Materials and Energy Research Center

Iranian Association of Chemical Engineers

CONTENTS

AIMS AND SCOPE

Journal of Renewable Energy and Environment (JREE) publishes original papers, review articles, short communications and technical notes in the field of science and technology of renewable energies and environmental-related issues including:

- Generation
- Storage
- Conversion
- Distribution
- Management (economics, policies and planning)
- Environmental Sustainability

INSTRUCTIONS FOR AUTHORS

Submission of manuscript represents that it had neither been published nor submitted for publication elsewhere and is result of research carried out by author(s). Only the extended and upgraded articles presented in a conference and/or appeared in a symposium proceedings could be evaluated for publication.
Authors are required to include a list describing all the symbols and abbreviations in the paper. Use of the international system of measurement units is mandatory.

- On-line submission of manuscripts results in faster publication process and is recommended. Instructions are given in the JREE web sites: www.jree.ir
- References should be numbered in brackets and appear in sequence through the text. List of references should be given at the end of the paper. All journal articles listed in the References section must follow with article doi.
- Figure captions are to be indicated under the illustrations. They should sufficiently explain the figures.
- Illustrations should appear in their appropriate places in the text.
- Tables and diagrams should be submitted in a form suitable for reproduction.
- Photographs should be of high quality saved as jpg files.
- Tables' illustrations, figures and diagrams will be normally printed in single column width (8 cm). Exceptionally large ones may be printed across two columns (17 cm).

Journal of Renewable Energy and Environment

Research Article

Journal Homepage: www.jree.ir

Ex-Situ CO_2 Capture and Utilization Over the Bauxite Residue: Lifecycle and Economic Recovery Assessment

Kazem Kashefi[a*], Alireza Pardakhti[a], Majid Shafiepour[a], Azadeh Hemmati[b]

[a] *Department of Environmental Engineering, School of Environment, College of Engineering, University of Tehran, P. O. Box: 11155-4563, Tehran, Tehran, Iran.*
[b] *Department of Petroleum and Chemical Engineering, Science and Research Branch, Islamic Azad University, P. O. Box: 14515-775, Tehran, Tehran, Iran.*

PAPER INFO

Paper history:
Received 09 April 2020
Accepted in revised form 14 July 2020

Keywords:
Carbon Capture and Utilization,
Life Cycle Assessment,
Carbon Footprint,
Greenhouse Gas Emission

ABSTRACT

Carbon-dioxide Capture and Utilization (CCU) technology is an efficient process in the portfolio of greenhouse gas reduction approaches and is programmed to mitigate global warming. Given that the prime intention of CCU technologies is to prevent CO_2 emissions into the atmosphere, it remains to be seen if these approaches cause other environmental impacts and consequences. Therefore, the Life Cycle Assessment (LCA) approach was considered to account for all environmental aspects, in addition to the emission of greenhouse gases. In this study, the Life Cycle Inventory (LCI) methodology was employed to quantify the environmental impacts of indirect carbonation of Red Mud (RM), a waste byproduct of alumina production line in Jajarm Alumina Plant, Iran by CO_2 exhausted from the plant stacks based on International Organization for Standardizations (ISO) of ISO 14040 and ISO 14044. The results confirmed the reduction of CO_2 emission by 82 %. The study of carbon footprint based on ISO 14064 under the criterion of PAS 2050 revealed CO_2 emission equivalent to 2.33 kg/ ton RM, proving that CCU managed to mitigate the CO_2 emission by 93 % compared to the conventional technology employed in Jajarm Plant, which produced around 34 kg CO_2 per 1 ton RM. Furthermore, the economic evaluation of the process brought about 243 $/ton RM in profit via the sales of products including silica, aluminum, hematite, and calcium carbonate. The outcomes of the present study highlight that the intended CCU technology is a practicable approach for large-scale applications.

https://doi.org/10.30501/jree.2020.225900.1097

1. INTRODUCTION

Anthropogenic activities increase the emission of greenhouse gases (GHGs) into the atmosphere, which is one of the major causes of global warming. This is a crucial problem for the future of the earth and living species. Carbon dioxide, methane, nitrogen oxide, and halocarbons are the main GHGs, among which CO_2 is the most problematic GHG in terms of global warming. According to a report by the Intergovernmental Panel on Climate Change, the concentration of CO_2 in the atmosphere will reach 2100 ppm by 2100 [1]. In order to keep the average increase rate in the global temperature below 2 °C, the emission of CO_2 should be reduced by 50-85 % before 2050. In this respect, different strategies have been taken into practice to ensure the sustainability of the world climate [2–4]. These recommended strategies include reduction of requisition process, efficiency improvements, application of renewable sources, nuclear power, and Carbon Capture and Storage (CCS). CO_2 capture at the terminal point of industrial processes such as power plants, cement manufacturers, refineries, and steel mills in which an immense volume of CO_2 is exhausted could be one of the potential solutions for the management of global warming [5–7].

The CCS and CCU technologies are noteworthy and promising approaches to reducing GHG emissions. These techniques have received a warm welcome by many industrial communities [8]. Although CCS is an efficient technique for the reduction of CO_2, it is not a satisfactorily viable method in terms of some technical and economic barriers for large-scale applications. From an economic standpoint, it is a high-cost process with no profit that cannot attract industries to invest. From a technical viewpoint, the leakage of CO_2 and obstacles regarding the storage of captured CO_2 are the common limitations of this process. A promising alternative that has attracted many industries is CCU processes. This is because CCU technologies act successfully in CO_2 reduction and are economically rewarding methods as the production of value-added products during the process and trading them to the marketplaces return a part of the investments. These commercial products have made CCU technologies more affordable than the CCS approaches. In addition to this merit, CO_2 released from different flues can be used as a renewable energy source, which is an inexpensive and non-poisonous available source. Moreover, the precious merits of this approach such as the availability of CO_2 as a safe resource that can compete with low-price fossil fuels motivate researchers to direct their researches to CCU techniques [9–12].

*Corresponding Author's Email: kazem.kashefi@gmail.com (K. Kashefi)
URL: http://www.jree.ir/article_110470.html

Please cite this article as: Kashefi, K., Pardakhti, A., Shafiepour, M. and Hemmati, A., "Ex-situ CO_2 capture and utilization over the bauxite residue: Lifecycle and economic recovery assessment", ***Journal of Renewable Energy and Environment (JREE)***, Vol. 7, No. 4, (2020), 1-9. (https://doi.org/10.30501/jree.2020.225900.1097).

An effective method that has been widely expanded for CCU goals is mineral carbonation practices. Mineral carbonation is a natural weathering process in which the reaction of CO_2 with natural alkali rocks leads to the formation of carbonate rocks for a relatively long time [13]. Natural alkali sources are known as rocks with a high amount of magnesium and calcium in the form of silicate minerals such as serpentine, olivine, and wollastonite. This natural phenomenon has inspired researchers to establish a mineral carbonation process for the capture and storage of industrially emitted CO_2 over alkali minerals [14]. Two typical mineral carbonation methods are direct and indirect carbonation. The direct mineral carbonation consists of carbonation reactions taking place in a single step, while, indirect mineral carbonation proceeds in a multi-stage process. To be more specific, in the direct carbonation process, the extraction of metals and carbonation reactions proceeds in one reactor vessel at the high pressure. In contrast, indirect carbonation embraces reactions in several discrete steps. The first step is the leaching of minerals from the alkali waste by a suitable acid. Common acids include hydrochloric acid, sulfuric acid, nitric acid, acetic acid, ammonium chloride, oxalic acid, citric acid, ammonium acetate, sodium citrate, sodium acetate, ammonium citrate, and ammonium oxalate [15]. The second step, called the pH swing process, concerns the formation of metal hydroxides by the addition of basic agents to reach high-purity alkali metal (calcium or magnesium) solution. The third and final stage includes the carbonation reaction in which CO_2 reacts with alkali metals resulting in the creation of carbonates (namely calcium/magnesium carbonate). The characteristic benefit of this approach is the storage of CO_2 in the form of highly stable carbonates for quite a long time with no probability of CO_2 release and leakage to the atmosphere. The other privilege of the indirect mineral carbonation is that there is no need to separate CO_2 from the flue gas for obtaining high-purity CO_2 because impurities present in CO_2-containing effluent gas such as SO_x and NO_x cannot interfere with the carbonation process. Hence, the exhausted gas can be directly used without any extra purification process which will save cost and energy. In spite of the limitations owing to the high cost and energy penalty of this process for industrial application, the mentioned merits have attracted scientists' attention to put their effort into upgrading the process or a large-scale utilization [16–19].

It has been reported that an industry armed with CCS technique changes the emission pattern of CO_2 [3]. In the industrial application of a CCS or CCU, in addition to climate change, other environmental impacts should be considered to see whether the relief of climate change induces other environmental consequences or not. A powerful tool to facilitate proper recognition of the environmental impacts of CCS/CCU is the deployment of the LCA approach [20,21]. In the LCA approach, the environmental impacts of a product system or device during its life cycle from the cradle to the grave including extraction of raw materials, transportation, production, distribution, and disposal of wastes are considered [22–24]. Emissions and resource usage in all of these stages and their proportions relevant to the specific environmental impacts should be included in the life cycle inventory (LCI) [25,26]. LCA is a precious tool for decision-makers as it assists them to choose among the proposed options [27,28], and for the simple judgment and comparison of the processes, several standards were introduced such as International Organization for Standardizations (ISO) [25,26]. LCI characterizes environmental inventories which are itemized as follows: abiotic depletion potential (ADP), global warming potential (GWP), ozone layer depletion potential (ODP), human toxicity potential (HTP), freshwater aquatic ecotoxicity potential (FWAETP), marine aquatic ecotoxicity potential (MAETP), terrestrial ecotoxicity potential (TEP), photochemical oxidation potential (POP), acidification potential (AP), and eutrophication potential (EP) [3]. In addition, economic evaluation has been considered as a key strategy for the estimation of the process potential for real application and its economic recovery [29–31].

In the current study carried out for the first time, 1) environmental impacts of indirect carbon mineralization of RM, the waste of Jajarm plant, were assessed by the LCA methodology. 2) The carbon footprint quantification was employed for a better understanding of GWP by calculation of GHG emissions of CCU under the boundary of the system. 3) The economic investigation was carried out to estimate the pecuniary value of the products and the cost compensation of the initial investment. 4) The outcomes of this study are highly beneficial to predicting the feasibility of the CCU process for commercial and real applications in the Jajarm plant.

2. ALUMINA PRODUCTION PLANT

Bayer method is the most common method in the production of aluminum from the bauxite mineral source. Bauxite is a well-known aluminum ore containing 30 to 54 % alumina and different percentages of silica, iron oxides, and titanium dioxide. In this method, sodium hydroxide solution at a temperature of 175 ºC is used to wash the bauxite rock and convert alumina into aluminum hydroxide, which is soluble in sodium hydroxide solution. Other components of bauxite ore are not soluble in sodium hydroxide solution; therefore, they can be separated from aluminum hydroxide by filtration. The aluminum hydroxide powder is obtained via cooling and, then, is heated to 980 ºC to separate alumina and water in order to achieve pure alumina.

$$2\,Al(OH)_3 \rightarrow Al_2\,O_3 + 3\,H_2O \quad (1)$$

Alumina plant of Iran (Jajarm complex) is the only alumina production plant in Iran, which is located in Jajarm, North Khorasan. It was established in 2003 with the alumina production capacity of 280,000 ton/ year. The Jajarm plant produces alumina via the Bayer method and it needs 348,000 ton of ground lime per 1 ton of alumina. About 500,000 ton of RM is produced annually and about 7 million ton of RM has been accumulated so far [32]. The composition of RM produced by the Jajarm plant was tested by XRF analysis (Table 1) and results confirm the great potential of RM for CCU as it is rich in calcium. The Jajarm plant includes seven main operational units, which are bauxite, dissolution, separation of RM, sedimentation, calcination, evaporation, desalting, and utility. Figure 1 depicts the overall process of alumina production of the Jajarm plant.

3. LIFE CYCLE ASSESSMENT

3.1. Methodology

LCA has been introduced as a holistic evaluating method which appraises all resources, emissions, and energy streams

and their environmental consequences throughout the life cycle of a certain product or service or system [33]. LCA calculates resource usage and environmental emissions in all steps ranging from raw material consumption to waste disposal during the entire life cycle of a product. Figure 2 shows the life cycle stages of a product briefly. This is a remarkable decision-making tool that allows institutions and program developers to take a vivid perspective regarding the environmental damage of a product [26,34,35].

Table 1. XRF analysis of RM

Component	Composition (wt %)
Fe_2O_3	35.77
CaO	14.21
Al_2O_3	15.88
L.O.I	10.61
SiO_2	11.73
Na_2O	5.28
TiO_2	4.41
MgO	1.24
Cl	0.17

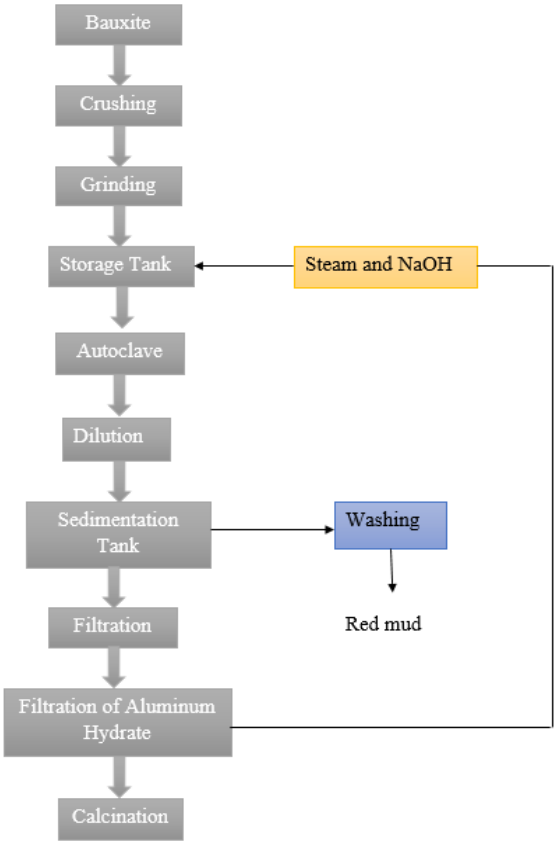

Figure 1. The overall process of alumina production of the Jajarm plant

Figure 2. The stages of the life cycle of a product

Owing to the widespread applications of the LCA method, several ISO standards have been described to help researchers to apply proper LCA criteria. Due to the complexity of the quantification process, accession of computer-aided technologies is truly beneficial due to their high accuracy and simplicity. The computational software weights the target process for its sustainability, LCA, and environmental impacts. Among the computational tool, GaBi tenders a simple, precise, and fast analysis for LCA and inventory assessment of a product system [36]. In this study, LCA was carried out based on the standards of ISO 1404 and ISO 14044 and the scenario is outlined as in the following steps:

1. Specification of the goal and scope: The initial attempt in LCA is the accurate specification of the aim of the LCA implementation for a given product and ascertaining of the system boundaries.
2. Life cycle inventory (LCI): In this step, all environmental inventories and inputs and outputs of the given product system are quantified. This stage is highly complicated since many elements in each life cycle stage should be accounted which necessitates a comprehensive database set to model the value chain of the processes. However, all the essential databases are not available. In such cases, LCA proceeds by postulating the ungiven data and checking the accuracy of the assumed data via the sensitivity analysis.
3. Life cycle impact assessment: The next step is the measurement of the environmental impacts resulting from interventions. This assessment embraces the classification of analogous interventions of a system in a category including global warming, acidification, etc. and calculation of those environmental impacts. The environmental impacts are classified as the items described in Table 2. A concise explanation of some of these categories is described below [20,26,37].

Global warming

The unpleasant phenomenon of global warming is entangled with the emission of greenhouse gases. The global warming categorization in LCA is estimated as the equivalent CO_2 through the assessment of the global warming potential of each chain during 100 years. Indeed, the environmental impact of global warming defined by the LCA just focuses on the emission of greenhouse gases resulting from human activities. Different greenhouse gases possess different potentialities in global warming. Therefore, the calculation of their contribution is comparatively complicated. The main greenhouse gases include CO_2, CH_4, and N_2O and the global warming potential attributed to them are defined as 1, 25, and 298 kg of equivalent CO_2 per kg of substance [38].

Resource depletion

In order to specify the resource depletion, the collection of the value of all energy inputs such as fossil fuels involved in the manufacture of the system is calculated.

Smog air

Smog air is a phenomenon associated with the formation of near-ground ozone (photosmog or summer smog). The ozone equivalent is the parameter used for the quantitative study of the environmental impact of the ozone creation potential of the system.

Acidification

The release of acidic substances, known as proton, into the atmosphere is called acidification. This impact is addressed in LCA as kg of equivalent SO_2. The acidic materials such as

SO_2, NO_x, HCl, H_2S, and NH_3 are considered in this category with acidification potentials of 1, 0.7, 0.88, 1.88, and 1.88 kg of equivalent SO_2 per kg of substance, respectively [38].

Eutrophication

The increase of the phosphoric and nitric contents of water and soil is known as eutrophication. This increment disarranges the natural balance of the ecosystem's components, which can give rise to the challenging issues. In the LCA studies, eutrophication of water and soil is defined as two separate parameters. In this study, air-oriented emissions were taken into account as the main cause of the soil eutrophication. The equivalent kg of $PO4^{3-}$ was used to address soil eutrophication.

Human toxicity

Human toxicity in LCA methodology is described as the toxic impacts of components on human health in a way that shorts human lifetime. This term is divided into two categories of cancer and non-cancer diseases.

4. Interpretation of the results: The final stage is the interpretation of the obtained values and quantities in order to make a comprehensive deduction and figure out the deficiencies. A beneficial strategy in order to judge the deficiencies is known as the sensitivity analysis [38].

Table 2. The life cycle impact categorizations

Life cycle impact category	Unit
Global warming	Tons of CO_2 equivalents
Stratospheric ozone depletion	Tons of Halon equivalents
Ground level ozone	Tons of projected ozone
Acidification	Tons of SO_2 equivalents
Eutrophication	Tons of phosphate equivalents
Aquatic toxicity	Tons of toxic equivalents
Human health	Equivalent tons of toxics
Fossil fuel depletion	Tons of oil equivalent
Mineral depletion	Tons of mineral equivalent (by mineral)
Water depletion	Cubic meters of water equivalent, (surface & groundwater)
Land use	equivalent hectares of endangered species and non-endangered species habitat
Resource depletion	Equivalent energy

3.2. Goal and scope of LCA

The aim of this LCA study is the projection of the environmental footprint of the carbonization of RM via an indirect route which could be beneficial in the future perspective of Jajarm Alumina Production Plant equipped with CCU technology. In this study, the specific environmental impacts of carbon capture via LCA were investigated and categorized based on different environmental classifications by GaBi software based on the ReCiPe methodology.

3.3. Process description and boundary

A proper process boundary designation is the key step in the cogent conclusion of an LCA study [39,40]. Figure 3 describes the system boundaries of the CCU process of the Jajarm plant. This process boundary covers the transfer of RM residue over the distance of about 1 km to the place that flue gas of the plant is exhausted and final calcium carbonate and side-products are produced. A brief description of the process is given below:

1. The RM extraction for leaching precious minerals including Al, Fe, and Ca was carried out using HCl (1M) at 80 °C at the initial step of the mineral carbonation. Indeed, 21 g dry powdered RM was added to the reactor comprising HCl and was agitated at a speed of 600 rpm by a magnetic stirrer upon atmospheric pressure. The reactor was covered with a condenser to prevent evaporation occurrence and preserve the temperature at a constant level as this reaction is exothermic. After completing the extraction in 2 h, the resultant slurry was separated from solid particles via centrifuging (9900 rpm, 15 min) and, then, vacuum filtration.
2. The second step concerns the production of Ca-enriched solution via the pH swing process. To be more specific, NaOH (1M) was employed to precipitate impurities present in the leached solution. pH increased from 2.3 (initial pH of the solution) to 4, 5, 7.5, and 9.5. At each step, the precipitants were separated using centrifuging (9900 rpm, 15 min) and vacuum filtration.
3. Next, the CO_2 recovery from the stacks (stacks A, B, and C) of the Jajarm plant was taken into account. The recovery of CO_2 from the stacks of the plant was performed via an amine scrubbing column. A mixture of CO_2 (10 % Vol.) and N_2 with a flow rate of 2 l/min was fed into the bubble column filled with 20 L of NaOH (1M). The conversion rate of CO_2 was about 99.53 %.
4. The suggested process ended in the production of the stabilized calcium carbonate. The reaction proceeded in ambient conditions to avoid any extra regulation with respect to the reaction conditions and, accordingly, less energy was required for the process. The prepared Na_2CO_3 was added to the final ca-enriched leachate, obtained in the first step, at a rate of 20 ml/min over a magnetic stirrer (250 rpm). After the reaction, a milky solution and white solid of Ca_2CO_3 were obtained which were centrifuged and filtered using a vacuum pump [13]. The conversion rate was achieved at 32.71 %.

The resultant product was transported to trucks to carry it for further commercial applications. It is noteworthy to mention that the environmental impacts relevant to those applications which utilized calcium carbonate product were not included in LCA. The functional unit was selected based on 1 t RM.

4. CARBON FOOTPRINT

The carbon footprint calculates GHG emissions during the life cycle of a product system or device [6,41]. This is a simple approach that includes carbon emissions as well as other non-carbon GHG emissions; however, the results are reported as the CO_2 equivalent [42,43].

According to the GHG Protocol Product Standard, there are obligations with respect to the emission of GHG. The carbon footprint strategy has been developed as the momentous agenda of societies in order to reduce the rising amount of CO_2 in the course of the life cycle of a product, system, or service [44].

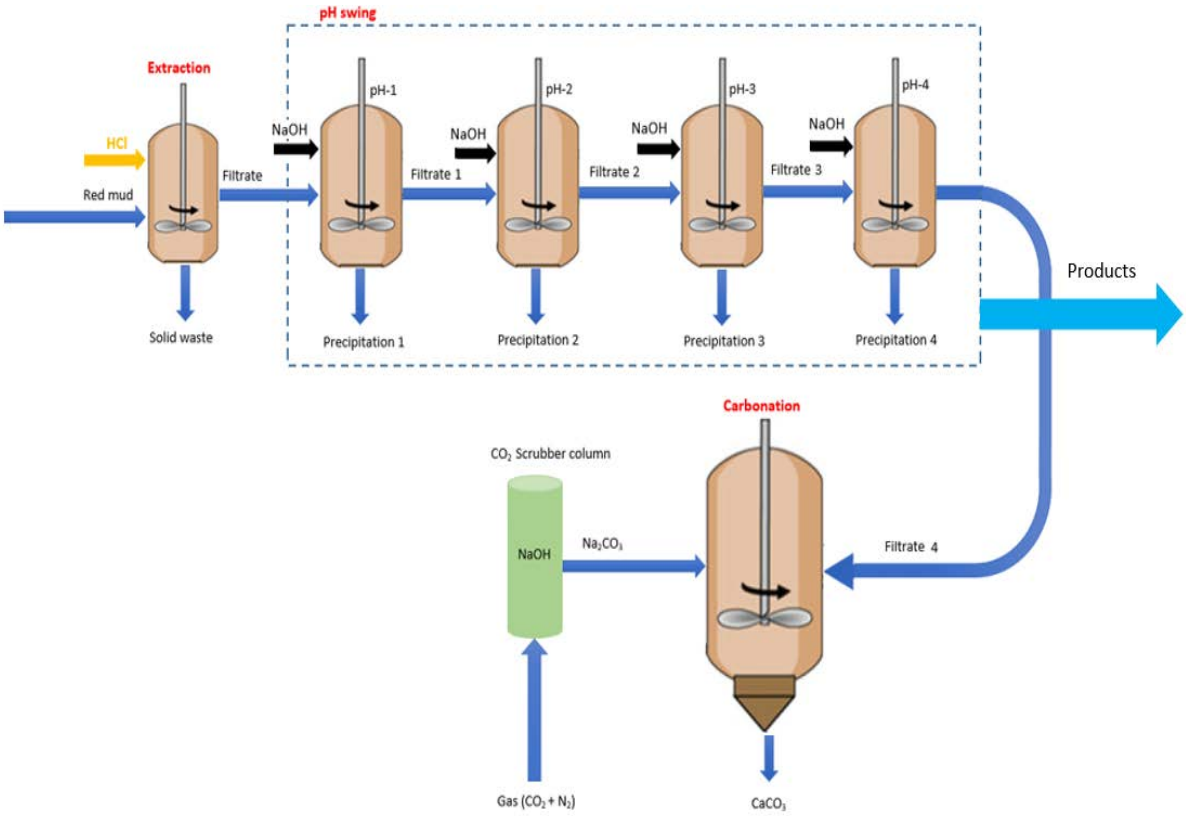

Figure 3. Schematic diagram of the system boundary of LCA

4.1. Methodology

The applied methodology for carbon footprint assessment in the current study is the Publicly Available Specifications (PAS) 2050. The LCA methodology cataloged in ISO 14040 based on the PAS 2050 framework is a highly attended standard for assessing products' carbon footprint. Although the ISO 14040 series represent the significantly applied LCA guidelines for the estimation of GHG emissions of a product or service, they lack a proper and accurate basis for the assessment of GHG emissions for the developing projects. An alternative standard exerted for assessing GHG emissions is ISO 14064 which considers carbon footprint at the organizational level. ISO 14064 seeks to provide institutions with a comprehensive assessment of direct and indirect GHG emissions of a product or service during the LCA and suggest strategies for mitigating GHG emissions. In the current study, ISO 14064 under the PAS 2050 criteria was used for the assessment of GHG emissions of RM carbonation process, which is expressed in CO_2 equivalent according to the GWP of each GHG defined by IPCC [41]. The tiers of GHG emissions based on ISO 14064 are illustrated as the following items: Tier 1) direct emissions from resources presented inside the system boundary; Tier 2) indirect emissions related to the energy use of an operational sector such as consumption of electricity, heat, and steam required for the production of a product; Tier 3) indirect emissions attributed to sources or operation of sectors beyond the allocated system boundary.

The emission equation according to ISO 14064 is defined as follows:

$$E_{tot} = \sum(EF_i \times AF_i) \quad (2)$$

where E_{tot} is the total emission of the process, and EF_i and AF_i are the emission factor and the activity factor of the individual resource of i, respectively [45,46].

4.2. System boundary and functional unit

ISO 14064 delineates the carbon footprint system boundaries as two specific boundaries, namely the organizational boundaries and the operational boundaries. The organizational boundaries are assigned to identify facilities of an organization that cause GHG inventory and they should be considered in the inventory analyses. According to the equity share definition, ISO 14064 takes the systems or devices under consideration which possesses the GHG emissions' portion of above 1 % of the predicted emissions of the functional unit.

The operational boundaries specify activities involved in the GHG inventory. In this context, direct emissions of GHG and those indirect emissions due to the supply of essential energies such as heat, steam, or electricity for the production of a product are considered in inventory calculations. The indirect emissions of GHG associated with the activities outside the defined boundary may or may not be taken into account. It is worth noting that the indirect emissions resulting from

electricity generation should be cited, but the citation of other emissions is optional, e.g., consideration of capital goods, transportation vehicles of employees or costumers [47,48].

The allocated system boundary for the carbon footprint of carbon mineralization of the Jajram plant was the same boundary defined in the LCA study (see Figure 1). As described before, PAS 2050 criteria just quantify the emissions of systems or devices that cause the GHG emissions beyond 1 % of the anticipated emissions for the functional unit. Additionally, the emissions associated with capital goods such as the construction of site and infrastructure and transportations were not taken into account. In the current study, no direct emission was accounted for in the process since none of the facilities consumed energy directly. Therefore, no direct emissions were expected. The only source of GHG emissions in this process was related to electricity use. As discussed above, the required energy for electricity generation out of the boundary of the system is considered as indirect GHG emissions. In order to compute the amount of indirect GHG emissions related to electricity consumption, the electricity use of all electrical facilities and the emission factor of each facility were used [49]. The emission factor can be calculated according to the following equation:

$$E_{ID,GE,CO_2} = \frac{EI_{grid} \times EF_{GE,CO_2}}{1-TDL} \quad (3)$$

where E_{ID,GE,CO_2} is the indirect emission of CO_2 resulting from the utilization of electricity, E_{ID,GE,CO_2} is the emission factor of the electricity network (ton $_{CO2}$/ MWh), EI_{grid} is the amount of received electricity (MWh), and TDL is the electricity loss.

According to the balance sheet of China in 2016, E_{ID,GE,CO_2} and TDL were considered as 0.6607 and 0.123, respectively.

5. RESULTS AND DISCUSSION

5.1. LCA methodology

The results of the simulation of the ex-situ CCU process of the Jajarm plant are given in Table 3. Table 3 summarizes the details of each environmental impact category assessed by GaBi software. As was mentioned in our previous work [13], the CO_2 mineralization process was intended to capture CO_2 to prevent the increase of global warming. Accordingly, the climate change category was chosen as the most critical life cycle impact for comparison and decision. According to the LCI results, compared to the conventional process that produced 34 kg CO_2, with equipment of the process with CCU, CO_2 eq. emission reduced about 28.13 kg/ ton RM, which means around release of 82 % CO_2 eq. into the atmosphere can be avoided. Moreover, the results showed that the share of each step in emission was about 40.2 %, 29.3 %, 24.6 %, and 5.9 % for pH swing, scrubbing column, extraction, and carbonation steps, respectively.

Table 3. The results of life cycle impact categories for the proposed CCU process

Life cycle impact category	Value	Unit
Climate change (ind. biogenic carbon)	5.87×10^{0}	kg CO_2 eq.
Acidification	1.54×10^{-3}	Kg SO_2 eq.
Ozone depletion	6.3×10^{-9}	kg CFC-11 eq.
Human toxicity, cancer effects	2.52×10^{-11}	CTUh
Human toxicity, non-cancer effects	1.3×10^{-10}	CTUh
Human health, Particulate air	1.14×10^{-5}	kg PM2.5 eq.
Eutrophication	2.24×10^{-3}	Kg N eq.
Smog air	2.52×10^{-3}	kg O_3 eq.
Ecotoxicity (freshwater)	1.31	CTUe
Resource depletion, mineral, fossil, and renewable	3.67×10^{-7}	kg MJ surplus energy eq.

5.2. Carbon footprint methodology

The CCU technology reduces the CO_2 emission of the Jajarm Plant. The CHG emissions during the CCU process were calculated based on the PAS 2050 scenario using ISO 14064. The total equivalent emissions associated with the main electricity-consuming instruments are summarized in Table 4. The total equivalent CO_2 emission is 2.33 kg which means a reduction of about 93 % of the equivalent CO_2 emission to the atmosphere. This value is lower than the results acquired by LCA in the climate change category. This is due to the fact that carbon footprint considers the emissions related to electronic consumption, while LCA is a holistic analysis. Therefore, the total emission estimated by LCA is higher than the carbon footprint.

Table 4. The results of carbon footprint methodology for the essential apparatus

Instrument	Equivalent emission CO_2 (ton CO_2eq/1 ton extraction)	EI_{grid}	Consumed electricity (MW)	Consumed time (min)
Electrical stirrer	0.0011	0.0015	0.003	30
Industrial centrifuge	0.0011	0.0015	0.006	15
Scrubber column	0.00013	0.0011	0.00035	30

5.3. Economical assessments

The process of CCU of CO_2 emitted from the stacks of the plant was considered in an indirect mineralization procedure. One of the best privileges of this process is its low capture cost as it proceeds in ambient conditions, namely environmental temperature and pressure and no necessity for the separation and purification of exhausted gas to achieve high-purity CO_2. Apart from the economic efficiency of the operational conditions, the production of side products and calcium carbonate as the main product made the process economically more recoverable. Table 5 describes the price of the generated products and the estimated amount of their sell. The total pecuniary value of these side and main products was estimated at around 243 $/ ton RM, which can compensate some portion of the initial investments. Moreover, by using RM as a suitable and easy available feed source, the costs regarding transporting the raw material for CCU goals are cut down, thus making the process more economically profitable. Furthermore, 29.4 ton RM is required for capture of 1 ton CO_2.

Table 5. The economic assessment of the products produced during the CCU

Product	Purity (%)	Price per 1 t product ($)	The amount of obtained product per 1 t RM (kg)	The estimated value ($)
Silica	65	50	53	3
Aluminum	70 -80	110-160	173	23
Hematite	60	200-400	642	193
Calcium carbonate	98	260-300	78.5	24

6. CONCLUSIONS

CCU technologies have been developed as promising techniques in the portfolio of GHG reduction and global warming abatement. In addition to these environmental merits, the acquirement of valuable products during the CCU process is another privilege of this process as it brings about economic recovery to the system. The former merit is highly attended as mitigation of CO_2 emission has become the priority of decision-makers and program managers. Nevertheless, it should be ascertained that GHG mitigation strategies would not bring about other environmental impacts. In this regard, an LCA approach has been employed as a holistic assessment tool to account for all environmental aspects of a product during its life cycle.

This paper studied the environmental impacts of indirect mineral carbonation of CO_2 exhausted from the stacks of Jajarm plant by RM, the alkaline waste of the plant, using LCA guideline. The estimation was carried out by GaBi software under the criteria of ISO 14044 and ISO 14040 in the LCA framework. The result of the climate change category revealed that the emission reduction of about 28.13 kg CO_2 eq/ton RM (around 82 %) can be achieved by the equipment of the conventional process with CCU technology. The carbon footprint calculations based on the PAS 2050 perspective using ISO 14064 showed GHG emission of about 2.33 kg CO_2 eq. According to the mentioned results, achieved for the first time, mineralization of CO_2 released from the flues of Jajarm plant over the mineral residue of the plant is a feasible approach that can be used on a large scale. The outcomes of this work would be highly beneficial for further investigations by researchers since a holistic guideline has been provided here. Further research works can consider the emission of transportation for more accurate analysis. Furthermore, the economic study pointed to the economic recovery of about 243 $/ t RM which is obtainable by the trade of the by- and main-products including silicate, alumina, hematite, and calcium carbonate. The convenient and easy-to-use operational conditions of the process as well as its cost efficiency due to the generation of valuable products can be seen as the greatest merits of this CCU technique.

The LCA-based outcomes suggest that after utilizing CCU in the Jajarm plant for mineral carbonation of RM by CO_2 exhausted from the plant, the emission of GHCs reduced dramatically, which supports the implementation of CCU technology for the real application in Jjarm plant. Additionally, carbon footprint results and economic evaluation confirmed the reduction of GHG emission and showed the promising profitability of the suggested process, which can attract investors to finance this technology.

7. ACKNOWLEDGEMENT

This research was carried out in collaboration with the Faculty of Environmental Engineering, The University of Tehran.

NOMENCLATURE

LCA	Life Cycle Assessment
LCI	Life Cycle Inventory
GHG	Greenhouse Gas
GWP	Global Warming Potential
ISO	International Organization for Standardization
CCS	Carbon Capture and Storage
CCU	Carbon Capture and Utilization
ADP	Abiotic Depletion Potential
ODP	Ozone layer Depletion Potential
HTP	Human Toxicity Potential
FWAETP	Freshwater Aquatic Ecotoxicity Potential
MAETP	Marine Aquatic Ecotoxicity Potential
TEP	Terrestrial Ecotoxicity Potential
POP	Photochemical Oxidation Potential
AP	Acidification Potential
EP	Eutrophication Potential
RM	Red Mud
HCl	Hydrochloric acid

REFERENCES

1. Jeon, J. and Kim, M.-J., "CO_2 storage and $CaCO_3$ production using seawater and an alkali industrial by-product", ***Chemical Engineering Journal***, Vol. 378, (2019), 122180. (https://doi.org/10.1016/j.cej.2019.122180).
2. Brandão, M., Levasseur, A., Kirschbaum, M.U.F., Weidema, B.P., Cowie, A.L., Jørgensen, S.V., Hauschild, M.Z., Pennington, D.W. and Chomkhamsri, K., "Key issues and options in accounting for carbon sequestration and temporary storage in life cycle assessment and carbon footprinting", ***The International Journal of Life Cycle Assessment***, Vol. 18, (2013), 230-240. (https://doi.org/10.1007/s11367-012-0451-6).
3. Koornneef, J., van Keulen, T., Faaij, A. and Turkenburg, W., "Life cycle assessment of a pulverized coal power plant with post-combustion capture, transport and storage of CO_2", ***International Journal of***

Greenhouse Gas Control, Vol. 2, (2008), 448-467. (https://doi.org/10.1016/j.ijggc.2008.06.008).

4. McDonagh, S., Wall, D.M., Deane, P. and Murphy, J.D., "The effect of electricity markets, and renewable electricity penetration, on the levelised cost of energy of an advanced electro-fuel system incorporating carbon capture and utilisation", ***Renewable Energy***, Vol. 131, (2019), 364-371. (https://doi.org/10.1016/j.renene.2018.07.058).
5. Arning, K., Offermann-van Heek, J., Linzenich, A., Kaetelhoen, A., Sternberg, A., Bardow, A. and Ziefle, M., "Same or different? Insights on public perception and acceptance of carbon capture and storage or utilization in Germany", ***Energy Policy***, Vol. 125, (2019), 235-249. (https://doi.org/10.1016/j.enpol.2018.10.039).
6. Markewitz, P., Kuckshinrichs, W., Leitner, W., Linssen, J., Zapp, P., Bongartz, R., Schreiber, A. and Müller, T.E., "Worldwide innovations in the development of carbon capture technologies and the utilization of CO_2", ***Energy and Environmental Science***, Vol. 5, (2012), 7281-7305. (https://doi.org/10.1039/C2EE03403D).
7. Laude, A., Ricci, O., Bureau, G., Royer-adnot, J. and Fabbri, A., "CO_2 capture and storage from a bioethanol plant : Carbon and energy footprint and economic assessment", ***International Journal of Greenhouse Gas Control***, Vol. 5, No. 5, (2011), 1220-1231. (https://doi.org/10.1016/j.ijggc.2011.06.004).
8. Vreys, K., Lizin, S., Van Dael, M., Tharakan, J. and Malina, R., "Exploring the future of carbon capture and utilisation by combining an international Delphi study with local scenario development", ***Resources, Conservation and Recycling***, Vol. 146, (2019), 484-501. (https://doi.org/10.1016/j.resconrec.2019.01.027).
9. Harrison, B. and Falcone, G., "Carbon capture and sequestration versus carbon capture utilisation and storage for enhanced oil recovery", ***Acta Geotechnica***, Vol. 9, (2014), 29-38. (https://link.springer.com/article/10.1007%2Fs11440-013-0235-6). (https://doi.org/10.1007/s11440-013-0235-6).
10. Perdan, S., Jones, C.R. and Azapagic, A., "Public awareness and acceptance of carbon capture and utilisation in the UK", ***Sustainable Production Consumption***, Vol. 10, (2017), 74-84. (https://doi.org/10.1016/j.spc.2017.01.001).
11. Bruhn, T., Naims, H. and Olfe-Kräutlein, B., "Separating the debate on CO_2 utilisation from carbon capture and storage", ***Environmental Science and Policy***, Vol. 60, (2016), 38-43. (https://doi.org/10.1016/j.envsci.2016.03.001).
12. North, M. and Styring, P., "Perspectives and visions on CO_2 capture and utilisation", ***Faraday Discussions***, Vol. 183, (2015), 489-502. (https://doi.org/10.1039/c5fd90077h).
13. Kashefi, K., Pardakhti, A., Shafiepour, M. and Hemmati, A., "Process optimization for integrated mineralization of carbon dioxide and metal recovery of red mud", ***Journal of Environmental Chemical Engineering***, Vol. 8, No. 2, (2020), 103638. (https://doi.org/10.1016/j.jece.2019.103638).
14. Bodénan, F., Bourgeois, F., Petiot, C., Augé, T., Bonfils, B., Julcour-Lebigue, C., Guyot, F., Boukary, A., Tremosa, J., Lassin, A., Gaucher, E.C. and Chiquet, P., "Ex situ mineral carbonation for CO_2 mitigation: Evaluation of mining waste resources, aqueous carbonation processability and life cycle assessment (Carmex project)", ***Minerals Engineering***, Vol. 59, (2014), 52-63. (https://doi.org/10.1016/j.mineng.2014.01.011).
15. Kim, M.J., Pak, S.Y., Kim, D. and Jung, S., "Optimum conditions for extracting Ca from CKD to store CO_2 through indirect mineral carbonation", ***KSCE Journal of Civil Engineering***, Vol. 21, (2017), 629-35. (https://doi.org/10.1007/s12205-016-0913-7).
16. Mo, L., Carbon dioxide sequestration on steel slag, Carbon dioxide sequestration in cementitious construction materials, Woodhead publishing series in civil and structural engineering, Elsevier, (2018), 175-197. (https://doi.org/10.1016/B978-0-08-102444-7.00008-3).
17. Nduagu, E., Bergerson, J. and Zevenhoven, R., "Life cycle assessment of CO_2 sequestration in magnesium silicate rock-A comparative study", ***Energy Conversation and Management***, Vol. 55, (2012), 116-126. (https://doi.org/10.1016/j.enconman.2011.10.026).
18. Ji, L. and Yu, H., Carbon dioxide sequestration by direct mineralization of fly ash, Carbon dioxide sequestration in cementitious construction materials, Woodhead publishing series in civil and structural engineering, Elsevier; (2018), 13-37. (https://doi.org/10.1016/B978-0-08-102444-7.00002-2).
19. Chu, G., Wang, L., Liu, W., Zhang, G., Luo, D., Wang, L., Liang, B. and Li, C., "Indirect mineral carbonation of chlorinated tailing derived from Ti-bearing blast-furnace slag coupled with simultaneous dechlorination and recovery of multiple value-added products", ***Greenhouse Gases: Science and Technology***, Vol. 9, (2019), 52-66. (https://doi.org/10.1002/ghg.1832).
20. Zapp, P., Schreiber, A., Marx, J., Haines, M., Hake, J.F. and Gale, J., "Overall environmental impacts of CCS technologies-A life cycle approach", ***International Journal of Greenhouse Gas Control***, Vol. 8, (2012), 12-21. (https://doi.org/10.1016/j.ijggc.2012.01.014).
21. Cuéllar-Franca, R.M. and Azapagic, A., "Carbon capture, storage and utilisation technologies: A critical analysis and comparison of their life cycle environmental impacts", ***Journal of CO_2 Utilization***, Vol. 9, (2015), 82-102. (https://doi.org/10.1016/j.jcou.2014.12.001).
22. Hauschild, M.Z., Rosenbaum, R.K. and Olsen, S.I., Life cycle assessment: Theory and practice, (2017), 1-1216. (https://doi.org/10.1007/978-3-319-56475-3).
23. Atta, A.P., Diango, A., N'Guessan, Y., Descombes, G., Morin, C. and Jaecker-Voirol, A., Life cycle assessment, technical and economical analyses of jatropha biodiesel for electricity generation in remote areas of côte d'Ivoire, Refining ciomass residues for sustainable energy and bioproducts, Technology, advances, life cycle assessment, and economics, Elsevier, (2020), 523-542. (https://doi.org/10.1016/B978-0-12-818996-2.00024-7).
24. Van Hung, N., Migo, M.V., Quilloy, R., Chivenge, P. and Gummert, M., Life cycle assessment applied in rice production and residue management, Sustainable rice straw management, Springer, (2020), 161-174. (https://doi.org/10.1007/978-3-030-32373-8_10).
25. Jolliet, O., Antón, A., Boulay, A.-M., Cherubini, F., Fantke, P., Levasseur, A., McKone, T.E., Michelsen, O., Milà i Canals, L., Motoshita, M., Pfister, S., Verones, F., Bruce Vigon, B. and Frischknecht, R., "Global guidance on environmental life cycle impact assessment indicators: Impacts of climate change, fine particulate matter formation, water consumption and land use", ***The International Journal of Life Cycle Assessment***, Vol. 23, (2018), 2189-2207. (https://doi.org/10.1007/s11367-018-1443-y).
26. Hertwich, E.G., Aaberg, M., Singh, B. and Strømman, A.H., "Life-cycle assessment of carbon dioxide capture for enhanced oil recovery", ***Chinese Journal of Chemical Engineering***, Vol. 16, (2008), 343-353. (https://doi.org/10.1016/S1004-9541(08)60085-3).
27. Koroneos, C., Dompros, A., Roumbas, G. and Moussiopoulos, N., "Life cycle assessment of kerosene used in aviation", ***The International Journal of Life Cycle Assessment***, Vol. 10, (2005), 417-424. (https://doi.org/10.1065/lca2004.12.191).
28. Sills, D.L., Van Doren, L.G., Beal, C. and Raynor, E., "The effect of functional unit and co-product handling methods on life cycle assessment of an algal biorefinery", ***Algal Research***, Vol. 46, (2020), 101770. (https://doi.org/10.1016/j.algal.2019.101770).
29. Hoseinzadeh, S., Ghasemiasl, R., Javadi, M.A. and Heyns, P.S., "Performance evaluation and economic assessment of a gas power plant with solar and desalination integrated systems", ***Desalination and Water Treatment***, Vol. 174, (2020), 11-25. (http://hdl.handle.net/2263/73259). (http://doi.org/10.5004/dwt.2020.24850).
30. Hoseinzadeh, S., Yargholi, R., Kariman, H. and Heyns, P.S., "Exergeoeconomic analysis and optimization of reverse osmosis desalination integrated with geothermal energy", ***Environmental Progress and Sustainable Energy***, (2020), e13405. (https://doi.org/10.1002/ep.13405).
31. Kariman, H., Hoseinzadeh, S., Shirkhani, A., Heyns, P.S. and Wannenburg, J., "Energy and economic analysis of evaporative vacuum easy desalination system with brine tank", ***Journal of Thermal Analysis and Calorimetry***, Vol. 140, (2019), 1935-1944. (https://doi.org/10.1007/s10973-019-08945-8).
32. http://iranalumina.ir/ n.d.
33. Schreiber, A., Zapp, P. and Marx, J., "Meta-analysis of life cycle assessment studies on electricity generation with carbon capture and storage", ***Journal of Industrial Ecology***, Vol. 16, (2012), S155-S168. (https://doi.org/10.1111/j.1530-9290.2011.00435.x).
34. Jørgensen, A., Le Bocq, A., Nazarkina, L. and Hauschild, M., "Methodologies for social life cycle assessment", ***The International Journal of Life Cycle Assessment***, Vol. 13, (2008), 96. (https://doi.org/10.1065/lca2007.11.367).
35. Viebahn, P., Nitsch, J., Fischedick, M., Esken, A., Schüwer, D., Supersberger, N., UlrichZuberbühler, U. and Edenhofer, O., "Comparison of carbon capture and storage with renewable energy

technologies regarding structural, economic, and ecological aspects in Germany", ***International Journal of Greenhouse Gas Control***, Vol. 1, No. 1, (2007), 121-133. (https://doi.org/10.1016/S1750-5836(07)00024-2).

36. Carvalho, A., Matos, H.A. and Gani, R., "SustainPro—A tool for systematic process analysis, generation and evaluation of sustainable design alternatives", ***Computers and Chemical Engineering***, Vol. 50, (2013), 8-27. (https://doi.org/10.1016/j.compchemeng.2012.11.007).
37. Zhang, X., Singh, B., He, X., Gundersen, T., Deng, L. and Zhang, S., "Post-combustion carbon capture technologies: Energetic analysis and life cycle assessment", ***International Journal of Greenhouse Gas Control***, Vol. 27, (2014), 289-298. (https://doi.org/10.1016/j.ijggc.2014.06.016).
38. Pehnt, M. and Henkel, J., "Life cycle assessment of carbon dioxide capture and storage from lignite power plants", ***International Journal of Greenhouse Gas Control***, Vol. 3, No. 1, (2009), 49-66. (https://doi.org/10.1016/j.ijggc.2008.07.001).
39. Yuen, Y.T., Sharratt, P.N. and Jie, B., "Carbon dioxide mineralization process design and evaluation: Concepts, case studies, and considerations", ***Environmental Science and Pollution Research***, Vol. 23, (2016), 22309-22330. (https://doi.org/10.1007/s11356-016-6512-9).
40. Khoo, H.H., Bu, J., Wong, R.L., Kuan, S.Y. and Sharratt, P.N., "Carbon capture and utilization: Preliminary life cycle CO_2, energy, and cost results of potential mineral carbonation", ***Energy Procedia***, Vol. 4 (2011), 2494-2501. (https://doi.org/doi:10.1016/j.egypro.2011.02.145).
41. Xu, X., Cheng, K., Wu, H., Sun, J., Yue, Q. and Pan, G., "Greenhouse gas mitigation potential in crop production with biochar soil amendment—A carbon footprint assessment for cross-site field experiments from China", ***GCB Bioenergy***, Vol. 11, No. 4, (2019), 592-605. (https://doi.org/10.1111/gcbb.12561).
42. Weidema, B.P., Thrane, M., Christensen, P., Schmidt, J. and Løkke, S., "Carbon footprint: A catalyst for life cycle assessment?" ***Journal of Industrial Ecology***, Vol. 12, No. 1, (2008), 3-6. (https://doi.org/10.1111/j.1530-9290.2008.00005.x).
43. Frischknecht, R., Fantke, P., Tschümperlin, L., Niero, M., Antón, A., Bare, J., Boulay, A.-M., Cherubini, F., Hauschild, M.Z., Henderson, A., Levasseur, A., McKone, T.E., Michelsen, O., Milà i Canals, L., Pfister, S., Ridoutt, B., Rosenbaum, R.K., Verones, F., Vigon, B. and Jolliet, O., "Global guidance on environmental life cycle impact assessment indicators: Progress and case study", ***The International Journal of Life Cycle Assessment***, Vol. 21, (2016), 429-442. (https://doi.org/10.1007/s11367-015-1025-1).
44. Mulrow, J., Machaj, K., Deanes, J. and Derrible, S., "The state of carbon footprint calculators: An evaluation of calculator design and user interaction features", ***Sustainable Production and Consumption***, Vol. 18, (2019), 33-40. (https://doi.org/10.1016/j.spc.2018.12.001).
45. Scipioni, A., Manzardo, A., Mazzi, A. and Mastrobuono, M., "Monitoring the carbon footprint of products: A methodological proposal", ***Journal of Cleaner Production***, Vol. 36, (2012), 94-101. (https://doi.org/10.1016/j.jclepro.2012.04.021).
46. Matthews, H.S., Hendrickson, C.T. and Weber, C.L., "The importance of carbon footprint estimation boundaries", ***Environmental Science & Technology***, Vol. 42, (2008), 5839-5842. (https://doi.org/10.1021/es703112w).
47. Wintergreen, J. and Delaney, T., "ISO 14064, International standard for GHG emissions inventories and verification", ***Proceedings of 16th Annual International Emission Inventory Conference***, Raleigh, NC, (2006), 4. (https://www3.epa.gov/ttn/chief/conference/ei16/session13/wintergreen.pdf).
48. Garcia, R. and Freire, F., "Carbon footprint of particleboard: A comparison between ISO/TS 14067, GHG Protocol, PAS 2050 and Climate Declaration", ***Journal of Cleaner Production***, Vol. 66, (2014), 199-209. (https://doi.org/10.1016/j.jclepro.2013.11.073).
49. Pandey, D., Agrawal, M. and Pandey, J.S., "Carbon footprint: current methods of estimation", ***Environmental and Monitoring Assessment***, Vol. 178, (2011), 135-160. (https://doi.org/10.1007/s10661-010-1678-y).

Journal of Renewable Energy and Environment

Research Article

Journal Homepage: www.jree.ir

Feasibility Study of Powering Desiccant Evaporative Cooling Systems with Photovoltaic Solar Panels for Hot and Humid Climates of Iran

Ahmad Naderi Nobandegani, Mohammad Ahmadzadehtalatapeh*

Department of Mechanical & Marine Engineering, Chabahar Maritime University, P. O. Box: 99717-56499, Chabahar, Sistan and Baluchestan, Iran.

PAPER INFO

Paper history:
Received 14 April 2020
Accepted in revised form 27 July 2020

Keywords:
Buildings,
Energy Consumption,
Desiccant Evaporative Cooling System (DECS),
Indoor Air,
TRNSYS

ABSTRACT

In the present study, the performance of a Desiccant Evaporative Cooling System (DECS) under eight different designs to provide the desired indoor air conditions for administration buildings was explored via TRNSYS software. An administration building in Chabahar, Iran as a region with a high cooling load demand was considered for the study. The simulation results indicated that the two-stage desiccant cooling system (Des. H) was the most suitable design, and it enjoyed the potential to keep the indoor air conditions within the standard recommendations. It was also shown that Des. H is the superior design in terms of energy performance and can meet the space cooling load requirements. The study showed that Des. H had the highest COP value with 2.83. The possible application of solar energy to the regeneration process of the Des. H was also studied. The simulations revealed that Des. H with and without the solar panels had less energy consumption than the existing system. The study showed that the application of Des. H could ensure 26.97 % saving in power per year in comparison to the existing system. Moreover, it was demonstrated that the addition of PVT panels to Des. H could increase the rate of annual power saving to about 68.03 %.

https://doi.org/10.30501/jree.2020.225286.1096

1. INTRODUCTION

Energy consumption of air-conditioning systems accounts for a significant part of the world's energy demand, which is about 40 % [1]. High cooling load situations normally coincide with high solar radiation hours, which makes it possible to apply the solar radiation to ventilation systems by related technologies. To this end, Renewable Energy Organization of Iran has recommended a strategic program under the five-year national development vision plan [2]. Based on the proposed plan, Iran is determined to provide 10 % of its electric power demand from renewable resources by 2025 [3].

Solar, wind, biomass, and geothermal energy are considered as the primary sources of renewable energy. Characterized by an average solar radiation 2000 KWh/m^2 with 2800 hours of sunshine per year, which reaches 3200 hours in the central regions of the country, Iran can be considered a rich country in terms of solar energy. Therefore, the application of solar-related technologies has drawn considerable attention by the researchers [4].

The technology of solar-assisted Desiccant Evaporative Cooling System (DECS) is an interesting solution to common issues of buildings. This technology has an open cycle that works based on air dehumidification by solid adsorbent such as silica gel and lithium chloride-cellulose and water evaporation. One of the significant advantages of these systems is the possibility of using solar energy in the recovery line.

The literature review indicates that there are some valuable research studies on the subject [5-10]. For instance, Li et al. [5] examined the performance of a two-stage solar DECS powered by solar energy. It was shown that a two-stage desiccant cooling system could work well for 51 days in an environment that had an average humidity of 51.7 %. A two-stage rotary dehumidification wheel was reviewed by Ge et al. [6]. The primary purpose of this study was to investigate the effect of desiccant thickness on the system performance. It was found that the desiccant with a thickness of 100 mm was the optimal mode for achieving the highest system performance.

Enteria et al. [7] investigated the effect of various adsorbent materials on the performance of a rotary Desiccant Wheel (DW). The performance of two adsorbents including silica gel (SiO_2) and titanium dioxide (TiO_2) was investigated in the study. The results revealed that the application of the titanium dioxide as the moisture absorbent led to better performance. In another research, Liu et al. [8] examined the combination of a DW and a heat pump. In this system, the heat wasted by the gas cooler pump is used to regenerate the DW. The results indicated that the combination saved energy by about 50-90 %.

Preisler et al. [9], and Enteria et al. [7] investigated the performance of flat plate solar collectors to provide the required heat source for the desiccant cooling cycle. In

*Corresponding Author's Email: m_ahmadzadeh56@yahoo.com (M. Ahmadzadehtalatapeh)
URL: http://www.jree.ir/article_111047.html

Please cite this article as: Naderi Nobandegani, A. and Ahmadzadehtalatapeh, M., "Feasibility study of powering desiccant evaporative cooling systems with photovoltaic solar panels for hot and humid climates of Iran", ***Journal of Renewable Energy and Environment (JREE)***, Vol. 7, No. 4, (2020), 10-20. (https://doi.org/10.30501/jree.2020.225286.1096).

another research, Bourdoukan et al. [10] suggested the application of vacuum tube collectors instead of low-efficiency flat plate collectors in the DECS. The study showed that the fluid output temperature in the vacuum tube collectors was higher than the temperature provided by the flat plates for the regeneration process.

So far, solar energy has been used in Iran to generate electricity and provide hot water. However, use of solar energy in cooling systems has not received sufficient attention. Therefore, the main objective is to evaluate the performance of the DECS under different designs by replacing this system with the existing operating vapor compression cooling systems in hot and humid regions of Iran. The Chabahar Maritime University Administration Building (CMUAB) is considered as a case study and it is located in the southeast of the country. Of note, the south and southeast of Iran are the areas with high cooling load requirements.

2. RESEARCH METHODOLOGY

The primary purpose of this study is to investigate the potential of replacing the existing ventilation system with a DECS to establish the desired indoor air conditions for an administration building in Chabahar, Iran. For this purpose, first, the existing ventilation system, which is a compression refrigeration type, was simulated by TRNSYS. Then, the existing ventilation system was re-designed to be replaced with a DECS under different designs to determine the most desired configuration in terms of provided indoor air conditions and energy consumption.

3. BUILDING SIMULATION

3.1. Region climate conditions

Chabahar is located on the Makran Coast of the Sistan and Baluchestan province, Iran. It is located in the direction of the Indian subcontinent monsoon wind; therefore, Chabahar climate is moderate tropical with high Relative Humidity (RH) values [11]. Figure 1 shows the monthly mean ambient RH and temperature for the region.

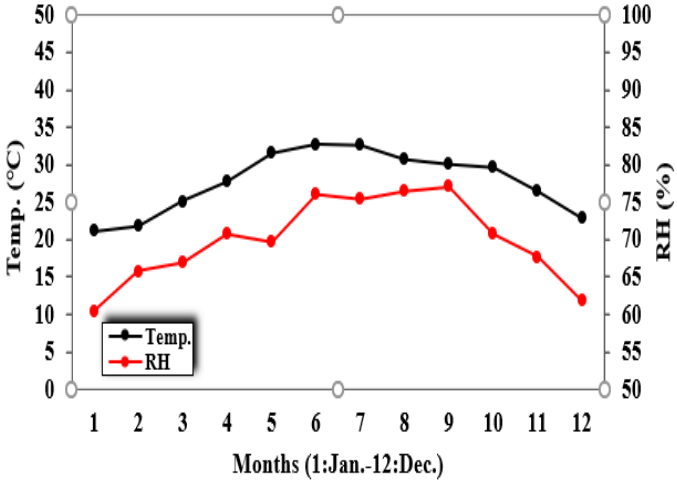

Figure 1. Monthly mean ambient air temperature and RH of the region (Chabahar) [11]

3.2. CMUAB characteristics

The considered CMUAB is located in Chabahar Maritime University, Chabahar, Iran. The building consists of three separate floors with 51 rooms. The ventilation systems of the floors are the same; however, the cooling capacity of the systems varies for the floors. Figure 2 illustrates the building overview and the plan view of the 1st and 2nd floor.

(a)

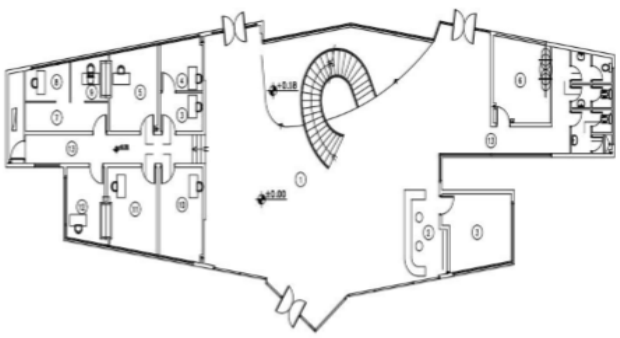

(b)

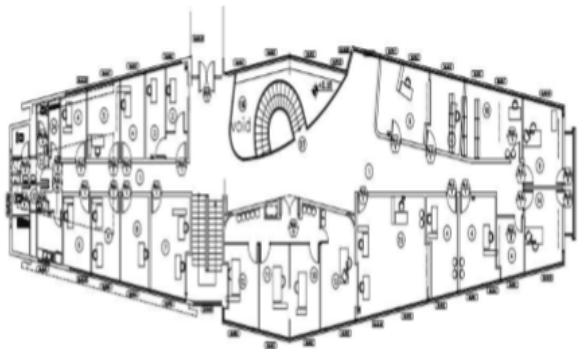

(c)

Figure 2. (a) CMUAB overview, (b) Plan view of the 1st floor, and (c) Plan view of the 2nd floor

In order to simulate the hourly performance of the considered building under the existing condition and the added DECS, the external walls structure, roof structure, and floor structure need to be determined and defined in the software. Therefore, thickness, material's type, and thermophysical properties of walls were obtained from the

administration department of the CMUAB. Figure 3 demonstrates the walls structure layout and the specifications of the CMUAB elements are tabulated in Table 1.

To determine the indoor air conditions and estimate the required cooling load, the building was simulated in TRNSYS software. The CMUAB was assumed as a single thermal zone (Type56a), and the required technical data for Type56a were defined. The functions and definitions are tabulated in Table 2.

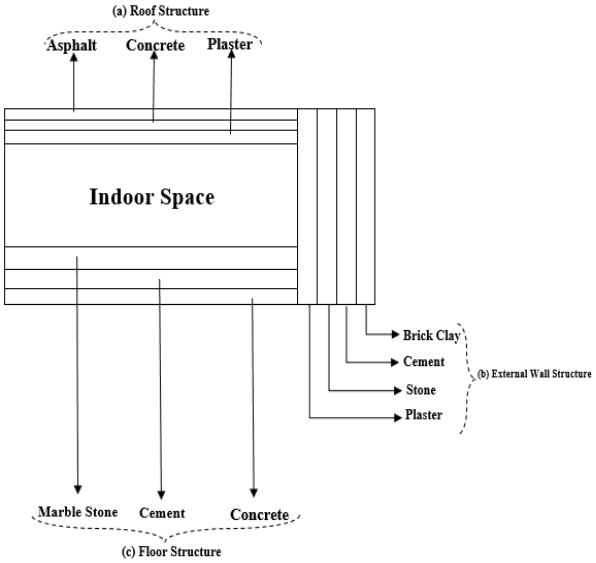

Figure 3. CMUAB roof, external walls, and floor structures layout: (a) Roof structure, (b) External wall structure, (c) Floor structure

Table 1. Specifications of the CMUAB elements

Eternal walls				
	d (m)	λ(w/mk)	ρ(kg/m³)	c (J/kg.k)
Stone	0.015	0.890	1920	790
Cement	0.001	0.580	1900	1000
Brick-Clay	0.20	1.185	2240	790
Plaster	0.015	0.580	800	1090
Floor				
Marble Stone	0.015	0.057	290	590
Cement	0.05	0.580	1900	1000
Concrete	0.30	0.580	1900	1000
Roof				
Asphalt	0.01	0.057	290	590
Concrete	0.30	0.580	1900	1000
Plaster	0.015	0.030	43.0	1210

Table 2. Components definitions (Fig. 7)

Lable	Description of the component	Function
	Equation	This component is used for calculation purposes.
	Region weather data	This component reads TRNSYS TMY2 format weather le to determine the outdoor condition.
	Building (space)	This component takes the inlet temperature, RH, and air flow to calculate the space temperature and RH.
	Ambient related data	This component takes the ambient air data and calculates the fictive sky temperature.
	Thermostat	This component controls the indoor temperature to turn the air conditioning on and off.
	Psychrometric calculator	This component takes any two properties of moist air and calculates all other properties.
	Direct evaporative cooler	This component takes the inlet dry and wet bulb temperatures to calculate the leaving dry and wet bulb temperatures.
&	Mixer	Input streamline mixer.
	EW	This component takes the inlet temperature and humidity ratio to calculate the leaving temperature and humidity ratio for the supply and return sides.
	Air heater	This component takes the inlet temperature and humidity ratio to calculate the leaving temperature and humidity ratio.
	Rotary desiccant	This component dries the humid air.
	Photovoltaic thermal collector series	This component generates electricity thermal energy simultaneously

4. CMUAB WITH THE DECS

In this study, different designs based on the DECS principle were investigated. To improve the performance of DECS, some energy converting units such as Direct Evaporative Cooler (DEC), Indirect Evaporative Cooler (IEC), Energy Wheel (EW), DW are normally recommended to be applied to the system. Figures 4 and 5 illustrate the schematic of DW and EW, respectively.

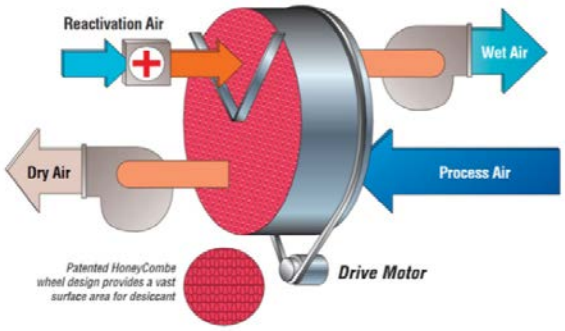

Figure 4. Schematic of a DW [12]

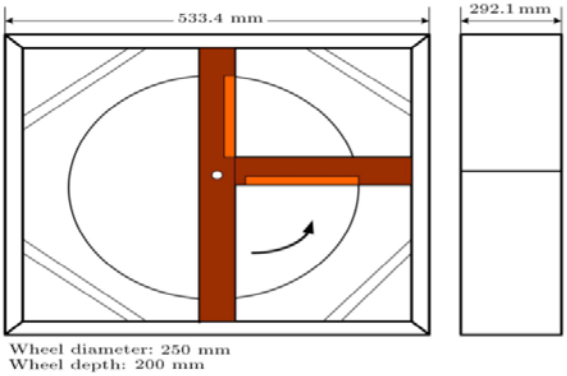

Figure 5. Schematic of an EW [13]

Eight different designs commonly proposed for the Heating, Ventilation, and Air Conditioning (HVAC) systems were examined to determine the most proper design in terms of the established indoor air conditions and energy consumption. The designs are listed below:

1. Des. A: DECS operating in ventilation cycle (Pennington cycle);
2. Des. B: DECS operating in recirculation cycle;
3. Des. C: DECS operating in Duncle cycle;
4. Des. D: DECS operating in modified ventilation cycle;
5. Des. E: DECS operating in modified recirculation cycle with pre-cooling;
6. Des. F: DECS operating in ventilation cycle with double series EW;
7. Des. G: Two-stage DECS operating in ventilation;
8. Des. H: Two-stage DECS operating in recirculation cycle.

More details regarding the design and simulation process will be explained in the subsections below.

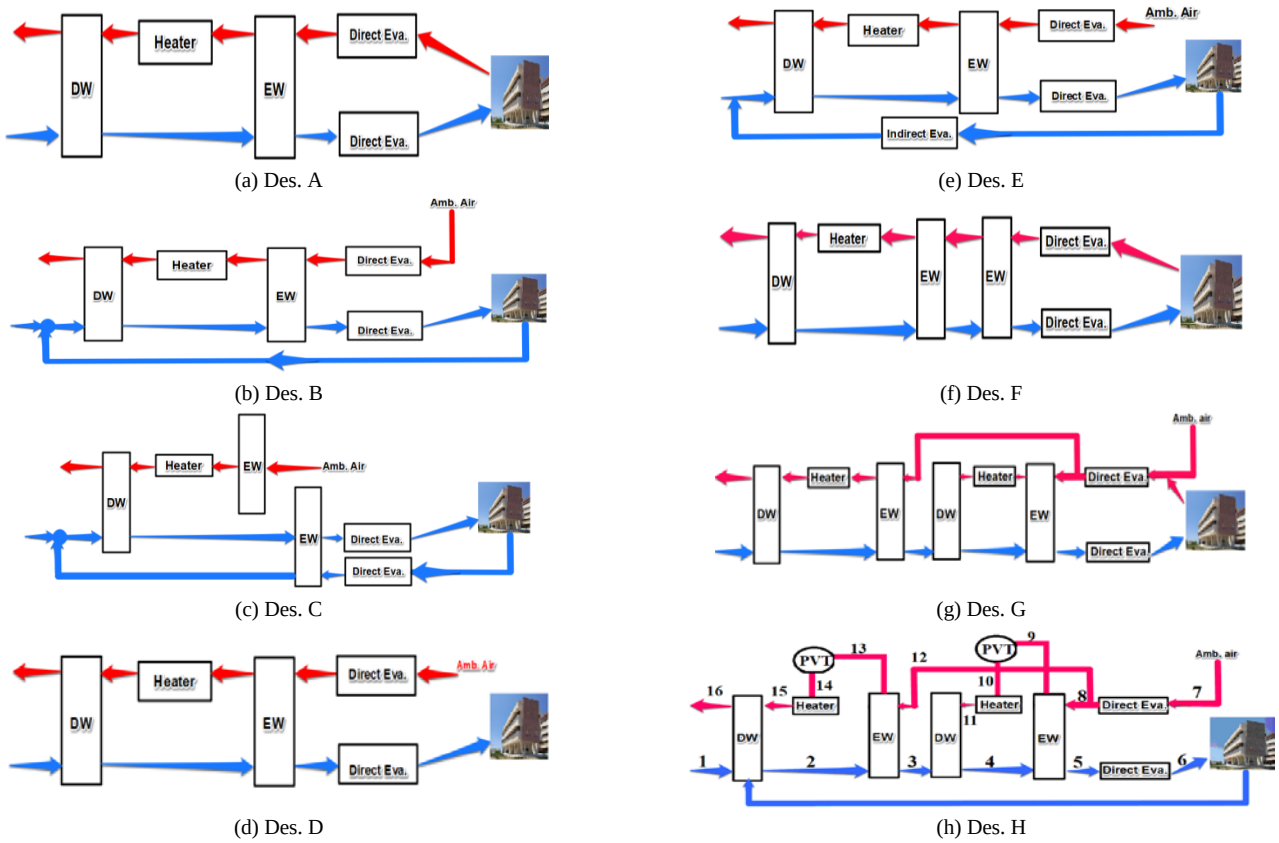

(a) Des. A (e) Des. E

(b) Des. B (f) Des. F

(c) Des. C (g) Des. G

(d) Des. D (h) Des. H

Figure 6. The schematic diagram of desiccant-based cooling systems

4.1. Des. A: DECS operating in ventilation cycle (Pennington cycle)

One of the most basic DECS is the Pennington cycle (Figure 6). This cycle consists of two streams of supply and regenerator. In this cycle, fresh outdoor air first passes through a rotary DW and is dehumidified, and its temperature increases. The warm air then passes through an EW and exchanges heat with the recovery stream.

The air after the EW passes through an evaporator unit before entering the building space. The return air from the building is cooled in another evaporator unit directly placed after the building and then, heated by an EW, as shown in Figure 6. Since the regeneration required temperature in DW is about 80-85 °C, air temperature must be sufficiently high enough before entering the DW. Therefore, a heater is typically employed [14].

4.2. Des. B: DECS operating in recirculation cycle

To enhance the performance of the Pennington open cycle, some modifications were made to the cycle (Figure 6). In the recirculation cycle, the process air uses the space return air, while the fresh outdoor air is used as the recovery air. Based on the performance principles of the recirculation cycle, using part of the space return air as the supply air reduces the provided air quality, which is the main disadvantage of this design [13].

4.3. Des. C: DECS operating in Dunkle cycle

In this design proposed by Dunkle (Figure 6), a heat exchanger was added to the recirculation cycle to increase the cycle performance [15].

4.4. Des. D: DECS operating in modified ventilation cycle

Des. D is recommended for the applications, where the building's exhaust air is not suitable for the outdoor air co-processing [16]. In this cycle, the ambient air is used in the recovery stream instead of the building's return air (Figure 6). Therefore, the system Coefficient of Performance (COP) value normally is lower than the unmodified system [17].

4.5. Des. E: DECS operating in modified recirculation cycle with pre-cooling

In this design, as illustrated in Figure 6, an IEC was embedded in the cycle to increase the cooling capacity. The IEC cools

the air passing through, before entering the DW. In this process, the ambient air is used as the regeneration air [18].

4.6. Des. F: DECS operating in ventilation cycle equipped with double series EW

EW thermal efficiency has a significant impact on the performance of the ventilation cycle. In this design, an extra EW was added to the ventilation cycle to achieve a possible improvement in the cooling capacity of the system [13]. In this design, the supply air passes through the rotary DW, two EWs, and a DEC before entering the space (Figure 6).

4.7. Des. G: Two-stage DECS operating in ventilation cycle

Des. G was proposed by Sopian et al. [18] to enhance cooling capacity and performance of the desiccant system. This design employs two rotary DWs, two EWs, and a direct evaporator in the supply air stream. Besides, in the regeneration line, two EWs, two rotary DWs, and one DEC are used (Figure 6).

4.8. Des. H: Two-stage DECS operating in recirculation cycle

Sopian et al. [18] also proposed Des. H, as a modified version of Des (Figure 6). Adding part of exhaust air from the building to the supply stream and using the ambient air in the regeneration line are the two significant modifications in this cycle. Fig. 7 represents the simulated layout of Des. H.

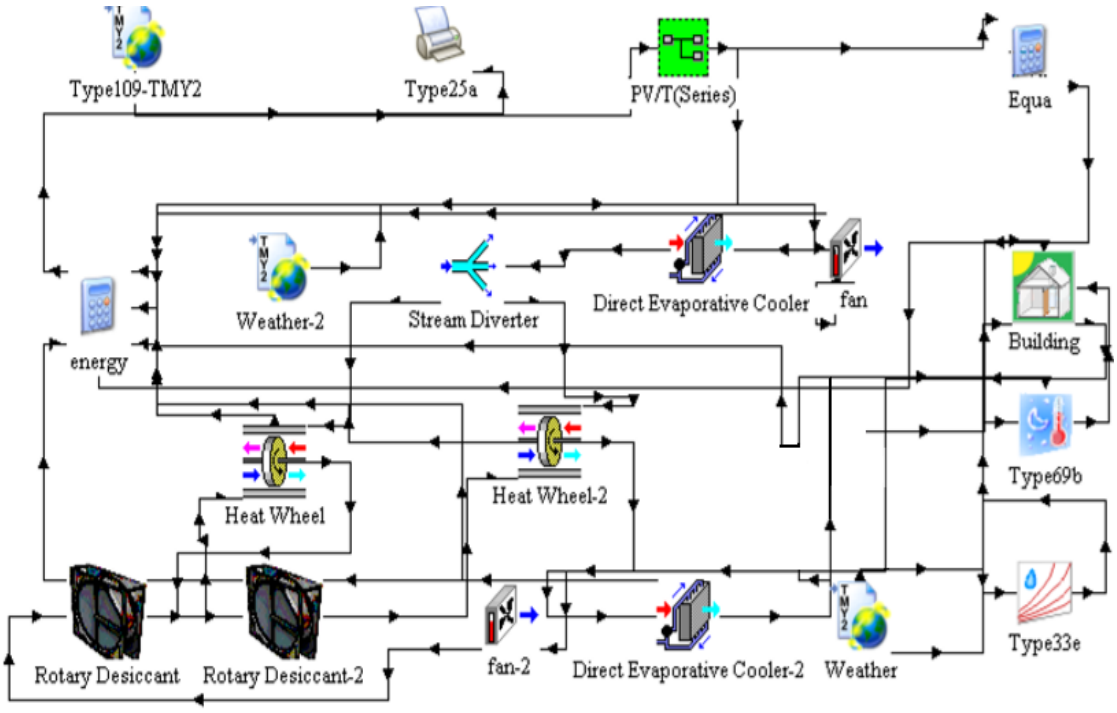

Figure 7. Simulation layout of Des. H in TRNSYS software

4.9. Building existing HVAC system

The existing HVAC system operating in the building is a simple compression cycle. Three Air Handling Units (AHU) with cooling capacities of 700, 1000, and 1300 were employed for the building. In order to simulate the AHUs in TRNSYS, the mathematical performance of the AHUs was extracted from the AHUs manuals. The mathematical equations were written in FORTRAN source codes and were added to the software library to be used as a user-defined component for the simulation process.

5. FEASIBILITY OF USING SOLAR ENERGY IN THE DECS

One of the most essential advantages of the DECS cycle is the possibility of using solar energy in the regeneration streamline. Therefore, in this study, the feasibility of providing thermal and electrical energy by the Photovoltaic Thermal collectors (PVT) was also explored. Prior to the feasibility study, the solar radiation potential of the region was evaluated. TMY data for the region were used for this purpose (Table 3). According to Table 3, the application of PVT panels is justified [19].

Table 3. Monthly mean and maximum solar radiation potential of Chabahar

Months	Mean. rad.	Max. rad.
	kjh/m^2	kjh/m^2
Jan.	2434.36	4109.01
Feb.	2845.16	4538.88
Mar.	3478.87	6148.55
Apr.	3800.72	7025.88
May	4308.42	7297.54
Jun.	4347.54	8386.38
Jul.	4101.90	8062.46
Aug.	3942.44	7659.19
Sep.	3627.56	6631.41
Oct.	3305.17	5163.19
Nov.	2818.02	4476.91
Dec.	2250.72	3928.05

Due to the space constraints on the building roof, the maximum number of 40 PVT panels can be installed. In addition, in order to install PVT panels, the latitude and longitude of the building site and the angle of the PVT panels need to be determined. It is clear that the optimum angle reduces the system waste and increases energy production. It was found that the optimum angle of the panels was about 27 degrees, as shown in Figure 8.

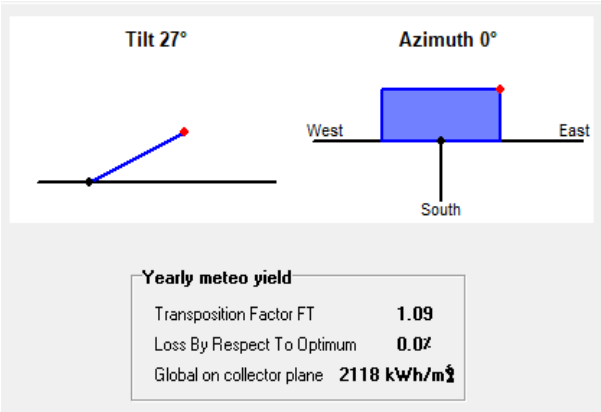

Figure 8. The optimum angle of the PVT panels

In order to optimize the arrangement of PVT panels, PVSYS software was employed. Based on the shadow tests conducted by the software, the sun has the most significant amount of radiation between 9:00 and 15:00 hours of a day; thus, the absence of shade on the panels is necessary at these hours. Therefore, the arrangement of the PVT panels in the four-row form was recommended. Figure 9 shows the arrangement of PVT panels on the CMUAB roof.

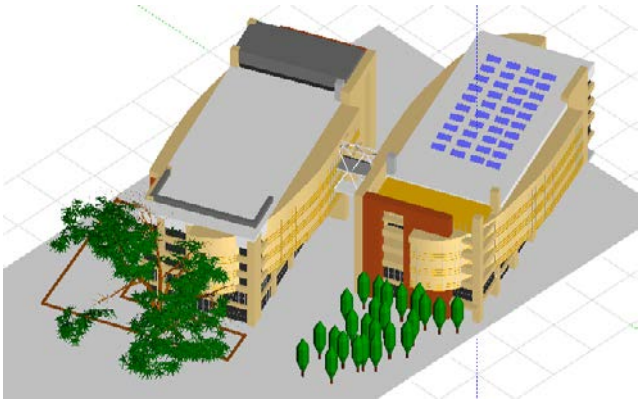

Figure 9. CMUAB with PVT panels

5.1. Solar collectors simulation results

As already mentioned above, one of the interesting characteristics of the DECS is the possibility of providing the desiccant required regeneration heat energy by renewable resources such as solar energy. In this section, the potential of airflow temperature being provided by different collectors, namely, G-BIPC, ETC, LPCC, PV-T, UTC, UAHC, and UBIP, was evaluated to determine the most desired collector for the application in DECS. To this end, the panels were considered in the two-row form to measure the temperature of the air passing through the panels. It should be noted that the air is driven through the panels by the fans. The study revealed that the panels are capable of providing the mean temperature values of 24.3 ℃ 44.41 ℃ 53.5 ℃ 41.3 ℃ 45.6 ℃ 43.1 ℃ and 42.4 ℃ for the air passing through for the G-BIPC, ETC, LPCC, PVT, UTC, UAHC, and UBIP panels, respectively (see Figure 10).

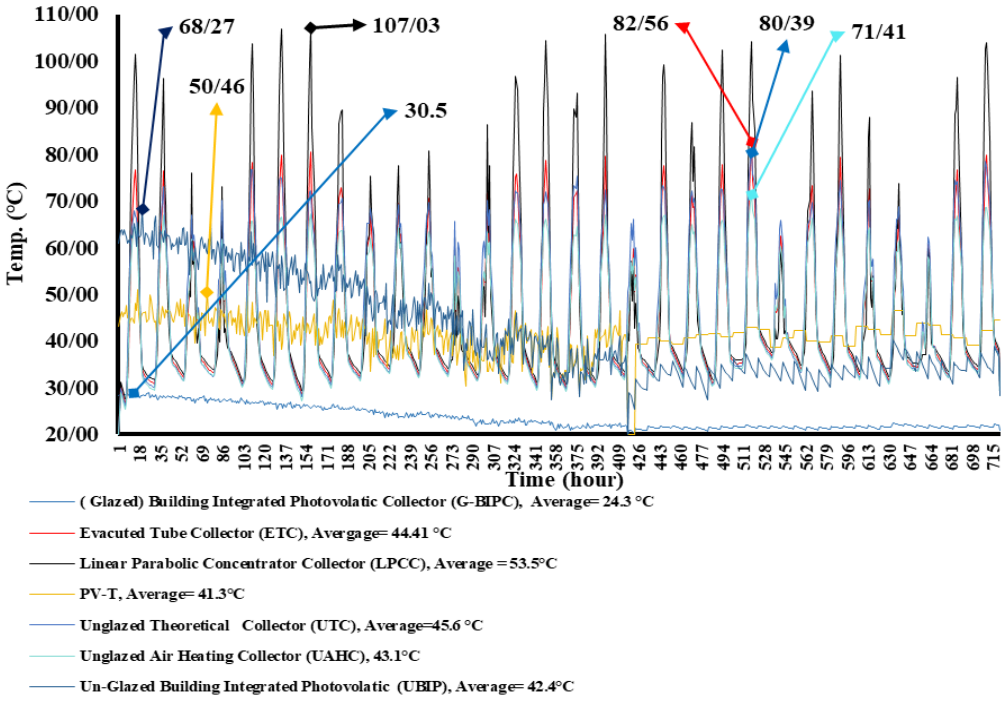

Figure 10. Airflow temperature provided by the solar panels

5.2. Photovoltaic thermal collectors (PVT)

Performance analysis indicates that for the present study, which is an energy-related case, the PVT panels are more desired than the solar thermal collectors, because PVT panels have the dual purpose of providing electrical energy by the PV cells and establishing a source of heat energy for possible low-grade temperature applications such as the DECS regeneration process.

This is achieved by the waste heat rejected into the air stream passing through the PVT panels, as illustrated in

Figure 11. In addition, heat rejection is useful for cooling the PV cells allowing higher power conversion efficiencies. Therefore, PVT panels are recommended for DECS application purposes in the present research.

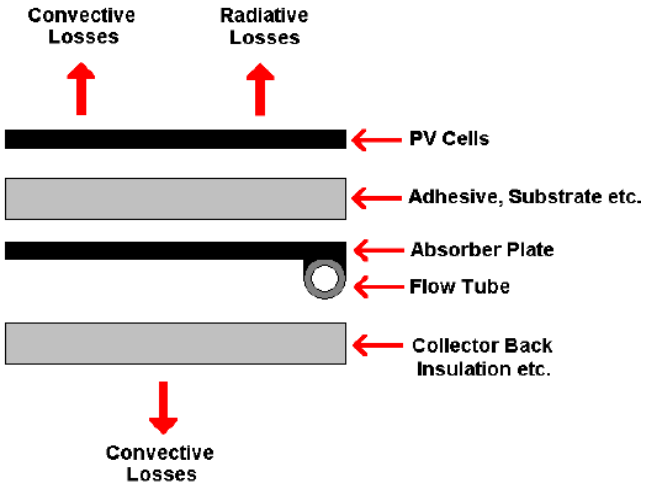

Figure 11. PVT panels layers

In order to define the PVT as a component in the TRNSYS library, the mathematical performance of the PVT panels was needed to be employed.

The efficiency of the PV cells is a function of the cell temperature and the incident solar radiation, as given by the following equation:

$$\eta_{PV} = \eta_{Nominal} \times X_{Cell.Temp} \times X_{Rad} \quad (1)$$

where:

$$X_{Cell.Temp} = 1 + Eff_T (T_{PV} - T_{ref}) \quad (2)$$

and

$$X_{Rad} = 1 + Eff_G (G_T - G_{ref}) \quad (3)$$

The collector's useful energy gain can now be calculated:

$$Q_u = \dot{m}C_P (T_{Fluid,out} - T_{Fluid,in}) \quad (4)$$

Moreover, the collector's useful energy gain per unit length can be calculated as:

$$Q' = Q'_{Fluid} = (\dot{m}C_P (T_{Fluid,out} - T_{Fluid,in}))/ LN_{tube} \quad (5)$$

The above mathematical performance equations were written using a FORTRAN source code to define the PVT as a component so that it can be used in TRNSYS studio.

6. SIMULATION RESULTS FOR THE BUILDING WITHOUT HVAC SYSTEM

In order to estimate the performance of the examined DECS on the building, the indoor air conditions without any cooling system (building without the HVAC system) need to be determined at the first phase of the study.

Then, possible improvements to the established indoor air conditions with the help of added DECS should be investigated. The simulation results of the indoor air conditions for the case of building without the HVAC system are tabulated in Table 4. In Table 4, the monthly meant indoor air temperature and RH are tabulated.

Table 4. Monthly mean indoor air temperature and indoor RH of the CMUAB (Building without HVAC)

Month	I.T. (°C)	I.RH (%)
Jan.	21.8	56.0
Feb.	22.7	57.3
Mar.	26.9	54.4
Apr.	28.3	48.0
May	33.3	41.2
Jun.	33.7	57.2
Jul.	33.9	68.1
Aug.	33.0	70.9
Sep.	32.1	66.7
Oct.	31.1	53.9
Nov.	26.8	57.1
Dec.	23.7	58.5

The simulation values were compared with the field measurements. The comparison shows less than 10 % deviation between the simulation results and fieldwork measurements. To determine the months in which the building requires the cooling load, the data tabulated in Table 4 were compared with the standard recommendations for thermal comfort, i.e.,.(20 °C-26.5 °C) and (45 %-65 %) [20]. These months were considered for further simulations by the DECS added to the building.

7. SIMULATION RESULTS OF THE BUILDING WITH THE ADDED DECS

7.1. Established indoor air conditions

Table 5 shows the mean indoor air and RH values established by the studied DECS designs added to the building. As explained above in the paper, the months which require cooling load were only considered for the simulations. For instance, as tabulated in Table 5, Des. A is only capable of providing standard indoor air conditions for March, April, May, June, and November. However, it does not have the potential to meet the standard indoor air conditions for July, August, September, and October. Figure 12 illustrates the established indoor air temperature in March until November (the months which require cooling load, Table 4) for the CMUAB without the HVAC system and CMUAB under Des. F to graphically compare the outcomes of adding Des. F as a representative of the configurations examined. However, for simplicity, all of the simulated values are tabulated in Table 5. The simulation indicated that Des. F is capable of providing mean values of 27.7 °C, 28.1 °C, 28.1 °C, and 27.5 °C for July, August, September, and October, respectively. The mean indoor air temperature at the working hours is also illustrated for a typical day in July by Des. F and Des. H in Figures 13 and 14, respectively, as the representative of the designs examined. According to the simulated values in Table 5, Des. G and Des. H have the capability to establish the desired indoor air conditions in the space in terms of indoor air temperature; however, Des. H has the potential to provide both of the temperature and RH values within the range recommended by the standards. Therefore, Des. H is the most

proper design and is recommended to be applied to the building. Des. H is capable of establishing the indoor air temperatures at 20.9 °C, 20.7 °C, 21.6 °C, 23.5 °C, 25.3 °C, 25.6 °C, 25.7 °C, 25 °C, and 23.8 °C in March, April, May, June, July, August, September, October, and November, respectively.

Table 5. Provided indoor air conditions by DECS designs (mean values)

Configs.		Months								
		Mar.	Apr.	May	Jun.	Jul.	Aug.	Sep.	Oct.	Nov.
Des. A	I.T. (°C)	22.8	22.3	23.5	25.6	27.5	27.9	27.9	27.2	26.0
	R.H. (%)	56.8	57.6	55.7	52.2	48.7	48.3	48.3	49.1	51.1
Des. B	I.T. (°C)	59.4	60.2	61.1	60.9	59.4	60.8	61.0	59.6	58.4
	R.H. (%)	23.2	22.5	24.2	26.6	29.0	29.6	29.7	28.8	27.0
Des. C	I.T. (°C)	64.8	65.9	66.2	65.2	64.0	65.2	65.5	64.4	63.5
	R.H. (%)	23.6	22.8	24.5	26.9	29.3	29.9	30.1	29.2	27.4
Des. D	I.T.(°C)	22.5	24.2	26.5	28.9	29.6	29.7	28.8	27.1	23.3
	R.H. (%)	59.4	60.2	61.1	60.7	59.2	60.5	60.7	59.4	58.3
Des. E	I.T. (°C)	22.4	21.8	23.4	25.8	28.1	28.7	28.9	27.9	26.2
	R.H. (%)	55.1	55.6	56.8	56.7	55.5	57.0	57.2	55.7	54.4
Des. F	I.T. (°C)	23.0	22.5	23.7	25.8	27.7	28.1	28.1	27.5	25.2
	R.H. (%)	59.0	59.9	58.0	54.5	51.1	50.7	50.7	51.5	53.5
Des. G	I.T. (°C)	24.7	20.2	21.1	23.1	25.0	25.4	25.4	23.4	20.4
	R.H. (%)	55.6	57.5	54.8	51.0	48.6	48.4	48.5	49.1	50.6
Des. H	I.T. (°C)	20.9	20.7	21.6	23.5	25.3	25.6	25.7	25.0	23.8
	R.H. (%)	58.7	59.0	57.6	53.8	50.4	50.1	50.1	51.0	52.8

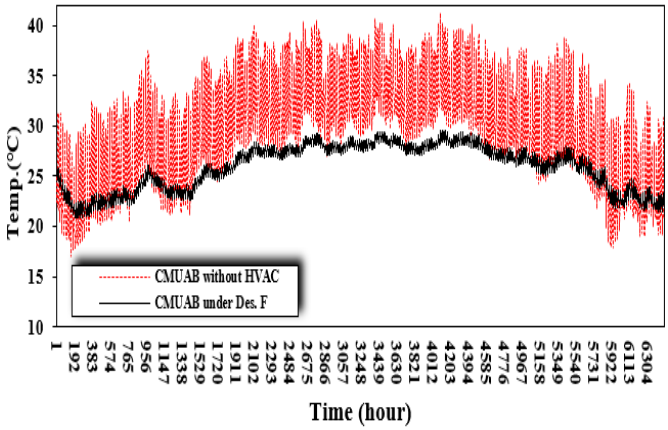

Figure 12. Hourly simulation responses of the existing space without DECS and existing space under Des. F in March untill November

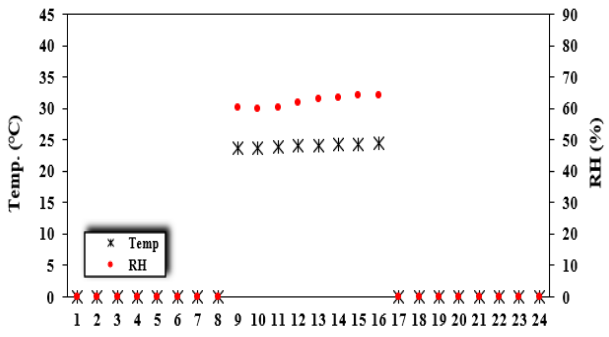

Figure 13. Hourly simulated indoor air conditions within eight working hours (8:00 am till 15:00 pm) for a typical day in July by Des. F

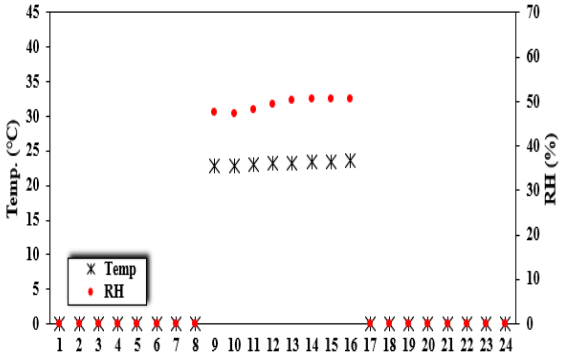

Figure 14. Hourly simulated indoor air conditions within eight working hours (8:00 am till 15:00 pm) for a typical day in July by Des. H

In Des. H, a fraction of indoor air (Bypass) is mixed with the fresh outdoor air and enters the first DW (latent wheel) unit which absorbs the moisture contents of the income air; therefore, the air temperature increases (temperature from 30.42 °C to 40.31 °C and humidity ratio from 0.02122 to 0.00963). Then, the DW leaving hot and dry air passes through the first EW unit (as the sensible heat transfer unit) to exchange heat with the regeneration line (temperature from 40.31 °C to 32.45 °C and humidity ratio remaining constant as 0.00963). In the next process, the air is further dehumidified by the second DW unit (temperature from 32.45 °C to 42.50 °C and humidity ratio from 0.00963 to 0.00835) and enters the second EW unit for the heat exchange with the return flow line (temperature from 42.50 °C to 33.43 °C and

humidity ratio remaining constant as 0.00835). The established air conditions by the units are outside the ASHRAE recommended standards scope; therefore, a DEC was employed before the building (temperature from 33.43 °C to 18.24 °C and humidity ratio of 0.00835 to 0.0112). The return flow line is divided into two branches and the return air passes through the same energy units. In order to provide a higher temperature gradient in the EW units, the air passes through the DEC first. In this line, thermal solar panels are planned to be used for reducing energy consumption. The Des. H air processes in the psychometric diagram are shown in Figure 15. Keeping the above mind, in Des. H, division of the air into two branches on the way back and the presence of bypass line have increased the design efficiency and improved the air quality of the indoor air compared to the other examined designs.

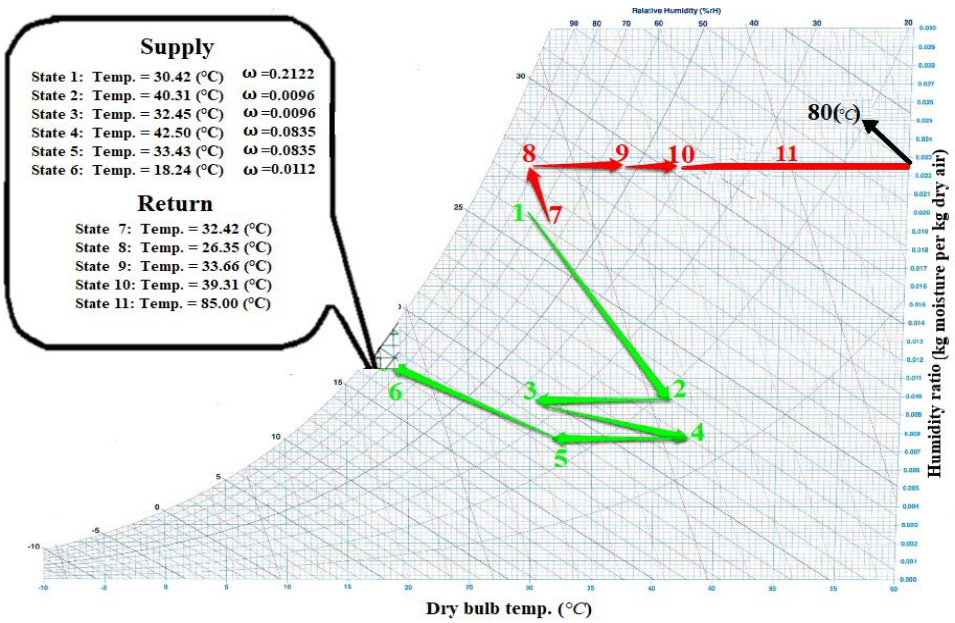

Figure 15. Air process under the Des. H in the psychometric diagram for typical July

7.2. COP analysis

As explained above, the Des. H has the most desired performance in terms of provided indoor air conditions. Therefore, the COP value for this design was also explored for the studied months of the year. The COP value is defined as the ratio of heat taken to the heat required. The heat taken is the amount of cooling load applied to the building by the supply streamline. Therefore, the COP value for Des. H as the two-stage DECS under the recirculation mode could be written as follows [5]:

$$COP = \dot{m}_s (h_1 - h_6) / \dot{m}_r (h_{12} - h_{11}) + \dot{m}_r (h_{15} - h_{14}) \quad (6)$$

The COP values for the Des. H in the studied months were determined, as shown in Table 6.

Table 6. The COP values for the Des. H

Months	COP value
Mar.	2.82
Apr.	1.42
May	1.36
Jun.	1.52
Jul.	1.62
Aug.	1.40
Sep.	1.50
Oct.	0.98
Nov.	1.98

The following equation is used to calculate the COP of other studied designs [5]:

$$COP = \Delta hs / \Delta h_r \quad (7)$$

The COP for the examined designs was determined for typical March, as the representative of the months of the year. As illustrated in Figure 16, Des. H has the highest COP value at 2.83.

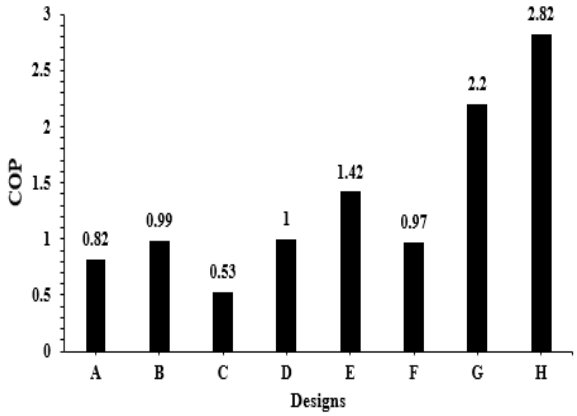

Figure 16. COP value for designs (A-H) for typical March

8. POWER CONSUMPTION BY Des. H

The power consumption of the building for the existing system, Des. H, and Des. H with the PVT is evaluated in this section. Figure 17 shows hour-by-hour power consumption by the Des. H for typical July. As illustrated in Figure 18, about 50.34 % savings in Des. H could be achieved by the application of PVT application.The study showed that the

application of Des. H, would ensure 26.97 % power saving per year, compared to the existing system. Moreover, it was proved that the yearly saving could be increased to about 68.03 % by adding PVT panels to Des. H.

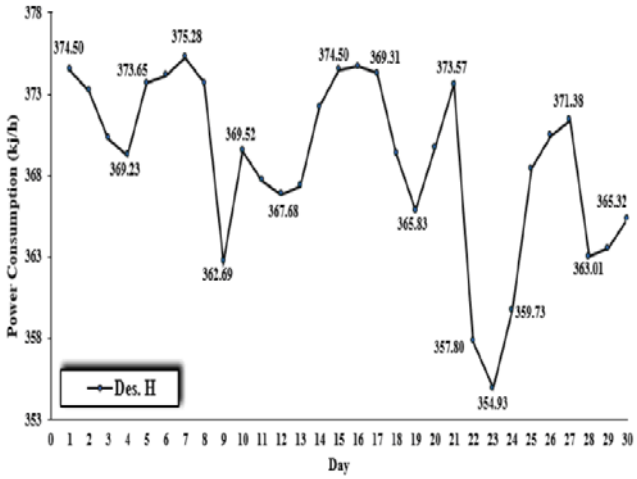

Figure 17. Hour-by-hour power consumption by Des. H for typical July

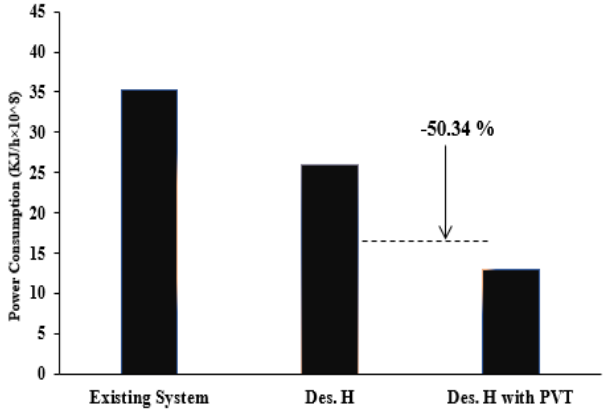

Figure 18. Power consumption by the existing system, Des. H and Des. H with the added PVT

9. CONCLUSIONS

The present study investigated the feasibility of solar-assisted DECS for buildings located in the high cooling load required region of Iran. To this end, the administration building in Chabahar Maritime University, Chabahar, Iran (CMUAB) was considered. In the first phase of the research, the CMUAB was simulated under the existing cooling system. Then, the feasibility of replacing the existing cooling system with solar DECS was explored. Eight different designs based on DECS were examined in terms of the provided indoor air conditions and energy performance to determine the most proper design for the building. The existing system and the building integrated with the DECS were studied for the whole year of operation. TRNSYS software was employed for this purpose, and the TMY weather data for the region were used as the input file for the program. Based on the simulation data, Des. H, as the two-stage DECS, had the potential to provide the required indoor air conditions for the studied months of the year. It was also found that Des. H had the highest COP value at 2.83 in March as the representative of the months examined.

The application of solar energy to the regeneration process in the Des. H was also explored. It was found that Des. H with and without the PVT had lower energy consumption than the existing ventilation system. It was also found that the application of Des. H ensured 26.97 % power saving per year, compared to the existing system. Moreover, it was shown that Des. H could reduce power consumption by about 68.03 % by adding the PVT panels.

10. ACKNOWLEDGEMENT

The authors would like to acknowledge the financial assistance from the Chabahar Maritime University, Iran to the authors to conduct the research.

NOMENCLATURE

C	Heat capacity (kj/s.k)
Cp	Specific heat (kJ/Kg.k)
d	Materials thickness (m)
Eff	Efficiency
FT	Transposition factor
G	Radiation (KJ/m^2.h)
h	Enthalpy
L	Collector tube length (m)
ṁ	Mass flow rate (Kg/h)
Q_U	Useful energy delivered by collector (Kj/h)
Q′	collector useful energy gain per unit length
$X_{Cell.Temp}$	Multiplier for the PV cell efficiency as a function of the cell temperature
X_{Rad}	Multiplier for the PV cell efficiency as a function of the incident radiation
Greek letters	
η	Efficiency
λ	Heat conductivity
ρ	Density of a Material
Δ	Gradient
ω	Absolute ratio
Subscripts	
Fluid,in	Inlet fluid (kg/h)
Fluid,out	Outlet fluid (kg/h)
Nominal	Refers to the reference conditions
r	Regeneration streamline
Rad	Sun radiation
ref	Reference ambient (°C)
s	Supply streamline
Abbreviations	
AHU	Air handling unit
Amb	Ambient
ASHRAE	American society of heating, refrigerating and air conditioning engineers
CMUAB	Chabahar maritime university administration building
COP	Coefficient of performance
DECS	Desiccant based evaporative cooling system
Des	Design
DW	Desiccant wheel
DEC	Direct evaporator cooler
Eva	Evaporator
ETC	Evacuated tube collector
EW	Energy wheel
G-BIPS	(Glazed) building integrated photovoltaic collector
HVAC	Heating, ventilation, and air conditioning
IEC	Indirect evaporative cooler
I.RH	Indoor relative humidity
I.T	Indoor temperature
LDCS	liquid desiccant cooling system
LPCC	Linear parabolic concentrator collector

N_{Tube}	Number of tube
PVT	Photovoltaic thermal collector
RH	Relative humidity
SDCS	Solid desiccant cooling system
Temp	Temperature
TMY	Typical meteorological year
TRNSYS	Transient system simulation software
UAHC	Unglazed air heating collector
UBIP	Un-glazed building integrated photovoltaic
UTC	Unglazed theoretical collector

REFERENCES

1. Karbassi, A.R., Abduli, M.A. and Mahin Abdollahzadeh, E., "Sustainability of energy production and use in Iran", ***Energy Policy***, Vol. 35, No. 10, (2007), 5171-5180. (https://doi.org/10.1016/j.enpol.2007.04.031).
2. Ghobadian, B., Najafi, G., Rahimi, H. and Yusaf, T.F., "Future of renewable energies in Iran", ***Renewable and Sustainable Energy Reviews***, Vol 13, No. 3, (2009), 689-695. (https://doi.org/10.1016/j.rser.2007.11.010).
3. Fadai, D., Shams Esfandabadi, Z.and Abbasi, A., "Analyzing the causes of non-development of renewable energy-related industries in Iran", ***Renewable and Sustainable Energy Reviews***, Vol. 15, No. 6, (2011), 2690-2695. (https://doi.org/10.1016/j.rser.2011.03.001).
4. Hosseini, S.E., Mohammadzadeh Andwari, A., Abdul Wahid, M. and Bagheri, G., "A Review on green energy potentials in Iran", ***Renewable and Sustainable Energy Reviews***, Vol. 27, (2013), 533-545. (https://doi.org/10.1016/j.rser.2013.07.015).
5. Li, H., Dai, Y.J., Köhler, M. and Wang, R.Z., "Simulation and parameter analysis of a two-stage desiccant cooling/heating system driven by solar air collectors", ***Energy Conversion and Management***, Vol. 67, (2013), 309-317. (https://doi.org/10.1016/j.enconman.2012.11.005).
6. Ge, T.S., Dai, Y.J. and Wang, Y.L., "Performance of two-stage rotary desiccant cooling system with different regeneration temperatures", ***Energy***, Vol. 80, (2015), 556-566. (https://doi.org/10.1016/j.energy.2014.12.010).
7. Enteria, N., Yoshino, H., Satake, A., Mochida, A., Takaki, R., Yoshie, R., Mitamura, T. and Baba, S., "Experimental heat and mass transfer of the separated and coupled rotating desiccant wheel and heat wheel", ***Experimental Thermal and Fluid Science***, Vol. 34, No. 5, (2010), 603-615. (https://doi.org/10.1016/j.expthermflusci.2009.12.001).
8. Liu, Y., Meng, D. and Sun, Y., "Feasible study on desiccant wheel with CO_2 heat pump", ***Proceedings of IOP Conference Series: Earth and Environmental Science***, Vol. 100, No. 1, (2017), 012209. (https://doi.org/10.1088/1755-1315/100/1/012209).
9. Preisler, A. and Brychta, M., "High potential of full year operation with solar driven desiccant evaporative cooling systems", ***Energy Procedia***, Vol. 30, (2012), 668-675. (https://doi.org/10.1016/j.egypro.2012.11.076).
10. Bourdoukan, P., Wurtz, E., Joubert, P. and Sperandio, M., "Potential of solar heat pipe vacuum collectors in the desiccant cooling process: Modelling and experimental results", ***Solar Energy***, Vol. 82, No. 12, (2008), 1209-1219. (https://doi.org/10.1016/j.solener.2008.06.003).
11. Ahmadzadehtalatapeh, M. and Khaki, S., "Application of phase change material (PCM) for cooling load reduction in lightweight and heavyweight buildings: Case study of a high cooling load region of Iran", ***Journal of Renewable Energy and Environment (JREE)***, Vol. 5, No. 2, (2018), 31-40. (https://doi.org/10.30501/jree.2018.88632).
12. Nie, J., Fang, L., Zhang, G., Sheng, Y., Kong, X., Zhang, Y. and Olesen, B.W., "Theoretical study on volatile organic compound removal and energy performance of a novel heat pump assisted solid desiccant cooling system", ***Building and Environment***, Vol. 85, (2015), 233-242. (https://doi.org/10.1016/j.buildenv.2014.11.034).
13. Ahmadzadehtalatapeh, M., "Solar assisted desiccant evaporative cooling system for office buildings in Iran: A yearly simulation model", ***Scientia Iranica***, Vol. 25, No. 1, (2018), 280-298. (https://doi.org/10.24200/SCI.2017.4323).
14. Ge, T.S., Li, Y., Wang, R.Z. and Dai, Y.J., "A review of the mathematical models for predicting rotary desiccant wheel", ***Renewable and Sustainable Energy Reviews***, Vol. 12, No. 6, (2008), 1485-1528. (https://doi.org/10.1016/j.rser.2007.01.012).
15. Pridasawas, W., "Solar-driven refrigeration systems with focus on the ejector cycle", Ph.D. Thesis, Royal Institute of Technology, KTH, Stockholm, (2006).
16. La, D., Dai, Y.J., Li, Y., Wang, R.Z. and Ge, T.S., "Technical development of rotary desiccant dehumidification and air conditioning: A review", ***Renewable and Sustainable Energy Reviews***, Vol. 14, No. 1, (2010), 130-147. (https://doi.org/10.1016/j.rser.2009.07.016).
17. Rafique, M.M., Gandhidasan, P., Rehman, S. and Al-Hadhrami, L.M., "A review on desiccant based evaporative cooling systems", ***Renewable and Sustainable Energy Reviews***, Vol. 45, (2015), 145-159. (https://doi.org/10.1016/j.rser.2015.01.051).
18. Sopian, K., Dezfouli, M.M.S., Mat, S. and Ruslan, M.H., "Solar assisted desiccant air conditioning system for hot and humid areas", ***International Journal of Environment and Sustainability***, Vol. 3, No. 1, (2014).(https://doi.org/10.24102/ijes.v3i1.447).
19. Keshavarz, S.A., Talebizadeh, P., Adalati, S., Mehrabian, M.A. and Abdolzadeh, M., "Optimal slope-angles to determine maximum solar energy gain for solar collectors used in Iran", ***International Journal of Renewable Energy Research***, Vol. 2, No. 4, (2012), 665-673. (https://ijrer.org/ijrer/index.php/ijrer/article/view/367).
20. ASHRAE, ASHRAE Standard 62.1-2016, Atlanta, USA, (2016).

Journal of Renewable Energy and Environment

Research Article

Journal Homepage: www.jree.ir

Feasibility Study of Using Renewable Energies in the Water and Wastewater Industry (Case Study: Tehran Water and Wastewater Company)

Ensieh Ozgoli[a], Younes Noorollahi[b*], Reza Arjmandi[a], Ali Mohammadi[a]

[a] *Department of Environment Management, Faculty of Natural Resources and Environment, Science and Research Branch, Islamic Azad University, P. O. Box: 1477893855, Tehran, Tehran, Iran.*
[b] *Department of Renewable Energy and Environmental Engineering, Faculty of New Sciences and Technologies, University of Tehran, Tehran, Tehran, Iran.*

PAPER INFO

Paper history:
Received 12 April 2020
Accepted in revised form 28 July 2020

Keywords:
Greenhouse Gases,
Prediction Model,
Electricity Consumption,
Renewable Energy,
Carbon Tax

ABSTRACT

Climate change refers to any significant and long-term alterations in global or regional weather conditions. The impact of climate change on the industrial plans is enormous, while the water supply sector has been challenged to examine how it could continuously operate in the current situation. Optimization of energy consumption and reduction of Greenhouse Gases (GHG) emissions are some of the priorities of water companies. The objective of the study is to propose a novel evaluation approach to the feasibility of using renewable energies (solar, wind, and biomass) in the water and wastewater industry. Tehran Water and Wastewater Company consists of six regional districts and forecasting of its energy consumption, power costs, and carbon tax rates for the next ten years was done by using the regression model. The results indicated that increase in water supply and electricity consumption was evidenced by the increase in Tehran's annual population. GHG emissions were calculated in two scenarios, the first of which is based on the total supply of required electricity from conventional power plants and the second is on the generation of approximately one-third by renewable energies. In addition to the higher emissions of carbon dioxide (CO_2) from diesel and oil power plants than the natural gas-fueled plants, by increasing the carbon tax to more than 30 USD per tonne of CO_2, it is expected that the emissions will be reduced by 30 % in all fossil-fueled power plant types. Results showed that a small amount of tax was not effective in reducing GHG emissions.

https://doi.org/10.30501/jree.2020.226666.1099

1. INTRODUCTION

Renewable energy sources that meet domestic energy needs are capable of delivering zero or near-zero emissions of air pollutants and GHG. The development of a renewable energy system enables it to solve the most important tasks of today such as improving the reliability of energy consumption and organic fuel economy, solving local energy and water supply problems, enhancing the living and working conditions of local people, and ensuring sustainable development. Remote areas in the desert and mountainous areas may require countries' commitments to international agreements on environmental protection [1]. Developing and implementing a renewable energy project in rural areas can create job opportunities and thus, minimize migration to urban areas [2]. Decentralized Renewable Energy Harvesting is one of the options to meet rural and small energy needs in a reliable, cost-effective, and environmentally sustainable manner [3, 4]. Renewable energy technologies are considered as clean and sustainable sources of energy for current and future economic and social needs. The optimal use of these resources could minimize environmental impacts and secondary waste [5]. Today, one of the most critical environmental problems globally that needs drastic action is the necessity of optimizing the production of energy using different types of renewable sources and, at the same time, reducing GHG emission. Widespread and persistent use of fossil fuels has turned carbon dioxide (CO_2) into the largest contributor of GHG emissions [6, 7]. Many economists [8] have long used carbon pricing as an efficient tool to reduce CO_2 emissions. A growing number of jurisdictions around the world are using this tool as an Emissions Trading System (ETS). Carbon pricing is an important policy tool for achieving cost-effective decarburization. The European Union has adopted the ETS as a key pillar of its policy mix to achieve short-term and long-term goals of GHG emissions [9].

In recent decades, increasing water usage for industrial, agricultural, and domestic needs and strictly enforcing water quality regulation have significantly increased water purification and transmission. Besides, a high volume of water usage in the agricultural sector is due to the intensified cultivation and expansion of irrigated farms to fulfill the increasing demand for food and biomass fuel supplies. These activities generally require a large amount of energy and lead to increased energy consumption in the water sector in many parts of the world, which finally influenced the GHG emissions [10, 11, 12, and 13]. In countries with very high

*Corresponding Author's Email: noorollahi@ut.ac.ir (Y. Noorollahi)
URL: http://www.jree.ir/article_111081.html

Please cite this article as: Ozgoli, E., Noorollahi, Y., Arjmandi, R. and Mohammadi, A., "Feasibility study of using renewable energies in the water and wastewater industry (Case study: Tehran water and wastewater company)", ***Journal of Renewable Energy and Environment (JREE)***, Vol. 7, No. 4, (2020), 21-29. (https://doi.org/10.30501/jree.2020.226666.1099).

freshwater harvesting, most of the total available water is used for irrigation, and the energy used in abstraction and transmission is often significant. Estimates for India indicate that GHG emissions to raise irrigation water could account for 6 % of the country's total emissions. In the US, agriculture is the largest consumer of electricity and water [13]. Due to the decreasing measures required to deal with climate change, the water sector has been challenged to examine how it currently operates. Energy efficiency optimization and GHG emission limitations are those that are a priority for water companies [14]. In Iran, one of the environmental issues is the rapid release of carbon. Since 1980, carbon emissions in Iran have increased by almost 450 %, from 33.1 million tons in 1980 to 146.8 million tons in 2008 [15]. Controlling growth and possibly reducing GHG emissions are important for not only the countries themselves but also the international community in pursuit of climate change strategies. According to 2008 statistics, Iran is ranked eighth in the world in GHG emissions. Further, a worrying factor is the growth rate of GHG emissions in the country, which has increased by 45 % in a decade with an increase in CO_2 emissions per capita from 4.78 ml in 1997 to 6.92 ml in 2007. This demonstrates the importance of Iran taking serious steps to control GHG emissions [16].

Raghuvanshi et al. [17] concluded that CO_2 emission as a combustion product of coal (fossil fuels) was responsible for over 60 % of the greenhouse effect. Yan et al. [18] also concluded that nearly 40 % of all CO_2 emissions in China came from the electricity sector. The reason is that China relies heavily on thermal power generation to meet its energy needs. Zhang et al. [19] also found that electricity production efficiency played an important role in reducing CO_2 emissions. Zhang et al. [19] concluded that coal products were the main fuel types of thermal energy generation, accounting for over 90 % of CO_2 from electricity generation.

Guo et al. [20] reviewed the available green energy and biomass energy that could be applied to wastewater treatment plants. Using renewable energy sources in these plants such as solar, wind, and biomass energy in different technologies has been summarized in their study. Moreover, several successful experiences of related companies have been obtained in this way. Also, advanced energy-efficient technologies for wastewater treatment were discussed and some control and management systems were proposed in that research.

Solar energy, which is considered the most abundant renewable energy source, can be introduced to water and wastewater companies. The application of solar thermal energy to this industries mainly includes three aspects: (a) the solar heat is collected through a heat collector to increase the reaction temperature and improve the treatment efficiency [21]; (b) the solar thermal is used to dewater the sludge or reduce the water content of some special wastewater in industrial wastewater treatment [22], and (c) the solar heat can be used for evaporation and desalination of special wastewater in industrial wastewater treatment.

Some researchers have suggested that photovoltaic power generation that provides electricity for sewage biological treatment could reduce the energy consumption of sewage treatment plants [23]. The power generated from a photovoltaic power station can satisfy the needs of a water treatment plant, which is in line with the "self-sufficiency" mode [24]. The electricity consumption takes up more than 30 % of production costs; therefore, cost reduction and efficient treatment are required intensively [25]. Han et al. applied solar power to drive the oxidation ditch without the battery, and the solar power system automatically started and stopped depending on the change in light intensity [26].

In previous researches, the issues of electricity consumption and the type of fuel consumed in the water and sewage industry have not been addressed. Thus, the purpose of the present study is to predict the GHG emissions over the next ten years and the effect of the carbon tax on the amount of GHG emitted by Tehran Water and Wastewater Company. It is also worth highlighting that the novelty of the proposed research is about the use of the predictive model to calculate the amount of electricity consumed and the carbon tax needed resulting from the usage of fossil fuels and renewable energy by Tehran Water and Wastewater Company.

2. MODELING APPROACH

2.1. Study area

Tehran is located at the center of Tehran province with an area of about 1.5 km2 and the respective latitude and longitude of 35°41′39″ N and 51°25′17″ E. The province is bordered by Mazandaran province to the north, Qom province to the south, Markazi province to the southwest, Alborz province to the west, and Semnan province to the east. According to the 1395 census (2016), the population of this province was 13,267,637, of which 12,452,230 lived in urban areas and 814,698 in rural areas [27]. Iran is one of the richest countries in the world in terms of various energy resources since it enjoys extensive resources of fossil fuels, such as petroleum and natural gas, and possessing high potentials of renewable energies, such as solar. Tehran is located on the sunbelt of the world with an insulation level of more than 5 kWh/m^2. Therefore, the country has good potential for using solar energy. The calculations show that the amount of practical solar radiation hours exceeds 2800 hours per year [28]. Therefore, due to the remarkable surface areas in different branches in Tehran, the application of this significant potential by the water and wastewater company can be a beneficial approach to generating some proportions of the electrical energy required by the country. Tehran is also the capital of Iran. The water and sewer companies of the six districts of Tehran including District 1, District 2, District 3, District 4, District 5, and District 6 within the districts of Tehran.

2.2. Forecasting model

This study applied predictive modeling has been used based on mathematical and computational methods to predict principal factors in energy consumption of the Tehran Water and Wastewater Company. Hence, a mathematical approach was used in the form of an equation-based model that described the pertained phenomenon considering all important characteristics of the company and its application. General Linear Methods (GLMs) include different techniques used in prediction issues. The most popular methods are Linear Regressor (LR), Lasso Regressor (Lasso), Ridge Regressor (Ridge), and Elastic Net Regressor (ElasticNet).

Linear regression provides the simplest and most widely used statistical model for predictive modeling. It is a linear model approach between response variables with one or more descriptive variables. In this case, it is assumed that one or more descriptive variables whose value is independent of the other variables or under the researcher's control can be effective in predicting the response variable whose value is

not dependent on the descriptive variables under the researcher's control. The purpose of regression analysis is to identify the linear model of this relationship. The dependent variable rather than the response variable and the independent variable rather than the descriptive variable are used. The form of the simple linear regression model is as follows [29]:

$$Y \approx \beta_0 + \beta_1 X \quad (1)$$

The parameters of this linear model include intercept (β_0) and slope of line (β_1). They are known as the model coefficients or parameters. Moreover, in training data, $\hat{\beta}_0$ and $\hat{\beta}_1$ are used to predict the model coefficients.

$$\hat{y} = \hat{\beta}_0 + \hat{\beta}_1 x \quad (2)$$

In Eq. (2), $\hat{y}$ shows a prediction of Y based on X = x. This symbol is used to indicate the estimated value of an unknown parameter or coefficient. It might be applied to signify the forecast value of the response. Since β_0 and β_1 are unknown, the estimation of coefficients by the data should be performed, as shown in Eq. (3).

$$(x_1, y_1), (x_2, y_2), \ldots, (x_n, y_n) \quad (3)$$

For making a linear model, available data will be used as in the following relation:

$$\hat{y}_i = \hat{\beta}_0 + \hat{\beta}_1 x_i \text{ for } i = 1 \ldots n \quad (4)$$

The above equation is used to make forecasting for Y based on the i^{th} value of X and $e_i = y_i - \hat{y}_i$ represents the ith residual, which is forecasted by this linear model. Then, the residual sum of squares (RSS) can be defined as Eq. (5):

$$RSS = e_1^2 + e_2^2 + \ldots + e_n^2 \quad (5)$$

The least-squares method chooses $\hat{\beta}_0$ and $\hat{\beta}_1$ for minimizing the RSS. Therefore, Eq. (6) and Eq. (7) minimizers will be obtained [30].

$$\hat{\beta}_1 = \frac{\sum_{i=1}^{n}(x_i - \bar{x})(y_i - \bar{y})}{\sum_{i=1}^{n}(x_i - \bar{x})^2} \quad (6)$$

$$\hat{\beta}_0 = \bar{y} - \hat{\beta}_1 \bar{x} \quad (7)$$

where $\bar{y} \equiv \frac{1}{n}\sum_{i=1}^{n} y_i$ and $\bar{x} \equiv \frac{1}{n}\sum_{i=1}^{n} x_i$ are the sample means. Eqs. (6, 7) represent least-squares coefficient estimates for general linear regression.

Furthermore, the slope of the line, generally linear regression, shows how sensitive the dependent variable is to the independent variable. That is, the value of the dependent variable changes by increasing one unit to the value of the independent variable. The width of the source represents the value of the dependent variable which is calculated as zero for the value of the independent variable. Alternatively, the constant value or the width of the source can be considered as the mean of the dependent variable for the independent variable [30].

In the present study, the independent variables are renewable energy potentials (solar, wind, and biomass), population rate, water consumption rate, current electricity consumption, and GHG emission values by using conventional power generators and current electricity prices. On the other hand, dependent variables including electricity consumption, renewables proportion, carbon tax, and electricity cost are predicted. Objective functions are aimed at forecasting energy consumption (in two scenarios), greenhouse gas emissions rate, and electricity cost.

3. RESULTS AND DISCUSSION

3.1. Forecasting energy consumption

Electricity consumption data of the six districts of Tehran Water and Wastewater Company from 2016 to 2019 were collected. Then, the prediction of electricity consumption for the year 2030 was made. Figure 1 shows the electricity consumption in Districts 1 to 6 of Tehran Water and Wastewater Company from 2016 to 2030 based on a million kWh. According to this chart, the total electricity consumption of the six districts of Tehran Water and Wastewater Company is increasing. The minimum and maximum values were calculated for District 5 (by 49.6 million kWh) and District 2 (by 123.8 million kWh), respectively, while different upward trends of Districts 2 and 5 were quite clear in this graph, directly depending on the rate of population rise for these reasons. Besides, Figure 2 indicates the graph of Tehran's total electricity consumption prediction up to 2030. This chart shows the sum of the lowest and highest amounts of the mentioned six districts of Tehran's electricity consumption predicted by 2030.

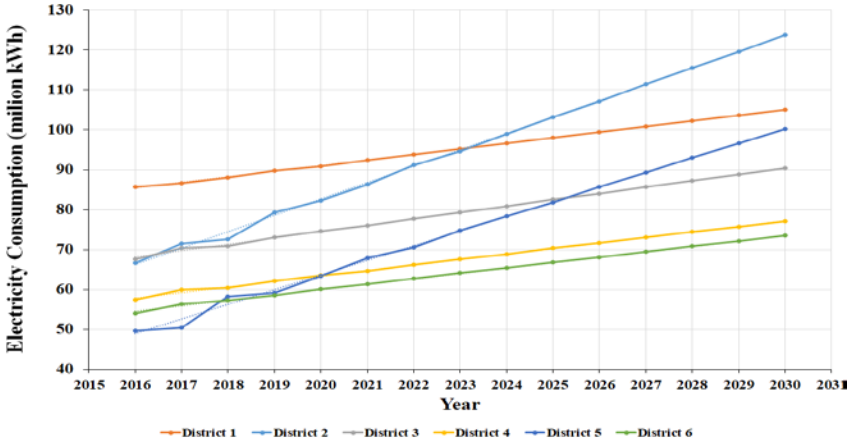

Figure 1. Current and expected values of electricity consumption in different districts of the Tehran Water and Wastewater Company

According to Figure 1, the slope of all graphs is positive. The coefficient of determination for all of the six districts is approximately 100 % except District 2 (which is 97 %). Therefore, it can be concluded that about 100 % of the changes in the dependent variable are explained by the independent variable. In these figures, the independent and dependent variables are time and amount of electricity consumption in Districts 1 to 6 of Tehran Water and Wastewater Company, respectively.

The electricity consumption rise can be described by the increase in Tehran's annual population and, consequently, it would cause a significant increase in the potable water supply of all districts of Tehran.

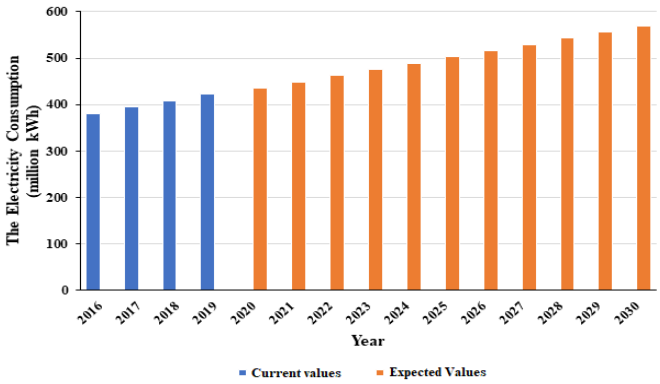

Figure 2. Current and expected total electricity consumption values of Tehran Water and Wastewater Company

3.2. Predicting energy consumption by using renewable energy

Table 1 shows the emission levels of GHGs and pollutants in power plants in grams per kWh. According to this table, the amount of pollutants emitted from diesel-fired power plants is higher than oil and natural gas-fired power plants. Also, although natural gas-fueled power plants have lower emissions than other types, the amounts of CH_4 and CO_2 emissions are still considerably high. It is important to highlight that the main objective of this study is to substitute the use of fossil fuel with renewable energies for electricity generation. Thus, it has been assumed that fossil fuel consumption was reduced by 30 % and replaced with renewable energies. As a result, GHG emissions would be declined. There are 72 water storages at different locations of Tehran under operation that provide an approximate volume of 2,065,000 m^3, and generating electricity from solar energy is possible by installing photovoltaic systems on their rooftops. Figure 3 shows a sample water storage tank covered by solar photovoltaic panels by a Spanish company [31]. Figure 4 shows the amount of electricity consumed by Tehran Water and Wastewater Company by 2030 (with 30 % renewable energy).

Table 1. Greenhouse gases emissions from power plants (gr/kWh) [32]

Type of power plant fuels	SO_2	N_2O	CH_4	CO_2
Natural gas	4×10^{-6}	0.4	17.99	201.8
Diesel	926×10^{-3}	2.2	35.97	266.5
Fuel oil (mazut)	508×10^{-3}	2.2	35.97	278.42

Figure 3. A water storage tank covered by solar photovoltaic panels [31]

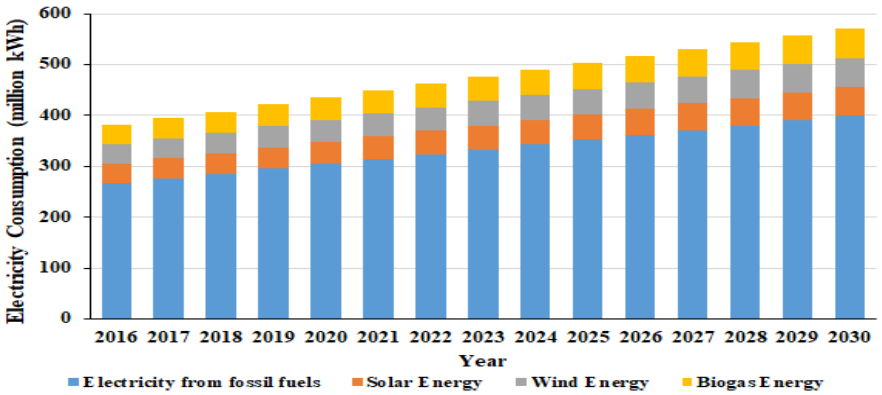

Figure 4. Electricity consumption prediction of Tehran Water and Wastewater Company by 2030 (Considering 30 % renewable energy)

Figure 5 shows the amount of CO_2 as the main GHG emitted from different types of fossils fuel power plants of Tehran Water and Wastewater Company by 2030 in thousand tons per kWh (with 30 % renewable energy). Two scenarios were designed to calculate GHG emissions. In the first scenario, the total electricity of the Water and Wastewater Company will be supplied by fossil fuel power plants by 2030 and, in the second scenario, 30 % of fossil energy will be replaced by renewable energy sources (solar, biomass, and wind power). This figure also compares the amount of GHG (CO_2) emitted in the two scenarios presented. As shows, CO_2 emission from oil fuel power plants is much higher than other types, and after the reduction of 30 % of fossil fuels, the CO_2 emissions from natural gas power plants have the lowest CO_2 emissions through all of the considered fossil power plants. Furthermore, it depicts the amount of GHG (CH_4) emitted from fossil-fueled power plants in Tehran Province to generate the required electricity of the Water and Wastewater Company by 2030 (with 30 % renewable energy). Moreover, Figure 5 indicates the amount of methane emission in both presented scenarios.

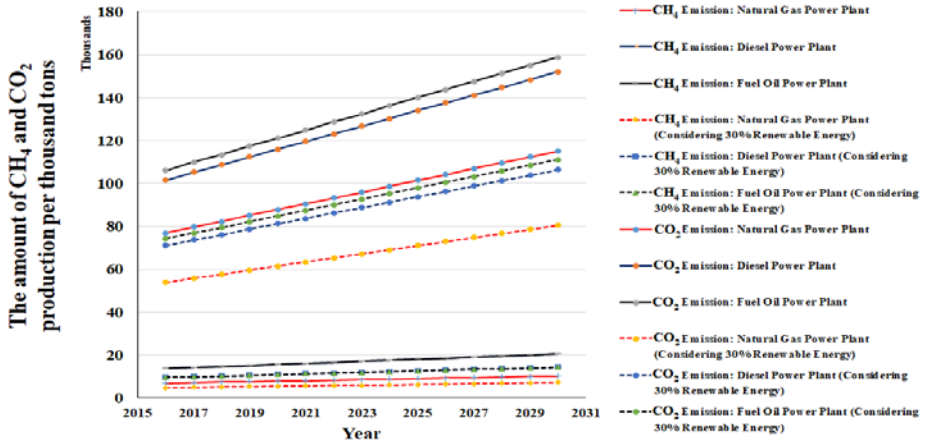

Figure 5. Comparing the amount of GHGs (CH_4 and CO_2) emitted in the two scenarios presented

Results also show that the emitted CO_2 from natural gas, diesel, and fuel oil-based power plants in 2030 is about 115,000, 152,000, and 158,000 tones, respectively, without using renewable energies. By generating one-third of the electricity demand in the case study from renewable energy sources, CO_2 emission will be reduced up to 30 % annually in the considered period. It is approximately the same for all fossil-fueled power plant types.

Figure 6 shows the amount of another principal GHG, N_2O, emitted from Tehran's Water and Wastewater equivalent fossil-fueled power plants by 2030 (with 30 % renewable energy). In addition, this figure compares the amount of N_2O emitted in the two presented scenarios. According to the presented figure, N_2O emission from the fuel oil power plants is higher than that of plants that use natural gas. Moreover, it shows the amount of emitted sulfur dioxide by Tehran Province Water and Wastewater Company equivalent fossil-fueled power plants by 2030 (with 30 % renewable energy). As Figure 6 shows, the amount of sulfur dioxide from diesel fuel plants is higher than that in other plants. Moreover, this figure demonstrates the difference in the amount of sulfur dioxide emitted between the use of renewable energy and the non-use of renewable energy.

By comparing the results of the proposed scenarios, it is perceptible that pollutant emissions from diesel-fueled power plants are higher than those from other types of plants (SO_2 emission of diesel-fueled power plants is approximately two times more than fuel oil plant, while other pollutants value are almost the same). Moreover, the significant CO_2 and methane emissions of the natural gas-fueled power plants are not comparable with renewable power plants. Thus, by replacing 30 % of fossil fuels with renewable energies, natural gas plants have the lowest GHG emissions among other plants. Additionally, the mentioned results are significantly comparable to previous studies reviewed in the introduction section [17-19]. It should be emphasized that the substitution of conventional power plants with renewable energy generators in the mentioned company causes a considerable reduction in GHG emission through time, as shown in Figures 5 and 6.

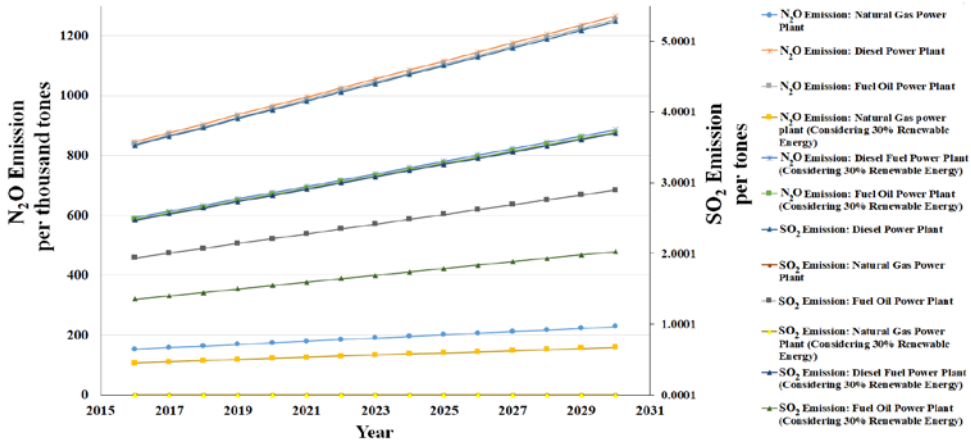

Figure 6. Comparing the amount of GHGs (N_2O and SO_2) emitted in the two scenarios presented

CO_2 emissions due to the fossil fuel consumption of Iran in 2016 were approximately 642,560,030 tons, an increase of about 2.22 % annually, while the global proportion of Iran's CO_2 emission was almost 1.8 % [33]. Due to the lack of recorded carbon tax for Iran, taxes were compared with other countries based on the share of GHG emissions in each state from different regions of the world and the position of Iran in global CO_2 emission. Based on the published data, Iran has almost 1.8 % of the world's CO_2 emission. Therefore, the Iranian tax should be equal to Australia because of the approximately equal share of these countries in the field of CO_2 emission. The tax rate for each tone of CO_2 is USD 10 [34]. Figure 7 shows the predicted carbon tax rate in million USD.

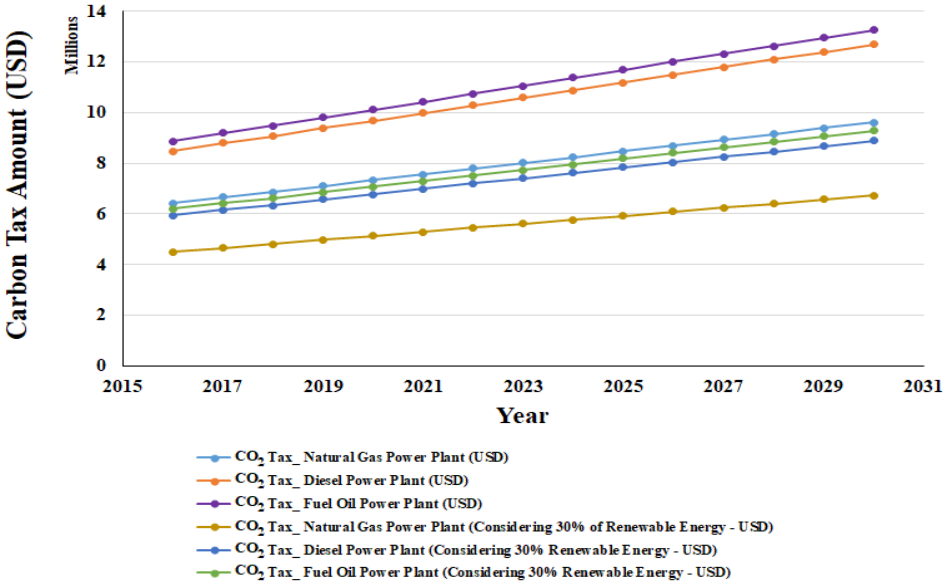

Figure 7. The carbon tax rate in USD from 2016 to 2030

Mardones and Flores [35] concluded that a tax of up to 10 USD per ton of CO_2 did not significantly change the use of fuel in industrial sources in Chile. However, if the tax is between 10 and 30 USD per ton of CO_2, then GHG emissions will decline rapidly due to the social and economic impacts. Furthermore, by increasing this tax to more than 30 USD per ton of CO_2, it is expected that the emissions will be reduced. Therefore, it should be noted that a small amount of tax (almost one-third of the planned value) does not have a significant effect on reducing GHG emissions.

Figure 8 illustrates the consumed electricity cost in the six districts of Tehran Water and Wastewater Company in million USD, and Figure 9 presents the cost of electricity consumption in the two proposed scenarios. Based on the results obtained, by replacing 30 % of the fossil fuel used by Tehran Water and Wastewater Company with renewable energies, 5,987,086.482 USD would be saved during the years 2016 to 2030. Therefore, the use of renewable energy in the water and wastewater industry could enhance the domestic economy as well as reduce GHG emissions.

It should be stressed that carbon tax has had a significant effect on reducing energy consumption in modern countries. The main outcomes of these rules are the substantial progress of energy management, energy efficiency, and the distribution of renewable energies. This issue has been emphasized in various scientific publications and on energy statistic websites [33, 34]. Therefore, legislating carbon tax on polluting industries of Iran (such as Water and Wastewater Companies) will create a greater tendency to establish energy conservation methods, particularly using such renewable energies as the green electricity generators.

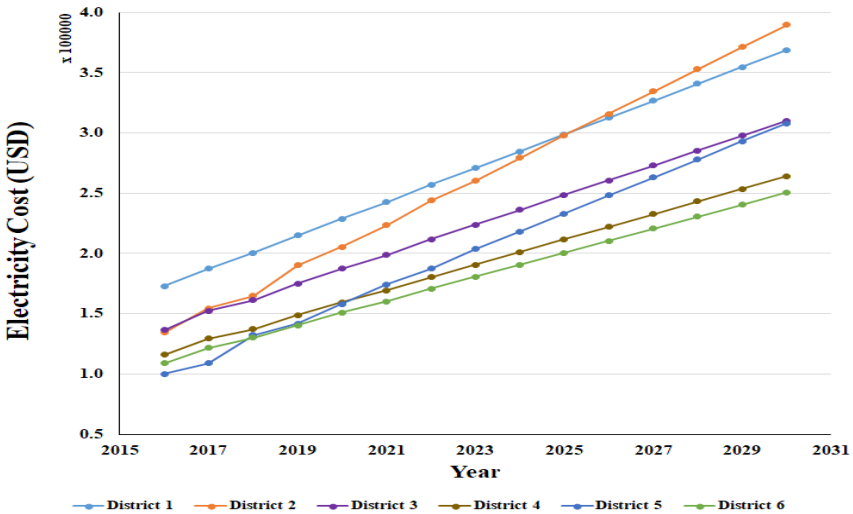

Figure 8. The electricity cost in six districts of the Water and Wastewater Organization

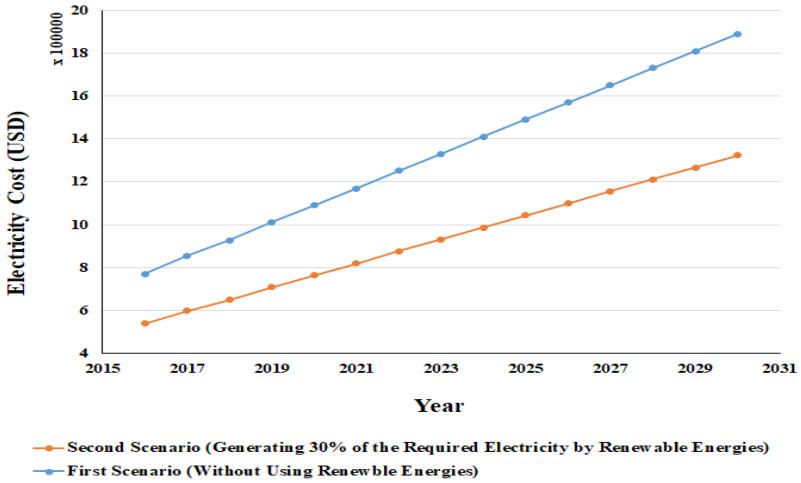

Figure 9. The electricity cost of the two proposed scenarios

Figure 10 shows the electricity cost of the proposed scenarios considering the effect of the carbon tax, while Figure 11 indicates the difference between the two graphs on fossil energy use without renewable energy and fossil energy use with 30 % renewable energy (cost in millions of USD).

It should also be pointed out that the economic benefits of using a proportion of the alternative energies in the mentioned case study will increase over time, based on Figure 11.

Besides, Districts 2 and 5 have the highest priorities for energy consumption management in the case study due to the predicted rates of demand for water supply and, consequently, infrastructure development in these two districts of the company. Therefore, the substitution of conventional electricity generation with renewable energy generators should be started from these two districts to control the power costs of the company efficiently.

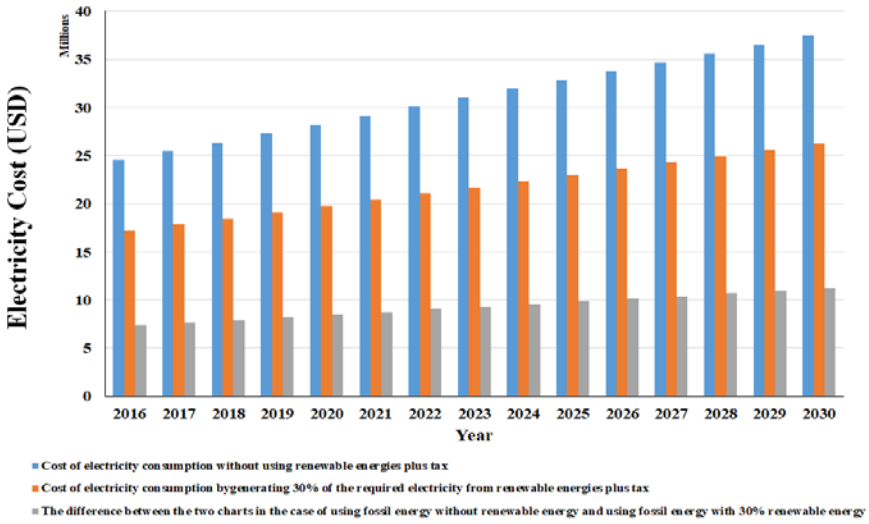

Figure 10. The electricity cost of the proposed scenarios considering the effect of the carbon tax

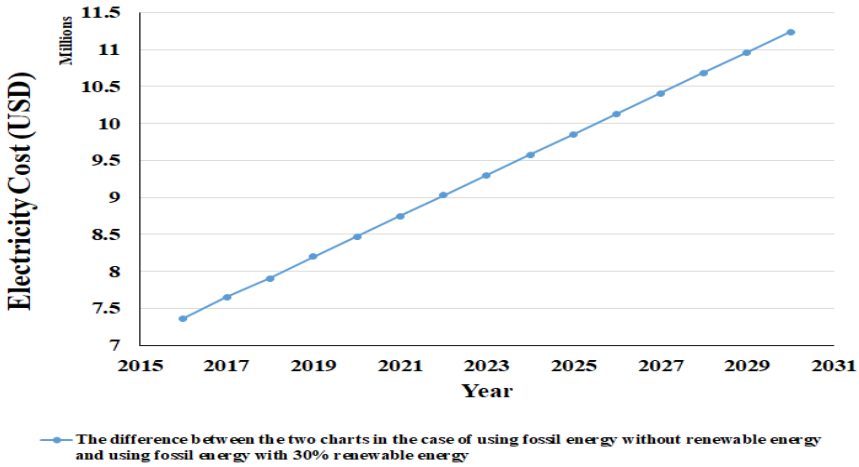

Figure 11. The difference between the two graphs on fossil energy use without renewable energy and fossil energy use with 30 % renewable energy (cost in millions of USD)

4. CONCLUSIONS

A comprehensive approach was mentioned in this study due to the current crisis in the field of high energy consumption to supply potable water and also sewage collection in urban applications. A significant potential to produce electricity from renewable energy sources is available in Tehran. For this reason, using some principal types of alternative energies such as solar, wind, and biomass can be specifically beneficial for the mentioned case study in this research. Urban water supply energy management is constrained by the attributes and realities of each city. In the presented research, the effective factors of energy consumption in Tehran Water and Wastewater Company were demonstrated. Moreover, a novel approach was proposed to predict the effect of renewable energy utilization in this sector on air pollution reduction.

Regarding the results, electricity consumption in the six districts of Tehran Water and Wastewater Company is a relatively straightforward trend, up to 2030. Therefore, the implementation of renewable energy and advanced technology was proposed for GHG mitigation potential in the power sectors. The presented approach offered sustainable potential of renewable energy technologies including solar, wind, and biomass power plants with carbon tax strategies. CO_2 emission will be decreased by about 30 % by replacing the conventional power plants with renewable energy plants based on the Tehran Water and Wastewater Company electricity demand.

Based on global warming issues, carbon tax which is one of the effective tools that a government imposes on any company that burns fossil fuels should be considered. For this reason, most debates are centered on oil, diesel, and natural gas-based power plants. The results showed that if carbon tax legislation contains tax imposition between 10 and 30 USD per ton of CO_2, an immediate reduction of greenhouse gas emissions will be predictable. Besides, by increasing carbon tax more than 30 USD per ton of CO_2, a significant decrease in air pollution of power generators will be expectable. Eventually, considering a fair amount of carbon tax is suggested to reduce GHG emissions due to energy consumption in water and wastewater companies.

5. ACKNOWLEDGEMENT

We thank our colleagues who provided insight and expertise that greatly assisted the research.

REFERENCES

1. Zakhidov, R.A., "Central Asian countries energy system and role of renewable energy sources", ***Applied Solar Energy***, Vol. 44, (2008), 218-223. (https://doi.org/10.3103/S0003701X08030201).
2. Moghadasi, M., Ghadamian, H., Farzaneh, H., Moghadasi, M. and Ozgoli, H.A., "CO_2 capture technical analysis for gas turbine Flue gases with complementary cycle assistance including non linear mathematical modeling", ***Procedia Environmental Sciences***, Vol. 17, (2013), 648-657. (https://doi.org/10.1016/j.proenv.2013.02.081).
3. Reddy, A.K.N. and Subramanian, D.K., "The design of rural energy centres", ***Proceedings of The Indian Academy of Sciences***, Vol. 2, (1979), 395-416. (https://doi.org/10.1007/BF02848936).
4. Ozgoli, H.A. and Ghadamian, H., "Energy price analysis of a biomass gasification-solid oxide fuel cell-gas turbine power plant", ***Iranian Journal of Hydrogen & Fuel Cell***, Vol. 3, (2016), 45-58. (https://doi.org/10.22104/ijhfc.2016.327).
5. Ozgoli, H.A., Ghadamian, H. and Pazouki, M., "Economic analysis of biomass gasification-solid oxide fuel cell-gas turbine hybrid cycle", ***International Journal of Renewable Energy Research***, Vol. 7, (2017), 1007-1018.
6. Friedlingstein, P., Jones, M.W., O'Sullivan, M., et al., "Global carbon budget 2019", ***Earth System Science Data***, Vol. 11, No. 4, (2019), 1783-1838. (https://doi.org/10.5194/essd-11-1783-2019).
7. Freestone, D., The united nations framework convention on climate change-The basis for the climate change regime, Oxford handbook of international climate change law, (2016). (http://doi.org/10.1093/law/9780199684601.003.0005)
8. Branger, F., Ponssard, J.P., Sartor, O. and Sato, M., "EU ETS, Free allocations, and activity level thresholds: the devil lies in the details", ***Journal of the Association of Environmental and Resource Economists***, Vol. 2, No. 3, (2015), 401-437. (https://doi.org/10.1086/682343).
9. Edenhofer, O., Flachsland, C., Wolff, C., Schmid, L.K., Leipprand, A., Koch, N., Kornek, U. and Pahlem M., "Decarbonization and EU ETS reform: Introducing a price floor to drive low-carbon investments", Mercator Research Institution on Global Commons and Climate Change (MCC), Berlin, (2017).
10. Curlee, T.R. and Sale, M.J., "Water and energy security", ***Proceedings of Water Security in the 21st Century Conference***, Netherlands, (2003).
11. "DoE U.S. energy demands on water resources, Report to congress on the interdependency of energy and water", U.S. Department of Energy, Washington D.C, (2006).
12. Goldstein, R. and Smith, W., "Water and sustainability, US electricity consumption for water supply and treatment- The next half century", Vol. 4., Electric power research institute (EPRI), Technical report, (2002).
13. Rothausen, S. and Conway, D., "Greenhouse-gas emissions from energy use in the water sector", ***Nature Climate Change***, Vol. 1, (2011), 210-219. (https://doi.org/10.1038/nclimate1147).
14. Frijns, J., "Towards a common carbon footprint assessment methodology for the water sector", ***Water and Environment Journal***, Vol. 26, (2012), 63-69. (https://doi.org/10.1111/j.1747-6593.2011.00264.x).
15. Marland, G., Boden, T.A. and Andres, R.J., "Global, regional, and national fossil-fuel CO_2 emissions", Carbon dioxide information analysis center, Oak Ridge national laboratory, U.S. department of energy, Oak Ridge, Tenn., USA, (2009).
16. Karimi, P., Qureshi, A.S., Bahramloo, R. and Molden, D., "Reducing carbon emissions through improved irrigation and groundwater management: A case study from Iran", ***Agricultural Water Management***, Vol. 108, (2012), 52-60. (https://doi.org/10.1016/j.agwat.2011.09.001).
17. Raghuvanshi, S.P., Chandra, A. and Raghav, A.K., "Carbon dioxide emissions from coal based power generation in India", ***Energy Conversion and Management***, Vol. 47, (2006), 427-441. (https://doi.org/10.1016/j.enconman.2005.05.007).
18. Yan, Q., Zhang, Q. and Zou, X., "Decomposition analysis of carbon dioxide emissions in China's regional thermal electricity generation, 2000-2020", ***Energy***, Vol. 112, (2016), 788-794. (https://doi.org/10.1016/j.energy.2016.06.136).
19. Zhang, M., Liu, X., Wang, W. and Zhou, M., "Decomposition analysis of CO_2 emissions from electricity generation in China", ***Energy Policy***, Vol. 52, (2013), 159-165. (https://doi.org/10.1016/j.enpol.2012.10.013).
20. Gou, Z., Sun, Y., Pan, S.Y. and Chiang, P.C., "Integration of green energy and advanced energy-Efficient technologies for municipal wastewater treatment plants", ***International Journal of Environmental Research and Public Health***, Vol. 16, No. 7, (2019). (https://doi.org/10.3390/ijerph16071282).
21. Mahmoodi, V., Bastami, T. and Ahmadpour, A., "Solar energy harvesting by magnetic-semiconductor nanoheterostructure in water treatment technology", ***Environmental Science and Pollution Research***, Vol. 25, (2018), 8268-8285. (https://doi.org/10.1007/s11356-018-1224-y).
22. Rodriguez, R., Espada, J.J., Gallardo, M., Molina, R. and Lopez-Munoz, M.J., "Life cycle assessment and techno-economic evaluation of alternatives for the treatment of wastewater in a chrome-plating industry", ***Journal of Cleaner Production***, Vol. 172, (2018), 2351-2362. (https://doi.org/10.1016/j.jclepro.2017.11.175).
23. Al-Aboosi, F.Y. and El-Halwagi, M.M., "An integrated approach to water-energy nexus in shale-gas production", ***Processes***, Vol. 6, (2018). (https://doi.org/10.3390/pr6050052).
24. Foteinis, S., Borthwick, A., Frontistis, Z., Mantzavinos, D. and Chatzisymeon, E., "Environmental sustainability of light-driven processes for wastewater treatment applications", ***Journal of Cleaner***

Production, Vol. 182, (2018), 8-15. (https://doi.org/10.1016/j.jclepro.2018.02.038).

25. Maldonado, M.I., Lopez-Martin, A., Colon, G., Peral, J., Martinez-Costa, J.I. and Malato, S., "Solar pilot plant scale hydrogen generation by irradiation of Cu/TiO_2 composites in presence of sacrificial electron donors", ***Applied Catalysis B: Environmental***, Vol. 229, (2018), 15-23. (https://doi.org/10.1016/j.apcatb.2018.02.005).
26. Han, C., Liu, J., Liang, H., Guo, X. and Li, L., "An innovative integrated system utilizing solar energy as power for the treatment of decentralized wastewater", ***Journal of Environmental Sciences***, Vol. 25, No. 2, (2013), 274-279. (https://doi.org/10.1016/S1001-0742(12)60034-5).
27. "Population and housing censuses", Statistical center of Iran, (Retrieved from: https://www.amar.org.ir/english/Population-and-Housing-Censuses), (Access date: 10/04/2020).
28. Dehghani, M.A. and Feylizadeh, M.R., "An overview of solar energy potential in Iran", ***International Journal of Current Life Sciences***, Vol. 4, (2014), 7173-7180.
29. Bangdiwala, S.I., "Regression: simple linear", ***International Journal of Injury Control and Safety Promotion***, Vol. 25, (2018), 113-115. (https://doi.org/10.1080/17457300.2018.1426702).
30. James, G., Witten, D., Hastie, T. and Tibshirani, R., An introduction to statistical learning, Springer, USA, (2015). (https://doi.org/10.1007/978-1-4614-7138-7).
31. "Casablanca storage tanks and drinking water plant", Project report, Eurofinsa Co., (Retrieved from: https://www.eurofinsa.com/en/casablanca-storage-tanks-and-drinking-water-plant), (2014).
32. Zabihian, F. and Fung, A., "Fuel and GHG emission reduction potentials by fuel switching and technology improvement in the Iranian electricity generation sector", ***International Journal of Engineering (IJE)***, Vol. 3, (2009), 159-173.
33. "Iran CO_2 emissions", Worldometer, (Retrieved from: https://www.worldometers.info/co2-emissions/iran-co2-emissions/), (Access date: 12/01/2020).
34. "These countries have prices on carbon, Are they working", The New York Times, (Retrieved from: https://www.nytimes.com/interactive/2019/04/02/climate/pricing-carbon-emissions.html), (Access date: 20/01/2020).
35. Mardones, C. and Flores, B., "Effectiveness of a CO_2 tax on industrial emissions", ***Energy Economics***, Vol. 71, (2018), 370-382. (https://doi.org/10.1016/j.eneco.2018.03.018).

JREE: Vol. 7, No. 4, (Autumn 2020) 30-43

Journal of Renewable Energy and Environment

Research Article

Journal Homepage: www.jree.ir

Adaptive Robust Control Design to Maximize the Harvested Power in a Wind Turbine with Input Constraint

Hossein Dastres, Ali Mohammadi, Behrooz Rezaie*

Department of Electrical and Computer Engineering, Babol Noshirvni University of Technology, P. O. Box: 47148-71167, Babol, Mazandaran, Iran.

PAPER INFO

Paper history:
Received 17 April 2020
Accepted in revised form 02 August 2020

Keywords:
Second-Order Sliding Mode Control,
Fast Integral Terminal Sliding Mode Control,
Input Saturation,
Maximum Power Point Tracking

ABSTRACT

This paper deals with the problem of maximizing the extracted power from a wind turbine in the presence of model uncertainties and input saturation. An adaptive second-order integral terminal sliding mode speed control method is utilized to address this problem. The presented method benefits from the advantages of several control techniques, i.e., adaptability, robustness, finite-time convergence, and the capability of coping with the input saturation. The robust nature of the designed controller causes its high performance in facing the uncertainties in the wind turbine model. In this paper, to compensate for the effect of input saturation, an auxiliary dynamic variable is added to the tracking error and also an adaptation law is designed so that the finite-time convergence of the closed-loop system can be achieved. Moreover, to reduce the mechanical stresses which are the result of the chattering phenomenon, a second-order sliding surface is employed. The finite-time convergence of the designed controller has been proven by the Lyapunov stability theorem in which the finite-time convergence of the tracking error to zero is guaranteed. Finally, to illustrate the effectiveness and satisfactory performance of the proposed controller, two comparative simulations are carried out. The results of this comparison show that the proposed controller has less error to track the optimal speed and when the model uncertainties and input saturation occur in the wind turbine system, the proposed controller is almost 3 % more efficient than the existing controllers.

https://doi.org/10.30501/jree.2020.224180.1093

1. INTRODUCTION

Using renewable energy sources such as wind, sea waves and solar systems have been intensely growing in recent years. These energy sources are great alternatives for other sources of energy which are mainly based on fossil fuels. Wind energy is an attractive resource which has received a great amount of attention because it is clean and also commonplace [1]. Two important and main objectives in the harvesting of the wind power are first, the extraction of the maximum power of the wind and second the reduction of the mechanical stress on the wind turbine. These two goals can be achieved thanks to the control strategies that are developed for various operation regions of the wind turbines. As shown in Fig. 1 four different operation regions can be defined for power extraction of the wind, using variable speed wind turbines (VSWTs). Regions 1 and 4 are in the middle of the cut-in and cut-out wind speed. Since the extracted wind power, is less than the losses in this state, it is necessary to turn-off the turbine and disconnect it from the grid in Region 1. However, in Region 4, the wind speed is so high that, the wind turbine may get damaged; hence, the wind turbine should be turned off. In Region 2, the wind speed is between the cut-in and nominal wind speed; in this region, the maximum power point tracking (MPPT) strategy is implemented to extract the maximum power from the wind power. In a wind turbine, the generator torque and the pitch angle are used to control the wind turbine velocity. To harvest the maximum power, in Region 2 the torque of the generator is used as the control input and the blade pitch, is considered to be constant. Region 3 is between the nominal and cut-out speed of the wind and to prevent the turbine to get damaged the pitch angle is used to control the system for regulating the wind turbine power at its rated value [2, 3]. In the literature, to control the harvested energy of the wind in VSWT, linear control methods like proportional-integral (PI), proportional-integral-derivative (PID) [4, 5], linear robust control [6-7], linear-quadratic (LQ) and linear-quadratic-Gaussian (LQG) [8-9] have been proposed. In these methods, the wind turbine model, is considered to be linear, however, in the wind turbine system there are unknown disturbance sources, uncertainties and highly nonlinear terms and the proposed methods cannot guarantee the robustness of the closed-loop system against these problems. When uncertainties and disturbances have high variations, these methods not only have poor performances, but also the stability of the closed-loop system cannot be guaranteed and also high precise results cannot be achieved [1, 3, and 10].

In order to make sure that the wind turbine system is stable in the presence of nonlinearities, uncertainties and disturbances, some of the more efficient nonlinear methods like sliding mode control (SMC) [3, 11], adaptive backstepping control [12] and robust nonlinear control [13]

*Corresponding Author's Email: brezaie@nit.ac.ir (B. Rezaie)
URL: http://www.jree.ir/article_111286.html

Please cite this article as: Dastres, H., Mohammadi, A. and Rezaie, B., "Adaptive robust control design to maximize the harvested power in a wind turbine with input constraint", ***Journal of Renewable Energy and Environment (JREE)***, Vol. 7, No. 4, (2020), 30-43. (https://doi.org/10.30501/jree.2020.224180.1093).

have been implemented. In [3], a sliding mode controller has been designed for maximizing the extracted power in a large scale variable speed wind turbine. In [11], an integral sliding mode controller and a PI controller have been designed for Regions 2 and 3 respectively, so that the generator torque is used to maximize the harvested power and the pitch angle is used to keep the wind turbine power at its rated power. Reference [12] presents a control scheme for a doubly-fed induction generator (DFIG) which is based on the adaptive pole placement control method which is an extension of the backstepping control method. To improve the output wind turbine power and also take into account the unknown disturbance sources and uncertainties, robust H∞ controller in combination with a PID controller has been presented in [14]. In [15], a neural network-based adaptive controller for Region 2 and 3 is designed so that the smooth transition between two modes can be ensured and the Radial-Basis-Function (RBF) Neural Network (NN) estimator is also utilized to approximate the uncertainties and disturbances in an adaptive control method. In this method to achieve the asymptotically stability, a restrictive assumption has been made on the wind turbine speed. Chattering problem, poor performance against the model parameter variation, low ability in the disturbance rejection and the lack of asymptotic stability are the disadvantages of these methods, respectively.

It is well known that the SMC method is robust against the different types of uncertainties and disturbances. However, it is not very sensitive to the variation of the system parameters.

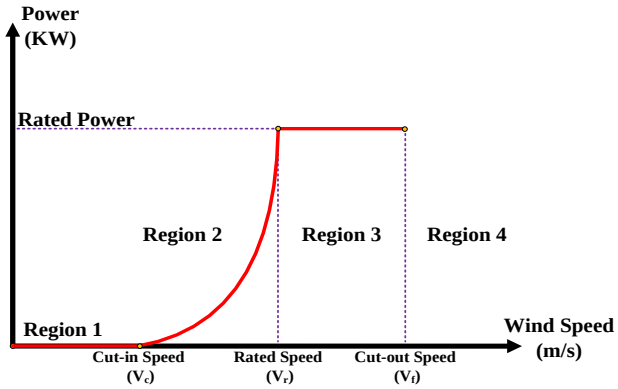

Figure 1. Four operating regions of wind turbine

Therefore, this method has been developed for a variety of systems like power systems [16], electrical machines [17] and spacecrafts [18]. Since, in the wind turbine system, many dilemmas such as nonlinear sources, disturbances and parameter uncertainties exist, so by applying this controller to the wind turbine, satisfactory results can be achieved. There are two important steps in the SMC method which include: (a) selecting a suitable sliding surface; (b) designing the control input so that the system state variables reach to the sliding surface. In the traditional SMC method, only asymptotic stability can be provided and the convergence of the tracking error to zero will not be ensured in the finite time [19]. In the second region, to improve the maximum extraction of the wind power, an optimal speed for rotor is needed. Hence, by exploiting large control effort, it is possible to obtain a faster convergence in control schemes with high precision, which is severely adverse in practical applications. However, implementing the terminal SMC (TSMC) with nonlinear terminal sliding surface can be a proper solution for the aforementioned problem. In the TSMC method, near the equilibrium point of the system, the singularity problem occurs and non-singular TSMC (NTSMC) can solve this problem [20]. Moreover, the chattering phenomenon appears if the TSMC approach is implemented and it is because of the excitation of unmodeled dynamics of the system with high frequency which causes actuators to get damaged [21]. A conventional technique to reduce the chattering phenomenon is substituting the sign function with saturation or sigmoid function which causes a steady-state error. Another approach, so-called as the higher-order sliding mode method, has been presented in reference [22] instead of the switching signal which can wipe out the chattering phenomenon. Furthermore, the tracking error convergence in finite-time is guaranteed by the higher-order sliding mode. Reference [23] implements the combination of two sliding surfaces, including the nonlinear terminal and PID sliding surface, to design the second-order fast TSMC. In the aforementioned paper, the uncertainty in the power coefficient model, and saturation in the electromagnetic torque has not been considered in the controller design procedure.

Another common problem in the control systems is the saturation nonlinearity in actuators which occurs because of the physical limitations and safety considerations. When the saturation occurs, the control input cannot be greater than its maximum and minimum limits, which not only does it reduce the performance of the system but can also cause instability in some cases. This issue has attracted a lot of attention in researchers which has led to the development of some methods to compensate for the input saturation. To compensate for the input saturation in a linear system the anti-windup compensator is an effective method. Reference [24] has presented the anti-windup PID control architecture for the linear systems. An investigation on the stability analysis for the problem of anti-windup design for a class of systems with discrete-time and time-varying, norm-bounded uncertainties and saturating actuators has been conducted by Zhang et al in [25]. When the saturation problem occurs in a nonlinear system, to design the actual input control law, usually there are two solutions available. The first solution is based on using the mean-value theorem to convert the input control to an affine form [26-28]. The second solution is based on defining an augmented error between the actual control input and the saturated control input and then designing an auxiliary dynamic variable to compensate for this error [29-32]. The previous researches studied the problem of input saturation in general systems and provided solutions to compensate for saturation. However, due to the safety considerations in Region 2 (the current limitation in electrical subsystem) and the physical limitations in Region 3 (limitation on the pitch angle because of limitation in servo actuator) in a wind turbine system, it is necessary for the saturation to be considered in the control input. Therefore, research on the design of an appropriate controller to compensate for the input saturation, especially for a wind turbine system seems to be a necessity. Reference [33] proposed an input-output feedback linearization nonlinear current controller to maximize the generated power in an Interior Permanent Magnet Synchronous Generator (IPMSG) driven by a wind turbine involved in magnetic saturation. In references [34, 35] to maximize the captured generated power in a variable speed wind turbine, the discrete sliding mode control is used. In these papers the saturation limitation is considered in the control input and to tackle this problem, in [34] the backstepping scheme is employed to construct an appropriate

sliding surface that can guarantee the stability of the control system. In [35], the gains of the controller are designed using the Linear Matrix Inequality (LMI) so that the closed-loop stability of the controller can be guaranteed in the presence of the input saturation. In this paper in order to have a linear system for easier controller design, it is assumed that the aerodynamic torque is a linear function. Reference [36] has developed a PI controller to control the current of a PMSG-based wind energy conversion system so that the presented controller has a good transient and asymptotically stability in the presence of the input saturation. References [33-36], have often either designed a linear controller only for the electrical subsystem of the wind turbine, or have assumed that the system is linear, and have designed a discrete-time sliding mode controller for the mechanical subsystem of the wind turbine.

Given that in the wind turbine both of the uncertainties and input saturation can occur, therefore considering the aerodynamic and mechanical model of the wind turbine with both uncertainties and input saturation is more general in practical applications. Moreover, to achieve a better precision and efficiency in the power generation, designing a controller with finite-time convergence for this model is very challenging. To the best of the authors' knowledge, according to the literature, the consideration of the uncertainties in the power coefficient and the dynamic model of the wind turbine as well as the consideration of the input saturation has not been studied. Based on the previous studies, the design of a high-precision robust controller with finite-time convergence has not been investigated yet. Therefore, designing a controller with a good performance against the model uncertainties and the input saturation, while the finite-time convergence is provided and the chattering and mechanical stresses problems are mitigated, can be very useful and efficient.

The main contribution of this paper is to propose a strategy, based on an adaptive fast TSMC in Region 2 of the operation area in the presence of the input saturation. At first, to reduce the mechanical stresses and to mitigate the chattering phenomenon, a second-order PI terminal sliding surface is considered. The integral term in the sliding surface can help to eliminate the steady-state error. Then, to ensure the finite-time convergence of the tracking error to zero, a nonlinear terminal surface is employed. Moreover, by adding a compensating variable to the tracking error, the second-order PI sliding surface is modified so that the input saturation can be compensated. The adaptation law for this dynamic compensating variable is designed so that the finite-time stability of the closed-loop system can be achieved. The simulation results show the superiority of the proposed scheme compared to the existing methods. The advantage of the proposed scheme is its ability to face the uncertainties in the model of the wind turbine as well as the input saturation which usually occurs in practice.

The outline of this paper is as follows. In Section 2, the wind turbine model is introduced. Section 3 presents the controller design procedure. The simulation results are given in Section 4. Finally, a conclusion for the proposed controller is presented in Section 5.

2. WIND TURBINE

As shown in Fig. 2, four subsystems can be considered to study the wind turbine characteristics. These subsystems are pitch servo subsystem, generator dynamic, aerodynamic subsystem and mechanical subsystem [37].

It is imperative to understand the principle of the wind turbine performance. According to Fig. 2, the wind speed causes the aerodynamic torque in the aerodynamic subsystem. To increase the efficiency of VSWT, some strategies such as flow control techniques [38, 39] can be utilized in this subsystem. As a result of the aerodynamic torque, the wind turbine blades start to rotate and this rotation leads to an angular velocity in the rotor side of the mechanical subsystem. The wind turbine and the generator are linked to each other via a gearbox thus, the generator shaft rotation speed, is higher than the rotor and the rotation of the generator leads to an electrical power in its output. To control the output electrical power, the electromagnetic torque and the pitch angle are used. To implement the maximum power point tracking strategy, the electromagnetic torque is used to capture the maximum power from the wind turbine in Region 2 and to fix the output power at its rated value in Region 3, the pitch servo subsystem is used. The servo subsystem increases the pitch angle by rotating the blades and as a result, the input aerodynamic torque is reduced and thus, the output power can be regulated at the nominal power.

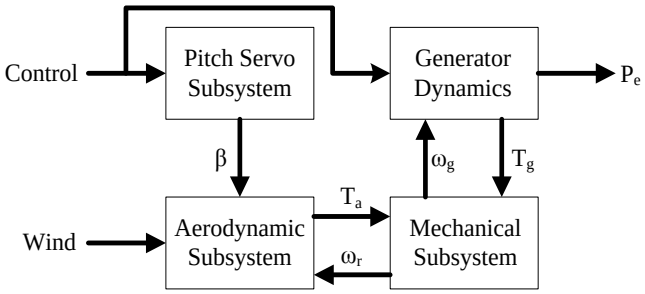

Figure 2. VSWT structure

The wind turbine captures the wind power or the aerodynamic power. This power is a function of two parameters; the wind speed V(t) and the power coefficient C_p, and the power coefficient itself depends on both the blade pitch angle β and also the tip speed ratio λ. To calculate the aerodynamic power, the following equation can be used [40]:

$$P_a = \frac{1}{2}\rho\pi R^2 C_p(\lambda,\beta)\, V^3(t) \quad (1)$$

In this equation, ρ represents the air density and R is the radius of the wind turbine rotor. In order to have a clear understanding of this equation, it is necessary to mention that the tip speed ratio λ is defined as:

$$\lambda = R\frac{\omega_r}{V} \quad (2)$$

where ω_r is the rotor speed. Therefore, the torque generated by the wind turbine is expressed as:

$$T_a = \frac{P_a}{\omega_r} = \frac{1}{2}\rho\pi R^3 \frac{C_p(\lambda,\beta)}{\lambda} V^2 \quad (3)$$

Due to the inherent uncertainties, the power coefficient is considered as follows:

$$C_p(\lambda,\beta) = \bar{C}_p(\lambda,\beta) + \Delta C_p(\lambda,\beta) \quad (4)$$

where $\bar{C}_P$ and $\Delta C_P(\lambda,\beta)$ are certain and uncertain terms of the power coefficient which are defined in Appendix A.

Note that, if the tip speed ratio has an optimum value, the power coefficient will be maximum that leads to maximum power extraction. To fix the tip speed ratio at its optimum value, the wind turbine speed should be controlled according to the input wind speed. To design an appropriate controller at first the dynamic model of the wind turbine should be described. As shown in Fig. 3, the model of the two-mass wind turbine is defined as follows [40]:

$$\begin{aligned} J_r\dot{\omega}_r &= T_a - T_{ls} - D_r\omega_r \\ J_g\dot{\omega}_g &= T_{hs} - T_e - D_g\omega_g \end{aligned} \tag{5}$$

where ω_r, ω_g and ω_{Ls} are the rotor, generator and low speed shaft angular velocities, respectively. T_e is the electromagnetic torque, T_{hs} is the high speed shaft torque and T_{ls} is the shaft torque in low speeds which is also known as the brake torque, and can be defined as:

$$T_{ls} = k_{ls}\left(\theta_r - \theta_{ls}\right) + D_{ls}\left(\omega_r - \omega_{Ls}\right) \tag{6}$$

where θ_{ls} and θ_r are the gearbox side and rotor side angular deviations, respectively.

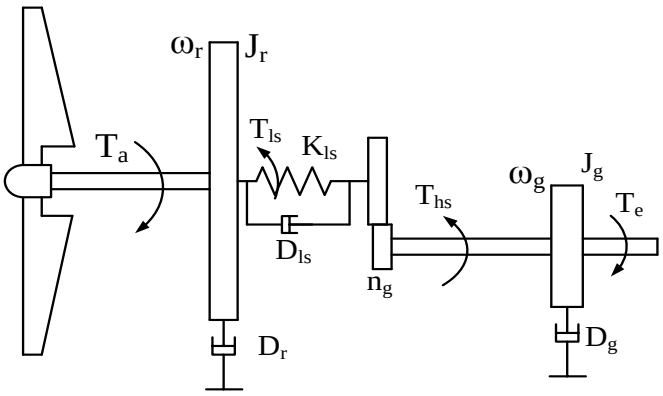

Figure 3. Two-mass wind turbine schematic

Moreover, J_g, J_r are the generator and the rotor inertias, respectively. In addition, D_r, D_g and D_{ls} are the external damping coefficients of the rotor, the generator and the damping coefficient of the low speed shaft respectively. Moreover, n_g is the gearbox ratio which is defined as:

$$n_g = \frac{\omega_g}{\omega_{Ls}} = \frac{T_{Ls}}{T_{hs}} = \frac{\theta_g}{\theta_{Ls}} \tag{7}$$

Using (9), (10) and (11), it can be obtained that:

$$J_t\dot{\omega}_r = T_a - D_t\,\omega_r - T_g \tag{8}$$

where, $J_t = J_r + n_g^2 J_g$ is the turbine total inertia, $D_t = D_r + n_g^2 D_g$ is the total external damping of the turbine and $T_g = n_g T_e$ is the torque of the generator in the rotor side.

D_t and J_t are considered to be uncertain with unknown bounds based on the deviation with respect to the rated values, i.e.:

$$\begin{aligned} D_t &= \bar{D}_t + \Delta D_t, \left|\Delta D_t\right| \le \rho_{D_t} \\ J_t &= \bar{J}_t + \Delta J_t, \left|\Delta J_t\right| \le \rho_{J_t} \end{aligned} \tag{9}$$

where $\bar{J}_t$ and $\bar{D}_t$ are the rated values. Moreover, ρ_{J_t} and ρ_{D_t} are known constants with positive values.

Considering (3), (4) and (9), we can rewrite (8) as:

$$\dot{\omega}_r = \frac{1}{\bar{J}_t}[\bar{T}_a - \bar{D}_t\omega_r - n_g T_e + d(\lambda,\beta,V,\omega_r)] \tag{10}$$

where:

$$\begin{aligned} d(\lambda,\beta,V,\omega_r) &= [0.5\rho\pi R^3 \frac{\Delta C_p(\lambda,\beta)}{\lambda} V^2 - \Delta D_t\omega_r(t)] \\ &- \frac{\Delta J_t}{\bar{J}_t + \Delta J_t}[0.5\rho\pi R^3 \frac{C_P(\lambda,\beta)}{\lambda} V^2 - D_t\omega_r(t) - n_g T_e] \end{aligned} \tag{11}$$

And $\bar{T}_a$ is the rated aerodynamic torque and is defined as follows:

$$\bar{T}_a = 0.5\rho\pi R^3 \frac{\bar{C}_p(\lambda,\beta)}{\lambda} V^2 \tag{12}$$

The overall system parametric uncertainty is shown by the term, d(λ, β, V, ω_r) depending on (A.3) in Appendix A and (9). Inherent physical limitations of a practical wind turbine can cause the wind speed, the rotor speed and the blade pitch angle to have bounded ranges [41]. Thus, by considering (A.3) and (9), it can be assumed that there is a positive constant like $\bar{\delta} > 0$ so that the overall system parametric uncertainty can be bounded as:

$$\left|d(\lambda,\beta,V,\omega_r)\right| \le \bar{\delta}, \qquad \bar{\delta} > 0 \tag{13}$$

As it is known, in region 2 in wind energy systems, generator torque or electromagnetic torque is used as the control input to control the wind turbine output power. This torque has a relationship with the current of the generator. Therefore the control input cannot be very large because a large control input causes a great increase in the amount of the current, and this can damage the generator. So, it is necessary to have a limitation for generating the control input torque for safety purposes. In other words, the control input should be practically feasible and have a reasonable range. Therefore, due to physical limitations and safety purposes [35], in this paper, it is assumed that the generator torque has saturation limitation as follows.

$$T_e = \text{sat}(u(t)) = \begin{cases} \text{sign}(u(t)) \times T_{e_{max}}, & \left|u(t)\right| > T_{e_{max}} \\ u(t) & , \left|u(t)\right| \le T_{e_{max}} \end{cases} \tag{14}$$

where $T_{e_{max}}$ is the maximum safe torque that can be applied to the system and u(t) is the control input that needs to be designed.

The control objective is to maximize the extracted power from the wind which depends on the power coefficient, and the power coefficient itself depends on λ and β. Therefore, based on the power coefficient curve, as shown in Fig. 4, maximum of c_p can be computed based on λ_{opt} and β_{opt}. Furthermore, ω_{ropt} can be calculated based on the wind speed variations. The power coefficient curve is drawn based on (A.1) for various pitch angles and is illustrated in Fig. 4 and it can be seen that, the maximum value of c_p occurs at $\beta = 0$.

$$C_P\left(\lambda_{opt},\beta_{opt}\right)=C_{P_{max}} \tag{15}$$

$$\omega_{r_{opt}}=\frac{\lambda_{opt}V}{R} \tag{16}$$

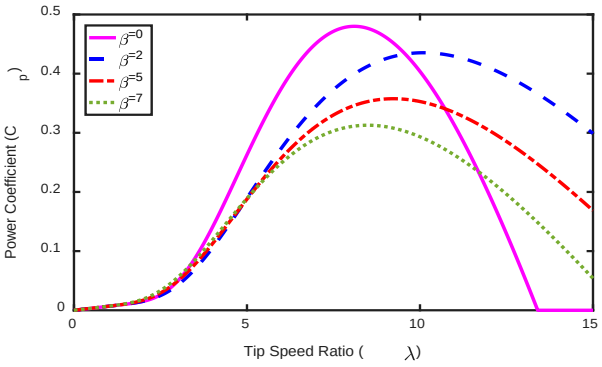

Figure 4. Power coefficient $C_P(\lambda,\beta)$ versus tip-speed ratio in different pitch angle

Note that in this paper, like many other papers, the generator dynamic (Electrical Model) is not taken into account which can be considered as a future work to address the problem of input saturation by considering the generator dynamic. It is worth to note, in this paper, similar to many works in the field of the MPPT strategy for the wind turbine, the speed control is investigated and direct power control is not considered. So according to the wind speed in region 2 and power coefficient curve (according to (A.1)), to achieve the maximum power, we should apply a generator torque to the wind turbine (according to (5)) that can regulate the turbine speed at its optimum value corresponding to the wind speed at each instant. Therefore, the power coefficient will has its maximum value, and the maximum power can be extracted from the input wind power. It is worth noting that in this strategy, the wind power is converted to the generator speed and there is no direct conversion between the generator torque and the wind power because the generator torque is determined by the controller.

Before presenting the controller design procedure, the following Lemma needs to be introduced. This Lemma is defined to prove the finite-time stability of the closed-loop system after applying the proposed controller.

Lemma 2.1 [42]: For any positive-definite function $V(t)$ which fulfills a differential inequality as:

$$\dot{V}(t)+\alpha\, V(t)+\beta\, V^{\ell}(t)\le 0 \tag{17}$$

where α and β are two positive coefficients, and ℓ is a fraction of two odd positive numbers with $1>\ell>0$, for the certain time t_0, note that the aforementioned function V(t), converges to zero in the finite-time t_r as:

$$t_r\le t_0+\frac{1}{\alpha(1-\ell)}\ln\left(\frac{\alpha\, V^{1-\ell}(t_0)+\beta}{\beta}\right) \tag{18}$$

3. CONTROLLER DESIGN

In this section, an adaptive second-order fast TSMC (SOFTSMC) is designed for harvesting the maximum power in a wind turbine (WT) system subjected to input control limitation. This method is performed in two main steps. First, the sliding surface is defined and in the second step, by considering the sliding dynamics, a controller is designed such that the tracking error will converge to zero in finite-time. In the first step, a fast terminal sliding surface is considered as below that can ensure that the sliding surface converges to zero in finite-time:

$$\sigma(t)=k_{1\sigma}\, s(t)^{\frac{p}{q}}+k_{2\sigma}\, s(t)+k_{3\sigma}\,\dot{s}(t) \tag{19}$$

Note that $k_{1\sigma}$ and k_{3s} are positive design parameters. In the second step, to decrease the mechanical stresses and mitigate the chattering and also to eliminate the steady state error, a second-order integral terminal sliding dynamic equation is considered as:

$$\dot{s}(t)+\gamma\, s(t)=k_p\, z(t))+k_I\int_0^t\left(k_{1I}\, z(\tau)^{\frac{p}{q}}+k_{2I}\, z(\tau)\right)d\tau \tag{20}$$

where $z(t)=e(t)+\eta(t)$. $e(t)$ and $\eta(t)$ are tracking error and auxiliary dynamic variables, respectively. Note that $\eta(t)$ is considered to compensate for the effect of input saturation. To achieve the finite-time convergence for the tracking error, the term $z(\tau)^{\frac{p}{q}}$ has been added into the sliding surface, where γ, k_p, k_I, k_{1I} and k_{2I} are positive design parameters. In addition, p and q are arbitrary positive odd constants so that the following inequality holds:

$$\frac{1}{2}<\frac{p}{q}<1 \tag{21}$$

The speed tracking error is defined as:

$$e(t)=\omega_r(t)-\omega_d(t)=\omega_r(t)-\omega_{r_{opt}}(t) \tag{22}$$

where $\omega_{r_{opt}}$ is the required rotor speed to achieve the maximum power in the wind turbine system.

As it is known, the conventional sliding surface is a combination of the error and the derivative of the error; however, by adding the integral of error and constructing a PID sliding surface, the steady-state error converges to zero. In [23], a PID second-order sliding surface has been used. In the proposed method, by adding the derivative of the sliding surface to the right hand side of the conventional PID sliding surface, not only the advantages of a conventional PID sliding surface are provided, but also the chattering is reduced. In this paper, a PI second-order sliding surface is employed for two reasons; first, the derivative of the tracking error in the aforementioned PID second-order sliding surface increases the order of the system and secondly, to compute the actual input control, the time derivative of the aerodynamic torque and the second order time derivative of the optimal rotor speed are needed.

In this paper, on the contrary to [23], in both aerodynamic (C_p) and mechanical models of the two-mass wind turbine, it is assumed that the model parameters are uncertain. Moreover, in this paper, the input saturation is also taken into account. To solve the saturation problem, a compensating dynamic term is added to the tracking error, and also the second-order

PI sliding surface is constructed based on this compensating variable. Then the adaptation law of this compensating dynamic term is designed so that the finite-time convergence of the closed-loop system can be ensured. Furthermore, the nonlinear integral term of the error, which was added to the second-order PI sliding surface, can ensure that the tracking error converges to zero in finite-time, while in [23] the tracking error is asymptotically stable and converges to zero in finite-time.

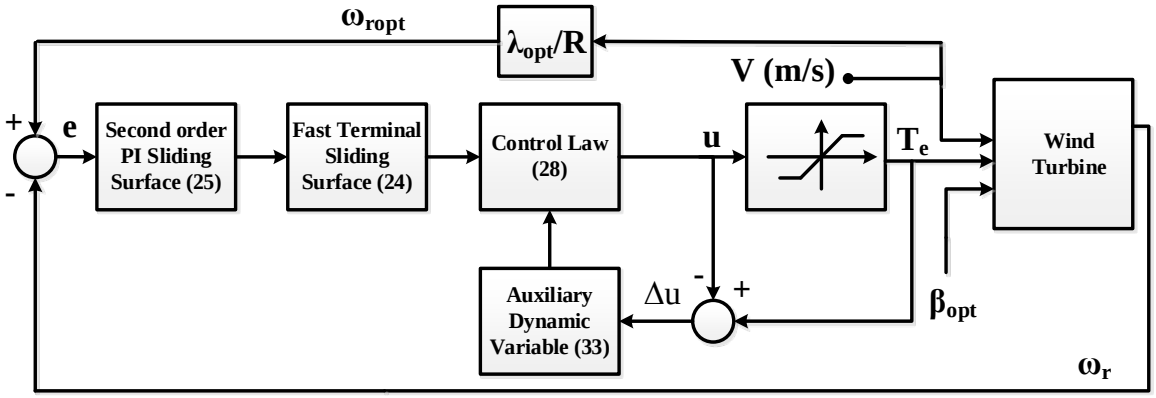

Figure 5. The closed-loop block diagram of the proposed controller

Theorem 1. In the dynamic model of the wind turbine (10), by applying the following control input and also by selecting the control parameters such that $b_4 > \frac{\alpha_1}{\alpha_3}\overline{\Delta u}$ and $b_2 > \alpha_2 \bar{\delta}$ hold, where $\overline{\Delta u}$ is the upper bound of $\Delta u = T_e - u$, then the overall system will be stable and the tracking error will converge to zero in finite-time:

$$u = -\frac{1}{\alpha_1}[-f - b_1\,\sigma(t) - b_2\,\mathrm{sign}(\sigma(t))) + \alpha_3\,b_3\,\eta(t) + \alpha_3\,b_4\,\mathrm{sign}(\eta(t))] \quad (23)$$

where:

$$f = \varphi(-\gamma s(t) + w) + k_{3\sigma}\,k_p\left[\frac{1}{\bar{J}_t}\left[\bar{T}_a - \bar{D}_t\omega_r\right] - \dot{\omega}_{r_{opt}}(t)\right] + k_{3\sigma}\left[k_{I_1} z(t)^{\frac{p}{q}} + \left(k_{I_2} + \frac{k_p}{k_{3\sigma}}\varphi\right) z(t)\right] \quad (24)$$

$$\varphi = k_{1\sigma}\frac{p}{q}s(t)^{\frac{p}{q}-1} + k_{2\sigma} - \gamma k_{3\sigma} \quad (25)$$

$$w = k_I \int_0^t (k_{1I}\, z(\tau)^{\frac{p}{q}} + k_{2I}\, z(\tau))\, d\tau \quad (26)$$

$$\alpha_1 = n_g k_{3\sigma}\frac{k_p}{\bar{J}_t},\ \alpha_2 = k_{3\sigma}\frac{k_p}{\bar{J}_t}, \alpha_3 = k_{3\sigma}k_p \quad (27)$$

Moreover, the adaptation law for the dynamic variable $\eta(t)$ which is defined to compensate for the input saturation is designed as:

$$\dot{\eta}(t) = -b_3\,\eta(t) + \frac{\alpha_1}{\alpha_3}\Delta u - b_4\,\mathrm{sign}(\eta(t)) \quad (28)$$

where b_3 and b_4 are positive arbitrary constants. Note that $-b_4\,\mathrm{sign}(\eta(t))$ is added to achieve the finite-time convergence in the proposed adaptive controller in the presence of the input saturation.

Proof. See Appendix B.

The augmented dynamic variable is designed to compensate for the input saturation problem. For a normal case, when the input saturation does not occur, this augmented variable is stable and converges to zero in the finite-time and when the saturation occurs, based on (28), the term Δu causes that $\eta \neq 0$, and therefore, according to (23), this variable helps the controller for the input saturation compensation.

The closed-loop block diagram of the proposed controller is shown in Fig. 5.

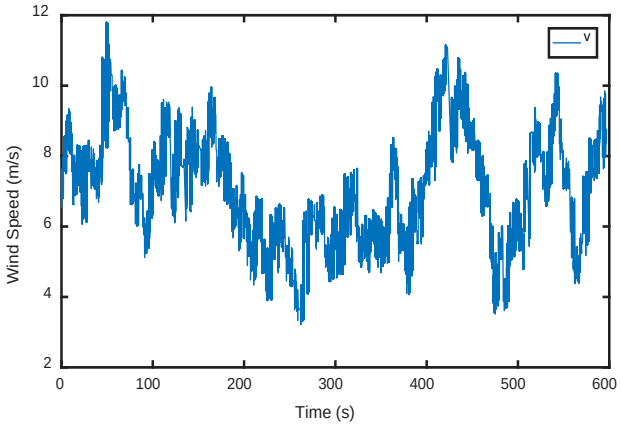

Figure 6. Wind speed profile

4. SIMULATIONS

To demonstrate the performance of the proposed controller against the parameter uncertainties and the input saturation, various simulations have been employed. The performance of the proposed controller is compared with some of the existing methods for two cases. In Case 1, the model uncertainties and the input saturation are not considered, while in Case 2, 60 % of the parameter uncertainty and the input saturation are considered. The wind speed in the wind turbine system is considered as shown in Fig. 6. Simulations are performed for 600 seconds, the mean value of the wind speed is 7.5 m/s and the turbulence intensity is 18 %. To have smooth signals, the optimal rotor speed after passing a low-pass filter is applied to the controller. By fitting Eq. (A.1) with the values of C_p for

the NREL 5-MW wind turbine, the rated values for $\bar{c}_i$, i=1 … 5 are as below [23]:

$$\bar{c}_1 = 0.5176,\ \bar{c}_2 = 116,\ \bar{c}_3 = 0.4,\ \bar{c}_4 = 5,\ \bar{c}_5 = 21,\ \bar{c}_6 = 0.0068 \quad (29)$$

The wind turbine parameters, used in these simulations, are selected the same as reported in [23] which are listed in Table 1.

In this paper, the MATLAB software is used to simulate the wind turbine model and the designed controller. The model of the wind turbine which is described in (5) and (6) is used and these differential equations have been implemented in Simulink environment. The ode45 solver has been employed to solve the differential equations. It is worth noting that the wind turbine model in (5) and (6) has been utilized in many of the references related to the control of the wind turbine. The details about this model and its validation can be found in [40, 43, 44] and references therein.

The proposed method is compared with conventional first order SMC (FOSMC) and two strategies that have been proposed in [23], named PID second-order SMC (SOSMC) and second-order fast TSMC (SOFTSMC).

Table 1. Wind turbine model parameters

R	21.65	m
ρ	1.308	Kg/m^3
J_g	34.4	$Kg.m^2$
J_r	3.25×10^5	$Kg.m^2$
D_r	27.36	N.m/rad/s
D_g	0.2	N.m/rad/s
K_{1s}	9.5×10^3	N.m/rad
D_{1s}	2.691×10^5	N.m/rad/s
P_{enom}	600×10^5	W
T_{emax}	3×10^3	N.m
β_{opt}	0	deg
λ_{opt}	8.1	-
n_g	43.165	-

The control law for the FOSMC is designed as:

$$\begin{cases} s = \dot{e} + k\,e \\ \dot{u} = \dfrac{\bar{J}_t}{n_g}\left[\dfrac{1}{\bar{J}_t}\left(\dot{\bar{T}}_a - \bar{D}_t\,\dot{\omega}_r - \ddot{\omega}_{ropt} + k\dot{e}\right) + k_{sw}\,\mathrm{sign}(s)\right] \end{cases} \quad (30)$$

The control parameters for this controller are chosen as:

k = 2 and k_{sw} = 0.1.

The control input for the SOSMC and the SOFTSMC are given in (31) and (32), respectively.

$$\begin{aligned} & s = \dot{e} + k\,e \\ & \dot{s} + \gamma s = k_p\,e + k_I \int_0^t e(\tau)\,d\tau + k_D\,\dot{e} \\ & \dot{u} = \frac{\bar{J}_t}{n_g(k_D - \gamma)}\left[(k\gamma - k_P)\,\dot{e} - k_I\,e + (\gamma - k_D)\,\ddot{\omega}_{ropt}\right. \\ & \left. - \frac{(\gamma - k_D)}{\bar{J}_t}\dot{\bar{T}}_a + \frac{(\gamma - k_D)\bar{D}_t}{\bar{J}_t}\dot{\omega}_r\right] - \beta_1 s - \beta_2\,\mathrm{sign}(s) \end{aligned} \quad (31)$$

where $k = 100,\ \gamma = 6, k_p = 5, k_I = 0.1, k_D = 50, \beta_1 = 0.1$ and $\beta_2 = 0.1$.

$$\begin{aligned} & s = \dot{e} + k\,e \\ & \dot{s} + \gamma s = k_p\,e + k_I \int_0^t e(\tau)\,d\tau + k_D\,\dot{e} \\ & \sigma = s^{\frac{p}{q}} + \dot{s} + s \\ & \vartheta = \frac{p}{q} s^{\frac{p}{q}-1} + 1 - \gamma \\ & \dot{u} = \frac{\bar{J}_t}{n_g(\vartheta + k_D)}\left[-(\vartheta k + k_P)\,\dot{e} - k_I\,e + (\vartheta + k_D)\,\ddot{\omega}_{ropt}\right. \\ & \left. + \frac{(\vartheta + k_D)}{\bar{J}_t}\left(\dot{\bar{T}}_a - \bar{D}_t\dot{\omega}_r\right) - k_{sw1}\,s - k_{sw2}\,\mathrm{sign}(s)\right] \end{aligned} \quad (32)$$

where

$$k = 100,\ \gamma = 6, k_p = 5, k_I = 0.1,$$
$$k_D = 50, k_{sw1} = 0.1, k_{sw2} = 0.01, p = 17$$

and $q = 19$.

Finally, based on (23)-(28), parameters of the proposed controller are selected as:

$$\gamma = 1, k_p = 1, k_I = 1, k_{1I} = 1, k_{2I} = 1, k_{1\sigma} = 1, k_{2\sigma} = 1,$$
$$k_{3\sigma} = 1\times10^3, b_1 = 20, b_2 = 0.1, b3 = 1, b_4 = 0.1, p = 17$$

and $q = 19$.

As previously mentioned, the simulations are performed for two cases. Case 1 is without the uncertainty and the input saturation, while in Case 2 both of the uncertainty and the input saturation are considered.

Fig. 7 to Fig. 12 illustrates the comparative results of Case 1 and Fig. 7, illustrates the rotor speed. It is obvious that the proposed controller has a better tracking performance compared to the existing methods. The proposed controller not only has less steady state error but also has a better dynamic performance. The generator speed for 4 controllers is shown in Fig. 8. The electromagnetic torque that is used as a control law is demonstrated in Fig. 9. As shown in the control law of the FOSMC, the chattering phenomenon has appeared. This can cause serious damage to the wind turbine and the rest of the controllers have no chattering. Low-speed shaft torque is demonstrated in Fig. 10 and according to this figure the Low-speed shaft in the FOSMC controller is involved in chattering problem that increases the mechanical stress on wind turbine. While, this problem does not appear in the proposed controller and also in the SOSMC and the SOFTSMC controllers. The electrical power P_e that is harvested from the wind turbine is depicted in Fig. 11 and the maximum power is captured by the proposed controller, and

as it can be seen from Figure 11, electrical power has many deviations due to the chattering phenomenon. The rotor speed tracking error is shown in Fig. 12 and it can be seen that the tracking error of the proposed controller is less than the others.

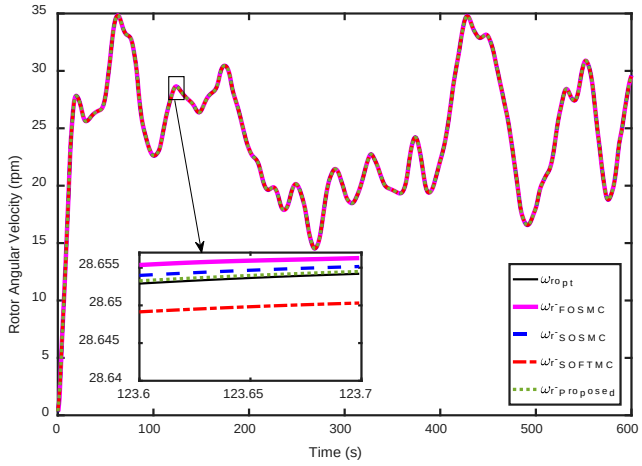

Figure 7. Rotor speed for Case 1

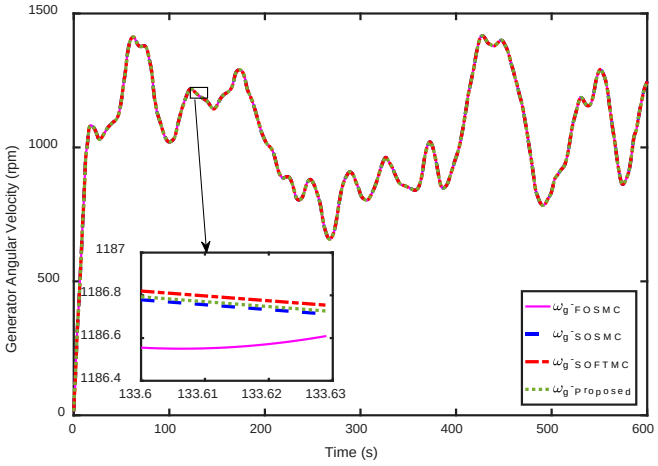

Figure 8. Generator speed for Case 1

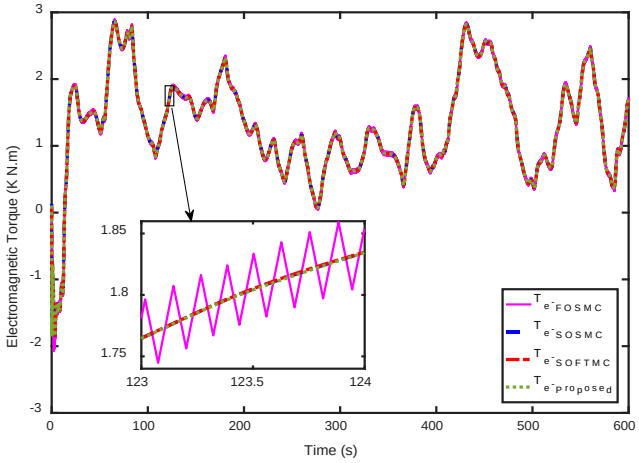

Figure 9. Electromagnetic torque (control input) for Case 1

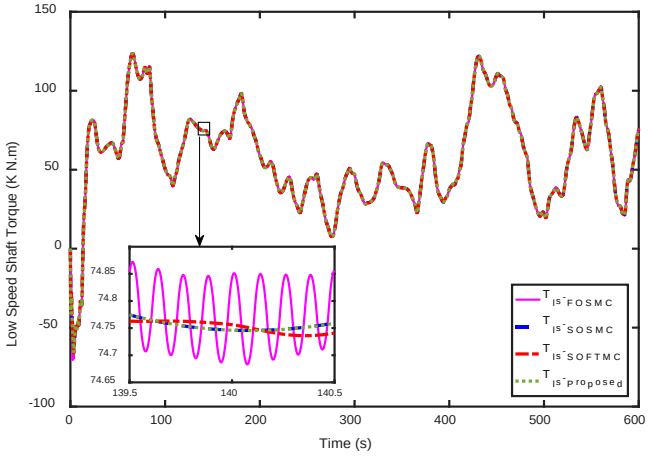

Figure 10. Low-speed shaft torque for Case 1

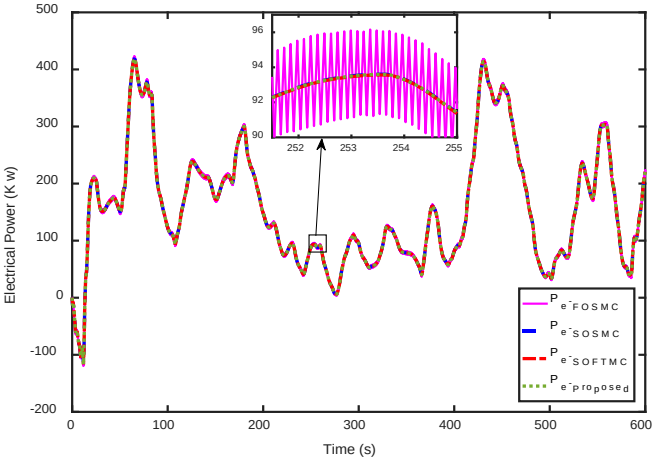

Figure 11. Electrical power for Case 1

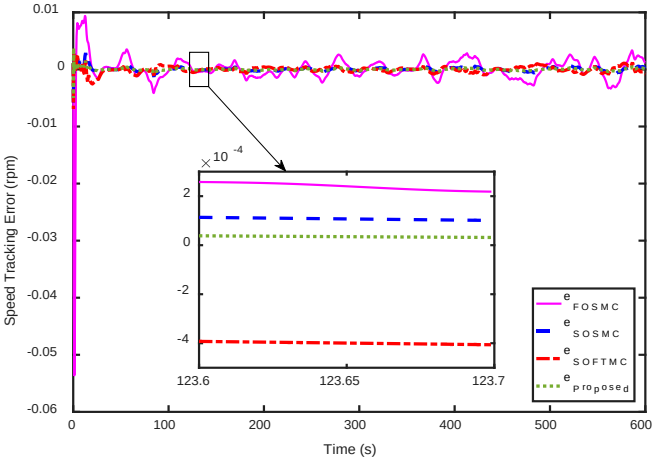

Figure 12. Rotor speed tracking error for Case 1

As mentioned earlier, given that the existing controllers are not designed for a wind turbine model involved in both uncertainties in the aerodynamic and the mechanical model as well as input saturation in the control law, therefore, due to taking into account the aforementioned uncertainties in the proposed controller design procedure as well as the design of an auxiliary dynamic variable to compensate for the input saturation, it is expected that the proposed controller has a better performance than the existing controllers in facing the aforementioned problems. Therefore, in the second case, the superiority of the proposed controller is more distinct than the aforesaid controllers. Fig.13 to Fig.18, show the results of applying above-mentioned controller to the wind turbine, for Case 2. Fig. 13 shows the rotor speed in the presence of model parameters uncertainties and input saturation. It is obvious that the proposed controller shows a very promising

performance and tracks the optimal rotor speed very faster than the other controllers which have been mentioned above. In Fig. 14, the generator speed for four controllers is shown. The electromagnetic torque which is the control input is shown in Fig. 15 for various controllers. As it is shown, the FOSMC is involved in the chattering. Fig. 16 shows the low-speed shaft torque for 4 different controllers and as in the previous case, the mechanical stresses caused by the chattering phenomenon which appeared in the Low-speed shaft torque, are reduced in the proposed controller. The extracted electric power is depicted in Fig. 17. Moreover, Fig. 18 shows the rotor speed tracking error. In this figure, the tracking error for the proposed controller is less than the other aforementioned controllers and the superiority of the proposed controller in Case 2 is more evident than Case 1. Therefore, the proposed controller not only has good steady-state properties, but also has better transient-state properties than the existing controllers, in the presence of input uncertainties and saturation.

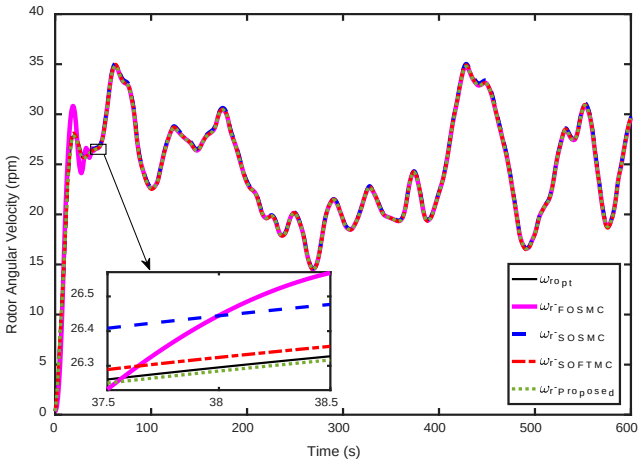

Figure 13. Rotor speed for Case 2

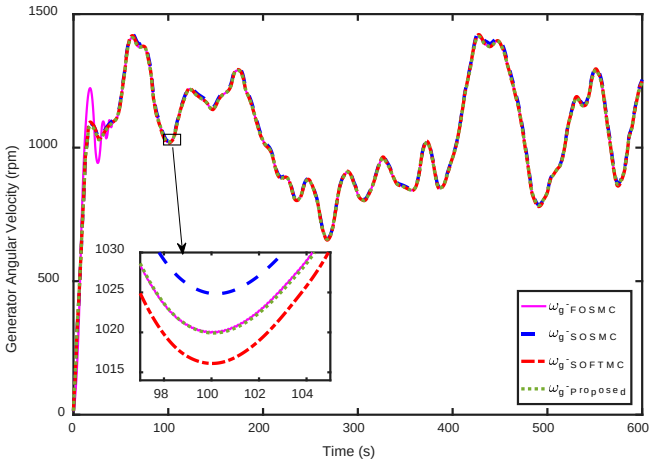

Figure 14. Generator speed for Case 2

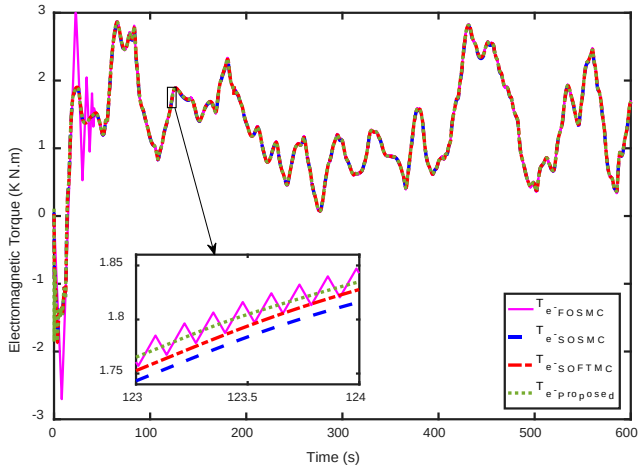

Figure 15. Electromagnetic torque (control input) for Case 2

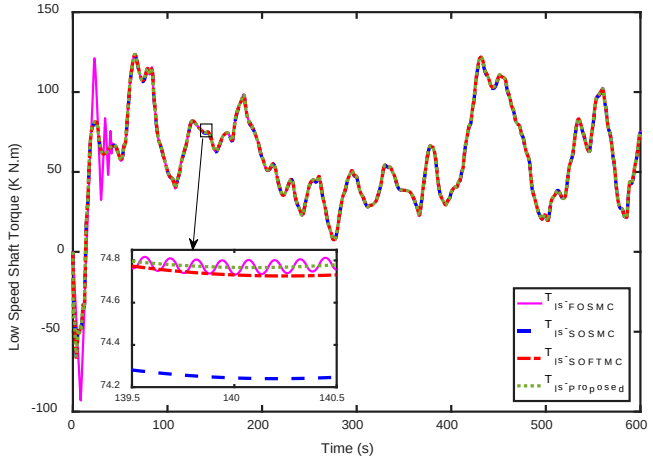

Figure 16. Low-speed shaft torque for Case 2

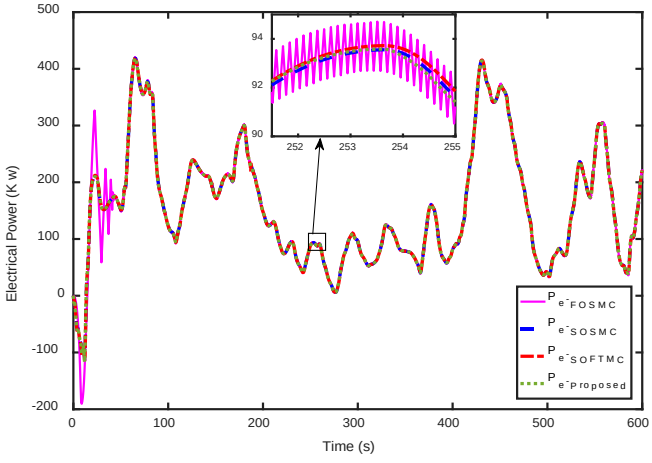

Figure 17. Electrical power for Case 2

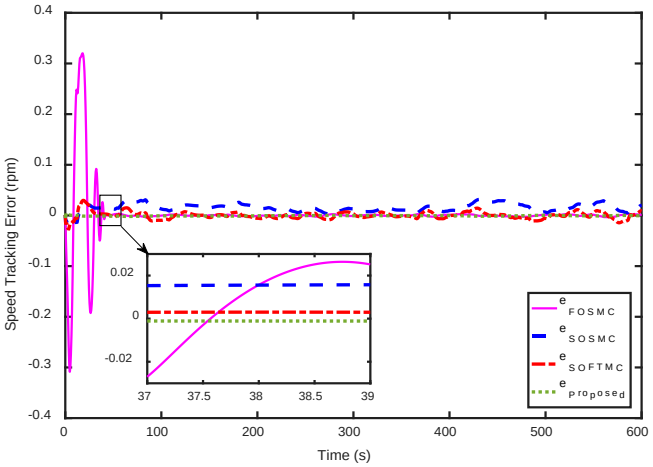

Figure 18. Rotor speed tracking error for Case 2

Finally, performance indices, i.e., integral of the absolute error (IAE) and the integral of the square error (ISE) and the integral of the time multiply absolute error (ITAE) have been calculated for these controllers as presented in the Table 2. It can be seen that the proposed controller in all three indices is superior to the other three controllers and it should be noted that in Case 2 the performance indices for the proposed controller are smaller than the others. Thus, the results of the proposed scheme are very promising and satisfactory, even when input saturation and uncertainties are considered in the wind turbine system. However, other existing controllers have less performance compared to this controller.

Table 2. Performance indices comparison for different controllers

	Case 1			Case 2		
Controller	IAE	ISE	ITAE	IAE	ISE	ITAE
FOSMC	0.8639	0.0058	228.44	6.9424	1.4379	327.4257
SOSMC	0.1636	9.3830e-05	47.5803	9.4274	0.1761	2.7936e+03
SOFTSMC	0.2322	1.7708e-04	65.8714	3.1197	0.0293	870.6477
Proposed	0.0830	2.7154e-05	23.8139	0.3886	3.8845e-04	95.1887

The aforementioned performance indices are computed using the criteria described by (34).

$$\begin{cases} IAE = \int \left| e(t) \right| dt \\ ISE = \int e^2(t) dt \\ ITAE = \int t \left| e(t) \right| dt \end{cases} \quad (33)$$

Table 3 is provided to evaluate the performance of the proposed controller and conventional existing controllers using the aerodynamic and electrical efficiency. Aerodynamic efficiency η_{aero} and electrical efficiency η_{elec} can be calculated using the following equations.

$$\eta_{aero}(\%) = \frac{\int_{t_i}^{t_f} P_a(t)\,dt}{\int_{t_i}^{t_f} P_{aopt}(t)\,dt} \times 100, \qquad \eta_{aero}(\%) = \frac{\int_{t_i}^{t_f} P_{elec}(t)\,dt}{\int_{t_i}^{t_f} P_{aopt}(t)\,dt} \times 100 \quad (34)$$

where $P_{aopt} = 0.5\rho\pi R^2 C_{pmax} V^3$ is the optimal aerodynamic power, P_{elec} is the electrical power, t_i is the initial simulation time and t_f is the final simulation time.

Table 3. Efficiency comparison for different controllers

	Case 1		Case 2	
Controller	η_{aero}	η_{elec}	η_{aero}	η_{elec}
FOSMC	90.22	88.72	85.233	82.088
SOSMC	94.357	92.04	89.427	86.781
SOFTSMC	95.82	93.49	90.119	87.521
Proposed	96.513	95.65	92.388	90.087

According to the Table 3, the FOSMC controller has the least efficiency in terms of the aerodynamics and electricity. However, the efficiency of the SOSMC controller and the SOFTSMC controller is almost the same, and the SOFTSMC controller is more efficient than the SOSMC controller. It is obvious that the proposed controller has the best efficiency rather than the existing controllers and by using this proposed controller the aerodynamic and electrical efficiency has been increased about 3 % in the Case 2.

5. CONCLUSIONS

The maximum power extraction from the wind in a wind turbine is difficult especially when there are model uncertainties in the system and the task becomes more challenging when the control input has saturation in its amplitude. Sliding mode controller is a suitable control method to deal with these inevitable uncertainties. But the conventional SMC causes the chattering problem that increases the mechanical stress on the wind turbine. By designing a second-order sliding mode controller the chattering problem can be avoided. However, to achieve high efficiency and precision in capturing the power, the terminal sliding mode control can provide satisfactory results thanks to its finite-time convergence properties. When the control input is constrained, the finite-time convergence of the control that is designed for normal condition i.e. without the input constraint cannot be guaranteed. Therefore, designing a controller that has a high precision and efficiency in the presence of model uncertainties and input saturation, as well as finite-time convergence properties, is practically effective. Given that in the previous works, the problem of finite-time controller design in the presence of the both uncertainties in the aerodynamic and the mechanical model, as well as input saturation in the control law, is not considered. However, in this paper, unlike the previous works, by considering the uncertainties and input saturation simultaneously, a finite-time convergent controller has been investigated. In this paper, to capture the maximum power, low mechanical stress, and to improve the tracking performance of the wind turbine system with parametric uncertainties in model and saturation in input, an adaptive second-order fast ITSMC has been proposed. It has been proven that the designed controller can achieve the zero tracking error in the finite-time even when the input saturation and the uncertainties of the system parameters are present. The augmented dynamic variable that was used to compensate for the input saturation was modified so that the finite-time convergence is ensured. Numerical Simulations are performed for two cases, without the uncertainty and the input saturation and with the uncertainty and the input saturation. In both cases, the proposed controller yielded satisfactory results and in the second case, the superiority of the proposed controller has been more evident than the others. As presented in Table 3, using the proposed controller in Case 2, the aerodynamic and electrical efficiency has been increased by almost 3 % compared to the SOFTSMC controller which is

the most efficient among the existing controllers. Meanwhile, in any kind of controller, the overshoot problem may occur, which can cause an illegal speed in the wind turbine, so in some applications, it is necessary that it should be guaranteed that the speed of the wind turbine can be constrained in a prescribed bound. Furthermore, in practical systems, input delay, sensors and actuator faults occur where may lead to damage to the wind turbine. Apart from that, because of the inherent model uncertainties in the wind turbine, designing a disturbance observer can reduce the input electromagnetic torque and the low-speed shaft torque significantly. Since in the existing controller these limitations are not considered, then the future works can concern the controller design in the presence of state constraint, the robust fault-tolerant control and input delay and disturbance observer design for the wind turbine system.

6. ACKNOWLEDGEMENT

The authors would like to acknowledge the support of the Babol Noshirvani University of Technology through Grant No. BNU/370632/2020.

NOMENCLATURE

C_p	Power coefficient
β	Blade pitch angle
λ	Tip speed ratio
ρ	Air density
R	Wind turbine rotor radius
ω_r	Rotor angular velocity
ω_g	Generator speed
ω_{Ls}	Low speed shaft angular velocity
T_e	Electromagnetic torque
T_{hs}	High speed shaft torque
T_{1s}	Low speed shaft torque
θ_{1s}	Gearbox angular deviation
θ_r	Rotor angular deviation
J_g	Generator inertia
J_r	Rotor inertia
D_r	Rotor damping coefficient
D_g	Generator damping coefficient
D_{1s}	Low speed shaft damping coefficient
n_g	Gearbox ratio
J_t	Total inertia of the turbine
D_t	Total external damping of the turbine
T_g	Generator torque in the rotor side

Abbreviations

VSWT	Variable speed wind turbine
MPPT	Maximum power point tracking
PI	Proportional-integral
PID	Proportional-integral-derivative
LQ	Linear-quadratic
LQG	Linear–quadratic–Gaussian
SMC	Sliding mode control
ISMC	Integral sliding mode control
TSMC	Terminal sliding mode control
ITSMC	Integral terminal sliding mode control
NTSMC	Non-singular terminal sliding mode control
FOSMC	First order sliding mode control
SOSMC	Second order sliding mode control
SOFTSMC	Second-order fast terminal sliding mode control
WT	Wind turbine
IAE	Integral of absolute error
ISE	Integral of square error
ITAE	Integral of time multiply absolute error
DFIG	Doubly-fed induction generator
NN	Neural network
RBF	Radial-basis-function
IPMSG	Interior permanent magnet synchronous generator
LMI	Linear matrix inequality

APPENDICES

Appendix A. Power coefficient properties

The power coefficient of the wind turbine C_p can be expressed as follows:

$$C_p(\lambda,\beta) = c_1\left(\frac{c_2}{\lambda_i} - c_3\beta - c_4\right)\exp\left(\frac{-c_5}{\lambda_i}\right) + c_6\lambda$$
$$\frac{1}{\lambda_i} = \frac{1}{\lambda + 0.08\beta} - \frac{0.035}{\beta^3 + 1} \quad (A.1)$$

The coefficients c_i, i= 1…5 are based on two parameters. The first parameter is the shape of the wind turbine blades and the second parameter is the aerodynamic performance of the blades. These coefficients are considered to be uncertain as:

$$c_i = \bar{c}_i + \Delta c_i \quad i = 1,2,...,5 \quad (A.2)$$

It is also assumed that the uncertainties $\Delta c_i\ i = 1,2,...,5$ are bounded with unknown bounds as follows:

$$|\Delta c_i| \le \rho_{c_i} \quad (A.3)$$

where ρ_{c_i} are the unknown positive constants.

Thus, the following functions can be defined:

$$h_1(\lambda,\beta) = \left(\frac{\bar{c}_2}{\lambda_i} - \bar{c}_3\beta - \bar{c}_4\right)$$
$$h_2(\lambda,\beta) = c_1\left(\frac{\Delta c_2}{\lambda_i} - \Delta c_3\beta - \Delta c_4\right) + \Delta c_1\, h_1(\lambda,\beta)$$
$$\bar{C}_p(\lambda,\beta) = \bar{c}_1 h_1(\lambda,\beta)\exp\left(\frac{\bar{c}_5}{\lambda_i}\right) + \bar{c}_6\lambda$$
$$\Delta C_p(\lambda,\beta) = \left[\bar{c}_1\, h_1(\lambda,\beta) + h_2(\lambda,\beta)\right] \times\left[\exp\left(\frac{\bar{c}_5}{\lambda_i}\right)\left(\exp\left(\frac{\Delta c_5}{\lambda_i}\right) - 1\right)\right] + h_2(\lambda,\beta)\exp\left(\frac{\bar{c}_5}{\lambda_i}\right) + \Delta c_6\lambda \quad (A.4)$$

Therefore, the power coefficient can be rewritten as:

$$C_p(\lambda,\beta) = \bar{C}_P(\lambda,\beta) + \Delta C_P(\lambda,\beta) \tag{A.5}$$

Appendix B. Proof of theorem 1

To analyze the stability and the finite-time convergence of the proposed controller, consider the following Lyapunov function:

$$V = \frac{1}{2}\sigma(t)^2 \tag{B.1}$$

Differentiating V with respect to time yields:

$$\dot{V} = \sigma(t)\dot{\sigma}(t) \tag{B.2}$$

Using (19), we have:

$$\begin{aligned}\dot{\sigma}(t) &= \frac{k_{1\sigma}\, p}{q} s(t)^{\frac{p}{q}-1}\dot{s}(t) + k_{2\sigma}\dot{s}(t) + k_{3\sigma}\ddot{s}(t)\\ &= \left(\frac{k_{1\sigma}\, p}{q} s(t)^{\frac{p}{q}-1} + k_{2\sigma}\right)\dot{s}(t) + k_{3\sigma}\ddot{s}(t)\end{aligned} \tag{B.3}$$

Moreover, from (20), (B.4) is obtained as:

$$\ddot{s}(t) = -\gamma\dot{s}(t) + k_p\dot{z}(t) + k_I\left(k_{1I} z(t)^{\frac{p}{q}} + k_{2I} z(t)\right) \tag{B.4}$$

For simplification, the terms $k_{I_1} = k_I k_{1I}$ and $k_{I_2} = k_I k_{2I}$ are defined. By substituting (B.4) into (B.3), (B.5) is obtained as:

$$\begin{aligned}\dot{\sigma}(t) = &\left(\frac{k_{1\sigma} p}{q} s(t)^{\frac{p}{q}-1} + k_{2\sigma} - k_{3\sigma}\gamma\right)\dot{s}(t) + \left(k_p\dot{z}(t)\right.\\ &\left. + k_{I_1} z(t)^{\frac{p}{q}} + k_{I_2} z(t)\right) k_{3\sigma}\end{aligned} \tag{B.5}$$

On the other hand, the time derivative of $z(t)$ can be calculated as follows:

$$\begin{aligned}\dot{z}(t) &= \dot{\omega}_r(t) - \dot{\omega}_{r_{opt}}(t) + \dot{\eta}(t)\\ &= \frac{1}{\bar{J}_t}\left[\bar{T}_a - \bar{D}_t\omega_r - n_g T_e + d(\lambda,\beta,V,\omega_r)\right] - \dot{\omega}_{r_{opt}}(t) + \dot{\eta}(t)\end{aligned} \tag{B.6}$$

Replacing (20) into (B.5), gives:

$$\begin{aligned}\dot{\sigma}(t) = &\left(k_{1\sigma}\frac{p}{q} s(t)^{\frac{p}{q}-1} + k_{2\sigma} - \gamma k_{3\sigma}\right)\times\left(-\gamma s(t) + k_p z(t)\right.\\ &\left. + k_I\left(\int_0^t \left(k_{1I} z(\tau)^{\frac{p}{q}} + k_{2I} z(\tau)\right) d\tau\right)\right.\\ &\left. + k_{3\sigma}\left(k_p\dot{z}(t) + k_{I_1} z(t)^{\frac{p}{q}} + k_{I_2} z(t)\right)\right.\end{aligned} \tag{B.7}$$

By substituting (25), (26) and (B.6) into (B.7), it can be obtained that:

$$\begin{aligned}&\dot{\sigma}(t) = \varphi(-\gamma s(t) + w)\\ &+ k_{3\sigma}k_p\left[\frac{1}{\bar{J}_t}\left[\bar{T}_a - \bar{D}_t\omega_r - n_g T_e + d(\lambda,\beta,V,\omega_r)\right]\right]\\ &- k_{3\sigma}k_p\left[\dot{\omega}_{r_{opt}}(t) + \dot{\eta}(t)\right]\\ &+ k_{3\sigma}\left[k_{I_1} z(t)^{\frac{p}{q}} + \left(k_{I_2} + \frac{k_p}{k_{3\sigma}}\varphi\right) z(t)\right]\\ &= \varphi(-\gamma s(t) + w) + k_{3\sigma}k_p\left[\frac{1}{\bar{J}_t}\left[\bar{T}_a - \bar{D}_t\omega_r\right] - \dot{\omega}_{r_{opt}}(t)\right]\\ &+ k_{3\sigma}\left[k_{I_1} z(t)^{\frac{p}{q}} + \left(k_{I_2} + \frac{k_p}{k_{3\sigma}}\varphi\right) z(t)\right] - \left(n_g k_{3\sigma}\frac{k_p}{\bar{J}_t}\right) T_e\\ &+ k_{3\sigma}k_p\dot{\eta}(t) + \frac{k_{3\sigma}k_p}{\bar{J}_t} d(\lambda,\beta,V,\omega_r)\end{aligned} \tag{B.8}$$

Using (24) and (27), (B.8) becomes:

$$\begin{aligned}\dot{\sigma}(t) &= f - \left(n_g k_{3\sigma}\frac{k_p}{\bar{J}_t}\right) T_e + \frac{k_{3\sigma}k_p}{\bar{J}_t} d(\lambda,\beta,V,\omega_r) + k_{3\sigma}k_p\dot{\eta}(t)\\ &= f - \alpha_1 T_e + \alpha_2\, d(\lambda,\beta,V,\omega_r) + \alpha_3\,\dot{\eta}(t)\\ &= f - \alpha_1 u - \alpha_1\Delta u + \alpha_2\, d(\lambda,\beta,V,\omega_r) + \alpha_3\,\dot{\eta}(t)\end{aligned} \tag{B.9}$$

By replacing (23), (30) and (B.9) into (B.1), (B.2) can be written as:

$$\dot{V} = \sigma(t)\left(-b_1\sigma(t) - b_2\, sign(\sigma(t)) + \alpha_2\, d(\lambda,\beta,V,\omega_r)\right) \tag{B.10}$$

Using (13), the following inequality is derived:

$$\begin{aligned}\alpha_2\,\sigma(t)\, d(\lambda,\beta,V,\omega_r) &\le |\sigma(t)|\,\alpha_2\,|d(\lambda,\beta,V,\omega_r)|\\ &\le |\sigma(t)|\,\alpha_2\bar{\delta}\end{aligned} \tag{B.11}$$

Considering (B.11), (B.10), the following inequality holds:

$$\dot{V} \le -2A_1 V - \sqrt{2}A_2 V^{\frac{1}{2}} \tag{B.12}$$

where $A_1 = b_1$ and $A_2 = b_2 - \alpha_2\bar{\delta}$.

Using (B.12) and according to Lemma 2.1, the time that it takes for V to tend to zero can be calculated as:

$$t_r = t_0 + \frac{1}{A_1} Ln\left(\frac{2A_1 V(t_0)^{\frac{1}{2}} + \sqrt{2}\,A_2}{\sqrt{2}\,A_2}\right) \tag{B.13}$$

when V converges to zero, based on (B.1), $\sigma(t)$ becomes zero, i.e.:

$$\dot{s}(t) + \frac{k_{2\sigma}}{k_{3\sigma}} s(t) + \frac{k_{1\sigma}}{k_{3\sigma}} s(t)^{\frac{p}{q}} = 0 \tag{B.14}$$

Using (B.14) and Lemma 2.1, the time, that it takes for s to become zero, can be calculated as below:

$$t_{s_1} = t_r + \frac{k_{3\sigma} q}{k_{2\sigma}(q-p)} \mathrm{Ln}\left(\frac{k_{2\sigma}\, s(t_r)^{1-\frac{p}{q}} + k_{1\sigma}}{k_{1\sigma}} \right) \quad \text{(B.15)}$$

when S converges to zero, consequently $\dot{s}$ tends to zero and based on (20), it can be deduced that:

$$\dot{s}(t) + \gamma s(t) = k_p\, z(t) + k_I \left(\int_0^t (k_{1I}\, z(\tau)^{\frac{p}{q}} + k_{2I}\, z(\tau))\, d\tau \right) = 0 \quad \text{(B.16)}$$

By differentiating (B.16), the following equation is obtained:

$$\dot{z}(t) + \frac{k_{I_1}}{k_p} z(t) + \frac{k_{I_2}}{k_p} z(t)^{\frac{p}{q}} = 0 \quad \text{(B.17)}$$

Now, based on Lemma 2.1 and (B.17), the time that it takes for $z(t)$ to become zero, is calculated as:

$$t_s = t_{s_1} + \frac{k_P\, q}{k_{I_2}(q-p)} \mathrm{Ln}\left(\frac{k_{I_2}\, z(t_{s_1})^{1-\frac{p}{q}} + k_{I_1}}{k_{I_1}} \right) \quad \text{(B.18)}$$

Since the time derivative of the Lyapunov Function is negative, so it can be concluded that the overall system is stable and all of the closed-loop signals are bounded. Therefore, Δu can be bounded by a positive constant like $\overline{\Delta u}$. It should be noticed that, if a Lyapunov function like $V = \frac{1}{2}\eta(t)^2$ is considered, and if the inequality $b_4 > \frac{\alpha_1}{\alpha_3}\overline{\Delta u}$ holds, according to the Lemma 2.1 and similarly to the previous proof, the auxiliary variable $\eta(t)$ converges to zero in finite-time. When $z(t)$ and $\eta(t)$ tend to zero in finite-time, based on $z(t) = e(t) + \eta(t)$, the speed tracking error $e(t)$ also converges to zero in finite-time t_s and therefore the proof is completed.

REFERENCES

1. Bagheri, P. and Sun, Q., "Adaptive robust control of a class of non-affine variable-speed variable-pitch wind turbines with unmodeled dynamics", ***ISA Transactions***, Vol. 63, (2016), 233-241. (https://doi.org/10.1016/j.isatra.2016.04.008).
2. Kumar, D. and Chatterjee, K., "A review of conventional and advanced MPPT algorithms for wind energy systems", ***Renewable and Sustainable Energy Reviews***, Vol. 55, (2016), 957-970. (https://doi.org/10.1016/j.rser.2015.11.013).
3. Mérida, J., Aguilar, L.T. and Dávila, J., "Analysis and synthesis of sliding mode control for large scale variable speed wind turbine for power optimization", ***Renewable Energy***, Vol. 71, (2014), 715-728. (https://doi.org/10.1016/j.renene.2014.06.030).
4. Hand, M.M., "Variable-speed wind turbine controller systematic design methodology: A comparison of nonlinear and linear model-based designs", ***National Renewable Energy Laboratory report TP-500-25540***, National Renewable Energy Laboratory, Golden, Colorado, (1999). (https://doi.org/10.2172/12172).
5. Ma, X., "Adaptive extremum control and wind turbine control", Ph.D. thesis, Informatics and Mathematical Modelling, Technical University of Denmark, DTU, DK-2800 Kgs. Lyngby, Denmark, (May 1997).
6. Steinbuch, M., "Dynamic modelling and robust control of a wind energy conversion system", Ph.D. thesis, Delft University of Technology, (November 1989). (ISBN: 90-9003143-X).
7. Bongers, P., "Modeling and identification of flexible wind turbines and a factorizational approach to robust control", Ph.D. thesis, Delft University of Technology, (1994). (ISBN: 90-370-0100-9).
8. Ekelund, T., "Speed control of wind turbines in the stall region", ***Proceedings of IEEE International Conference on Control and Applications (CCA)***, Glasgow, U.K., (1994), 227-232. (https://doi.org/10.1109/CCA.1994.381194).
9. Novak, P., Ekelund, T., Jovik, Y. and Schmidtbauer, B., "Modeling and control of variable-speed wind-turbine drive system dynamics", ***IEEE Control Systems Magazine***, Vol. 15, No. 4, (1995), 28-37. (https://doi.org/10.1109/37.408463).
10. Ebrahimkhani, S., "Robust fractional order sliding mode control of doubly-fed induction generator (DFIG)- based wind turbines", ***ISA Transactions***, Vol. 63, (2016), 343-354. (https://doi.org/10.1016/j.isatra.2016.03.003).
11. Saravanakumar, R. and Jena, D., "Validation of an integral sliding mode control for optimal control of a three blade variable speed variable pitch wind turbine", ***International Journal of Electrical Power & Energy Systems***, Vol. 69, (2015), 421-429. (https://doi.org/10.1016/j.ijepes.2015.01.031).
12. Bossoufi, B., Karim, M., Lagrioui, A., Taoussi, M. and Derouich, A., "Observer backstepping control of DFIG-generators for wind turbines variable-speed: FPGA-based implementation", ***Renewable Energy***, Vol. 81, (2015), 903-917. (https://doi.org/10.1016/j.renene.2015.04.013).
13. Şeker, M., Zergeroğlu, E. and Tatlicioğlu, E., "Non-linear control of variable-speed wind turbines with permanent magnet synchronous generators: A robust backstepping approach", ***International Journal of Systems Science***, Vol. 47, No. 2, (2016), 420-432. (https://doi.org/10.1080/00207721.2013.834087).
14. Moradi, H. and Vossoughi, G., "Robust control of the variable speed wind turbines in the presence of uncertainties: A comparison between H∞ and PID controllers", ***Energy***, Vol. 90, Part 2, (2015), 1508-1521. (https://doi.org/10.1016/j.energy.2015.06.100).
15. Jafarnejadsani, H., Pieper, J. and Ehlers, J., "Adaptive control of a variable-speed variable-pitch wind turbine using RBF neural network", ***IEEE Transactions on Control Systems Technology***, Vol. 21, No. 6, (2012), 216-222. (https://doi.org/10.1109/TCST.2012.2237518).
16. Saoudi, K. and Harmas, M.N., "Enhanced design of an indirect adaptive fuzzy sliding mode power system stabilizer for multi-machine power systems", ***International Journal of Electrical Power & Energy Systems***, Vol. 54, (2014), 425-431. (https://doi.org/10.1016/j.ijepes.2013.07.034).
17. Eker, I., "Second-order sliding mode control with experimental application", ***ISA Transactions***, Vol. 49, No. 3, (2010), 394-405. (https://doi.org/10.1016/j.isatra.2010.03.010).
18. Pukdeboon, C. and Kumam, P., "Robust optimal sliding mode control for spacecraft position and attitude maneuvers", ***Aerospace Science and Technology***, Vol. 43, (2015), 329-342. (https://doi.org/10.1016/j.ast.2015.03.012).
19. Chiu, C., "Derivative and integral terminal sliding mode control for a class of MIMO nonlinear systems", ***Automatica***, Vol. 48, No. 2, (2012), 316-326. (https://doi.org/10.1016/j.automatica.2011.08.055).
20. Feng, Y., Yu, X. and Man, Z., "Non-singular terminal sliding mode control of rigid manipulators", ***Automatica***, Vol. 38, No. 12, (2002), 2159-2167. (https://doi.org/10.1016/S0005-1098(02)00147-4).
21. Mondal, S. and Mahanta, C., "Adaptive second order terminal sliding mode controller for robotic manipulators", ***Journal of the Franklin Institute***, Vol. 351, No. 4, (2014), 2356-2377. (https://doi.org/10.1016/j.jfranklin.2013.08.027).
22. Feng, Y., Yu, X. and Han, F., "On nonsingular terminal sliding mode control of nonlinear systems", ***Automatica***, Vol. 49, No. 6, (2013), 1715-1722. (https://doi.org/10.1016/j.automatica.2013.01.051).
23. Abolvafaei, M. and Ganjefar, S., "Maximum power extraction from a wind turbine using second-order fast terminal sliding mode control", ***Renewable Energy***, Vol. 139, (2019), 1437-1446. (https://doi.org/10.1016/j.renene.2019.03.044).
24. Azar, A.T. and Serrano, F.E., Design and modelling of anti wind up PID controllers, Complex system modelling and control through intelligent soft computations, Vol. 319, Springer, Switzerland, (2015), 1-44. (https://doi.org/10.1007/978-3-319-12883-2_1).

25. Zhang, X., Zhao, J. and Li, X., "Stability analysis and design of uncertain discrete-time switched systems with actuator saturation using anti-windup and multiple Lyapunov functions approach", ***Asian Journal of Control***, Vol. 19, No. 1, (2017), 325-331. (https://doi.org/10.1002/asjc.1364).
26. Chen, M., Tao, G. and Jiang, B., "Dynamic surface control using neural networks for a class of uncertain nonlinear systems with input saturation", ***IEEE transactions on neural networks and learning systems***, Vol. 26, No. 9, (2014), 2086-2097. (https://doi.org/10.1109/TNNLS.2014.2360933).
27. Edalati, L., Sedigh, A.K., Shooredeli, M.A. and Moarefianpour, A., "Adaptive fuzzy dynamic surface control of nonlinear systems with input saturation and time-varying output constraints", ***Mechanical Systems and Signal Processing***, Vol. 100, (2018), 311-329. (https://doi.org/10.1016/j.ymssp.2017.07.036).
28. Chen, Q., Shi, L., Na, J., Ren, X. and Nan, Y., "Adaptive echo state network control for a class of pure-feedback systems with input and output constraints", ***Neurocomputing***, Vol. 275, (2018), 1370-1382. (https://doi.org/10.1016/j.neucom.2017.09.083).
29. Cui, R., Zhang, X. and Cui, D., "Adaptive sliding-mode attitude control for autonomous underwater vehicles with input nonlinearities", ***Ocean Engineering***, Vol. 123, (2016), 45-54. (https://doi.org/10.1016/j.oceaneng.2016.06.041).
30. Li, Y., Tong, S. and Li, T., "Adaptive fuzzy output-feedback control for output constrained nonlinear systems in the presence of input saturation", ***Fuzzy Sets and Systems***, Vol. 248, (2014), 138-155. (https://doi.org/10.1016/j.fss.2013.11.006).
31. Zhang, Q. and Dong, J., "Disturbance-observer-based adaptive fuzzy control for nonlinear state constrained systems with input saturation and input delay", ***Fuzzy Sets and Systems***, Vol. 392, (2019), 77-92. (https://doi.org/10.1016/j.fss.2019.06.014).
32. Dastres, H., Rezaie, B. and Baigzadehnoe, B., "Neural-network-based adaptive backstepping control for a class of unknown nonlinear time-delay systems with unknown input saturation", ***Neurocomputing***, Vol. 398, (2020), 131-152. (https://doi.org/10.1016/j.neucom.2020.02.070).
33. Qiao, W., Qu, L. and Harley, R.G., "Control of IPM synchronous generator for maximum wind power generation considering magnetic saturation", ***IEEE Transactions on Industry Applications***, Vol. 45, No. 3, (2009), 1095-1105. (https://doi.org/10.1109/TIA.2009.2018914).
34. Torchani, B., Sellami, A. and Garcia, G., "Variable speed wind turbine control by discrete-time sliding mode approach", ***ISA Transactions***, Vol. 62, (2016), 81-86. (https://doi.org/10.1016/j.isatra.2016.01.001).
35. Zaafouri, Ch., Torchani, B., Sellami, A. and Garcia, G., "Uncertain saturated discrete-time sliding mode control for a wind turbine using a two-mass model", ***Asian Journal of Control***, Vol. 20, No. 2, (2018), 802-818. (https://doi.org/10.1002/asjc.1594).
36. Errouissi, R., Al-Durra, A. and Debouza, M., "A novel design of PI current controller for PMSG-based wind turbine considering transient performance specifications and control saturation", ***IEEE Transactions on Industrial Electronics***, Vol. 65, No. 11, (2018), 8624-8634. (https://doi.org/10.1109/TIE.2018.2814007).
37. Thomsen, S.C., "Nonlinear control of a wind turbine", MS thesis, Informatics and Mathematical Modelling, Technical University of Denmark, DTU, DK-2800 Kgs. Lyngby, Denmark, (2006).
38. Hoseinzadeh, S., Bahrami, A., Mirhosseini, S.M., Sohani, A. and Heyns, P.S., "A detailed experimental airfoil performance investigation using an equipped wind tunnel", ***Flow Measurement and Instrumentation***, Vol. 72, (2020), 101717. (https://doi.org/10.1016/j.flwmeasinst.2020.101717).
39. Bahrami, A., Hoseinzadeh, S., Heyns, P.S. and Mirhosseini, S.M., "Experimental investigation of co-flow jet's airfoil flow control by hot wire anemometer", ***Review of Scientific Instruments***, Vol. 90, (2019), 125107. (https://doi.org/10.1063/1.5113592).
40. Hammerum, K., "A fatigue approach to wind turbine control", MS thesis, Informatics and Mathematical Modelling, Technical University of Denmark, DTU, DK-2800 Kgs. Lyngby, Denmark, (2006).
41. Colombo, L., Corradini, M.L., Ippoliti, G. and Orlando, G., "Pitch angle control of a wind turbine operating above the rated wind speed: A sliding mode control approach", ***ISA Transactions***, Vol. 96, (2020), 95-102. (https://doi.org/10.1016/j.isatra.2019.07.002).
42. Mobayen, S. and Tchier, F., "Nonsingular fast terminal sliding-mode stabilizer for a class of uncertain nonlinear systems based on disturbance observer", ***Scientia Iranica***, Vol. 24, No 3, (2017), 1410-1418. (https://doi.org/10.24200/SCI.2017.4123).
43. Elbaset, A.A., Mohamed, Y.S., El-Sayed, A.-H.M. and Ahmed, A.E.H.A., Wind driven doubly fed induction generator, Springer, (2018). (https://doi.org/10.24200/SCI.2017.4123).
44. Jing, X., "Modeling and control of a doubly-fed induction generator for wind turbine-generator systems", MS thesis, Marquett University, Milwaukee, USA, (2012).

Journal of Renewable Energy and Environment

Research Article

Journal Homepage: www.jree.ir

Biogas Potentiality Through Waste Management in Bangladesh

Parvez Mosharraf[a], Md. Saroyar Zahan[a], Dilip Kumar Das[b], Suman Chowdhury[a*]

[a] *Department of Electrical and Electronic Engineering, International University of Business Agriculture and Technology, Uttara Model Town, Dhaka 1230, Bangladeh.*
[b] *Department of Mathematics, International University of Business Agriculture and Technology, Uttara Model Town, Dhaka 1230, Bangladeh.*

PAPER INFO

Paper history:
Received 12 March 2020
Accepted in revised form 09 August 2020

Keywords:
Anaerobic Digestion,
Biogas,
Landfill,
Waste,
Power

ABSTRACT

This study offers an effective solution to meet the growing demands of biogas plants for energy. This paper presents a model and simulates the digestion process of biogas production from the organic and food processing waste that contains high moisture. Biogas is produced by bacteria through the bio-degradation of organic material under anaerobic conditions. According to the findings, in case of biogas production, the broiler chicken manure is approximately 88 %. From the analysis, it is observed that the chicken broiler waste is approximately 88 % more efficient than the unsorted waste. In addition, in the case of digestate, the cow manure is approximately 6.25 % more efficient than the garden waste. The present study aims to investigate the performance of different types of wastes regarding biogas production. To this end, different types of waste were considered in data analysis. According to the data analysis, biogas production is highly affected by the type of waste.

https://doi.org/10.30501/jree.2020.222856.1089

1. INTRODUCTION

Natural generation of biogas is an important part of bio-geochemical carbon cycle. It can be used both in rural and urban areas. Biogas contains 40 % to 60 % methane which is an excellent source of renewable energy. Biogas (bio fuel) is a mixture of gases that usually consist of a considerable amount of methane and some other constituents (carbon dioxide, (CO_2) 25-50 %, and some negligible amounts of N_2, H_2, H_2S and O_2). Biogas is produced in situations where organic matters decompose in the absence of Oxygen. Biogas is produced from highly moisturized content, like food wastes and animal manure is essential to the biological treatment method, namely anaerobic digestion. An environment devoid of oxygen is needed for bacteria to activate the anaerobic digestion process. In Bangladesh with a population of 160 million people, the increasing rate of energy consumption due to its industrial development and fast-paced process of urbanization is notable. To maintain and improve economic growth and achieve the Sustainable Development Goal (SDG), energy supply is required. Optimization of the anaerobic digestion process has a huge potential to produce maximum biogas and reduce the environment pollution through waste management within a short period prior to landfill [1]. Electrical Resistivity Tomography (ERT) techniques are applicable to address environmental and engineering issues [2]. Farm-based anaerobic digestion will play a key role in waste management and biomass energy production in the future. Anaerobic digestion technology is a suitable, viable option in the case of biogas productions. In addition, this technology can be used in fuel internal combustion engines to run a generator that produces electricity [3]. Normally, 40 % to 60 % of methane is obtained from manure, after 28 days of fermentation at a temperature of 40 ^{o}C [4]. The case study of Greece shows that this operation is profitable in 20 years at an energy efficiency level of 33 %. Moreover, biogas production is reduced with increase in the age of waste and disposal [5]. Disposed solid waste made by landfill produces enormous amount of biogas whose main constituent is methane which is responsible for global warming; in this respect regular study and data maintenance are necessary to reduce the green house gas (GHG) emission [6]. The rate and quality of biogas production depend on many factors such as waste type, temperature, humidity, moisturized components, period of fermentation, size of bacteria, and pH [7]. Since biogas can supply 25 % of all required bio-energy, EU has set a goal to provide 20 % of its required energy from renewable energy by 2020 [8]. If 33 % more volatile solids (VS) are added from fats, oil, grease (FOG) and food waste for anaerobic digestion, biogas production will increase to 60 % or more [9]. Biogas production along with anaerobic co-digestion process from animal manure and organic waste not only solves the energy problem but also protects the environment and helps the waste management sector. The biogas components depend on favorable environmental state and type of decomposing materials. Family based biogas plant is a solution to mitigating GHG emissions and decreasing the dependence of dung-based biogas plant, LPG or firewood used as kitchen fuel [10]. Olive oil industries are held

*Corresponding Author's Email: suman@iubat.edu (S. Chowdhury)
URL: http://www.jree.ir/article_111670.html

Please cite this article as: Mosharraf, P., Zahan, Md.S., Das, D.K. and Chowdhury, S., "Biogas potentiality through waste management in Bangladesh", ***Journal of Renewable Energy and Environment (JREE)***, Vol. 7, No. 4, (2020), 44-49. (https://doi.org/10.30501/jree.2020.222856.1089).

responsible for serious environmental repercussions since waste management is a costly arduous task, biogas production can be used as an alternative solution [11]. The quality of biogas is improved by mixing water chestnut, water hyacinth, and cow dung after a period of digestion [12]. A robust methodology to analyze and evaluate energy demand at every steps is required to improve biogas production at a particular biogas plant [13]. To obtain one unit of biogas, 0.56J non-renewable energy is required [14]. In the case of performance evaluation, data comparison on the routine basis is vital for different plants [15]. Food waste is the most suitable option for anaerobic digestion for its high biodegradability and methane output [16]. 90 % more methane is produced within 40-50 days of fermentation [17]. Large biogas plant can produce significant amount of gas used for industrial purposes [18]. Biogas production in Europe is gaining foothold and growing [19]. Under SNV (Netherlands Development Organization) project 600000 m^3 biogas was yielded from 300000 biogas plants until 2009 [20]. Biogas production is economically viable in Bangladesh [21]. Power produced from municipal and agricultural waste 80 % of which are organic in Hazaribagh (total area 0f 5.65 km^2) as one of the densely populated areas (population density of 32,856/km^2) of Dhaka city, can play a significant role in addressing the electricity crisis in this region through biogas production [22]. Bangladesh, one of the densely populated countries with more than 160 million people, is a 147000 km^2 land, 33 % of which enjoys electricity coverage [23]. The projected energy demands are predicted to be 19000 MW and 34000 MW by 2100 and 2030, respectively [24].

Since industries are still highly dependent on traditional energies (electricity, natural gas etc.), it is the most appropriate time for transition from this energy to renewable energies to solve the electricity crisis and kitchen fuel. The following sections discuss how the biogas production and usage will reduce the load of traditional energies and solve waste management problems, especially MSW problems in Bangladesh.

2. METHODOLOGY

1. Numerous studies on renewable energies were carefully investigated before conducting the actual research.

2. The present paper aims to solve two problems simultaneously: searching for alternative energy and managing waste with emphasis on biogas production and its popularity in Bangladesh.

3. Substrates (MSW, animal manure, food waste, fats, oil, plant waste, etc.) are stored for anaerobic digestion. The anaerobic digestion process is run around 40 days at temperatures of 35-45 ^oC for fermentation. Since the type of mixtures plays a vital role in improving both quality and quantity of gas, substrates of high biodegradability are added even more. After the suggested period of time, the inlet pipe opens to collect gas either already stored or being used, through dehumidified for cooking. It we can be connected to a generator unit so that it can be converted into electricity.

4. A MATLAB simulation was carried out to examine the potential of biogas production. Moreover, some related data were collected from online sources to investigate the overall performance of biogas production with regard to various types of waste.

5. Finally, results were achieved through data analysis.

A flowchart was also presented to show the working scheme throughout the research period (Figure 1).

3. BIOGAS POWER PRINCIPLE

There are a number of factors affecting the biogas production, considering the organic content of waste. These factors include time span and constitution of waste, humidity, temperature, pH-varying with depth of filling, population of microbes, and quality and quantity of alimentary substances [5, 6, 7]. The rate of biogas production is given by the first-order kinetic equation expressed in Equation (1) [6, 7, 9].

$$\frac{dC}{dt} = -kC \quad (1)$$

According to the above kinetic equation and empirical data, a numerical model called “Landfill Gas Emissions Model” was developed under the supervision of EPA (Environmental Protection Agency) and used to measure biogas generation. In the following Equation (2) shows how to measure biogas generation (considering time) [6, 7]:

$$LFG = 2L_0 R (e^{kc} - e^{-kt}) \quad (2)$$

Description of Parameters: LFG =amount of produced biogas during the year, L_0 =potential methane generation capacity (m^3/ton), R =average yearly quantity of waste disposal during the function of the landfill (ton), k =methane generation rate ($year^{-1}$), t= inactive year of the landfill, and c= years passed from the closure of the landfill.

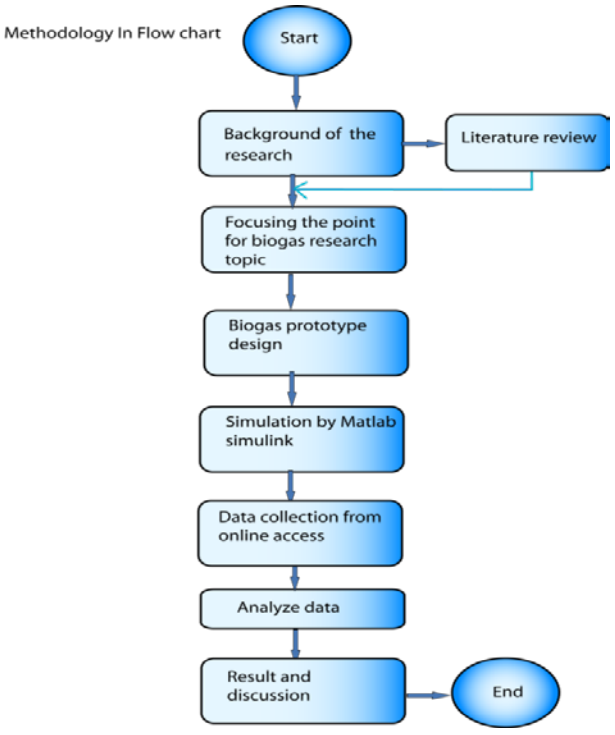

Figure 1. Flowchart of working throughout the research period

According to EPA (“Landfill Gas System Engineering Design Seminar”, 1994), the parameter ‘L_0’ fluctuates between 140-180 m^3/ton and, also the parameter ‘k’ experiences fluctuation as in the following:

->For wet climates between 0.1 - 0.35
->For dry climates between 0.02 - 0.1
->For intercalary climates between 0.05 – 0.1

In the case of the landfill of Volos, the following parameters are included to the biogas production model:

L_0= 120 m^3/ton for utmost secure reasons, k=0.05/year, R=70000 ton, t=25 year, and c=20 years.

Figure 2 shows the simulink model for simulating of biogas production. In addition Figure 3 represents the relationship between the amount of produced biogas and amount of methane gas. The amount of methane gas increases as the amount of biogas increases.

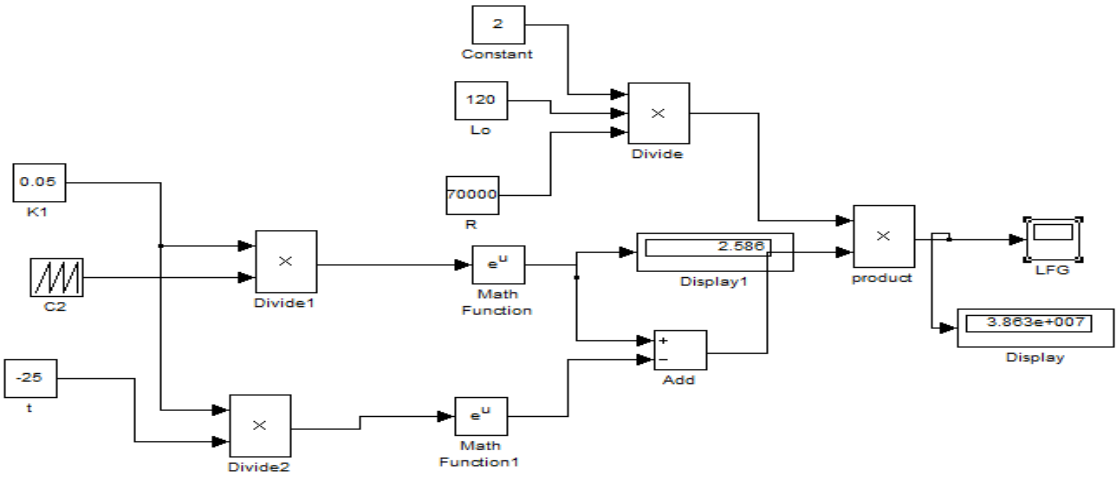

Figure 2. Simulation and calculation diagram

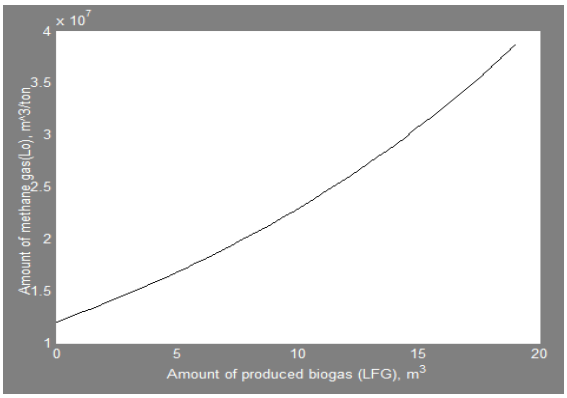

Figure 3. Amount of produced biogas vs amount of methane gas

4. DESIGN OF BIOGAS PRODUCTION

According to Figure 4, biogas is pumped from sewage pump and the waste comes to the biogas chamber, in biogas chamber, the organic matters will break down in the absence of oxygen casing to generate biogas. Then gas passes through the pipe and comes to the gas dehumidification/elaboration chamber where moisture and humidity are reduced. Following the biogas production the rest of the waste will pass out the outlet, which can be used in agricultural fields as a fertilizer. There are two pipes connected to the gas dehumidification; one for cooking purposes and the other connected to the gas generator.

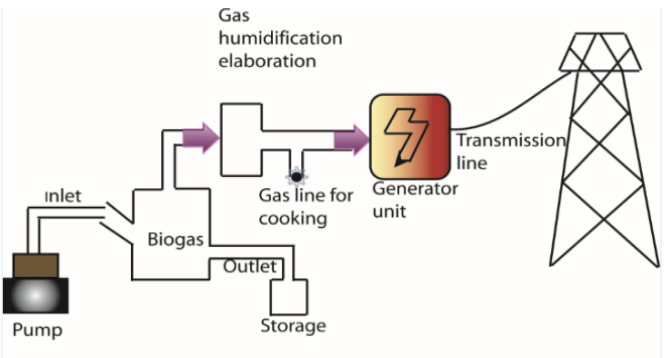

Figure 4. Proposed biogas system

Table 1. Biogas production and energy scenarios of Bangladesh [23, 25]

Waste category	Biogas (m^3)	Electricity (MW)	Percentage of generated electricity
Cattle dung	8670000	12211	50.4
Municipal waste	1634000	2301	9.5
Poultry waste	2153400	3033	12.5
Human excreta	4736000	6670	27.5
Total	17193400	24215	EMRED ~ 100

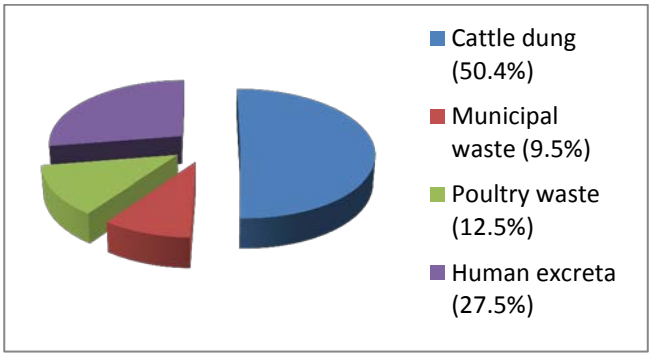

Figure 5. Amount of electricity production from different wastes

According to Figure 5, maximum amount of electricity is produced (50.4 %) from cattle dung using 23 million cattle in 2011. In addition, Table 1 shows the possibility of producing a considerable amount of electricity and biogas. Biogas can be used as an alternative to kitchen fuel and other needed energies in Bangladesh with more than 64 % [26] of people living in rural areas.

5. ESTIMATION

The biogas production, with considering various wastes, is estimated by biogas estimator software called Anaerobic Digestion Calculator [27].

Table 2. Biogas estimation for vegetable waste

Amount of waste (tons/year)	Total digestate (tons/year)	Biogas production (m^3/year)	Electricity production (kWh/year)	Capacity of biogas power plant (kW)
50	39.5	6,412.5	12,636	1.44
100	79	12,825	25,272	2.88
150	118.5	19,237.5	37,908	4.33
200	158	25,650	50,544	5.77
500	395	64,125	126,360	14.42
1,000	790	128,250	252,720	28.85
2,000	1,580	256,500	505,440	57.70

Table 2 shows that the efficiency of the to-be-digestated waste is around 90 %, whereas biogas production rate can reach 256500 m^3/year for the annual waste of 2000 tons.

Table 3 suggests that unsorted waste is 7.59 % more efficient than the wet vegetable waste with respect to digestate. However, vegetable waste is around 50.4 % more efficient than the unsorted waste regarding biogas production.

Table 3. Biogas estimation for unsorted waste

Amount of waste (tons/year)	Total digestate (tons/year)	Biogas production (m^3/year)	Electricity production (kWh/year)	Capacity of biogas power plant (kW)
50	42.5	4,263.5	8,401.5	0.95
100	85	8,527	16,803	1.91
150	127.5	12,790.5	25,204.5	2.88
200	170	17,054	33,606	3.84
500	425	42,635	84,015	9.6
1,000	850	85,270	168,030	19.2
2,000	1,700	170,540	336,060	38.36

Table 4. Biogas estimation for cow manure

Amount of waste (tons/year)	Total digestate (tons/year)	Biogas production (m^3/year)	Electricity production (kWh/year)	Capacity of biogas power plant (kW)
50	42.5	4,275	8,424	0.96
100	85	8,550	16,848	1.92
150	127.5	12,825	25,272	2.88
200	170	17,100	33,696	3.85
500	425	42,750	84,240	9.62
1,000	850	85,500	168,480	19.23
2,000	1,700	171,000	336,960	38.46

Table 4 represents almost the same amounts of manure as the ones shown in Table 3, while Tables 5 and 6 show an almost similar amounts of manure to the ones listed in Table 2. Finally, Table 7 shows that chicken broiler waste is the most efficient of all other wastes, as discussed in this paper.

Table 5. Biogas estimation for garden waste

Amount of waste (tons/year)	Total digestate (tons/year)	Biogas production (m^3/year)	Electricity production (kWh/year)	Capacity of biogas power plant (kW)
50	40	6,080	11,980.5	1.37
100	80	12,160	23,961	2.73
150	120	18,240	35,941.5	4.1
200	160	24,320	47,922	5.5
500	400	60,800	119,805	13.68
1,000	800	121,600	239,610	27.35
2,000	1,600	243,200	479,220	54.7

Table 6. Biogas estimation for organic waste

Amount of waste (tons/year)	Total digestate (tons/year)	Biogas production (m^3/year)	Electricity production (kWh/year)	Capacity of biogas power plant (kW)
50	40	6,056.5	11,934	1.36
100	80	12,113	23,868	2.72
150	120	18,169.5	35,802	4.09
200	160	24,226	47,736	5.45
500	400	60,565	119,340	13.62
1,000	800	121,130	238,680	27.25
2,000	1,600	242,260	477,360	54.49

Table 7. Biogas estimation for chicken broiler

Amount of waste (tons/year)	Total digestate (tons/year)	Biogas production (m^3/year)	Electricity production (kWh/year)	Capacity of biogas power plant (kW)
50	38	8015.5	15,795	1.8
100	76	16,031	31,590	3.61
150	114	24,046.5	47,385	5.41
200	152	32,062	63,160	7.21
500	380	80,155	157,950	18.03
1,000	760	160,310	315,900	36.06
2,000	1,520	320,620	631,800	72.12

6. CONCLUSIONS

Biogas is one of the important economical and environmentally-friendly energy sources used for the electricity generation. Biogas is considered an appropriate alternative to fossil fuel since biogas has no detrimental impacts on the environment. In addition, counted as its most notable advantage, it can be used to produce electricity and reduce the excessive demand for fossil fuels. The present study aims to show potential of wastes' to produce biogas. Among six different types of waste considered in this study, the chicken broiler waste has shown maximum efficiency. The data analysis suggests that vegetable waste has better efficiency than garden and organic wastes. Vegetable waste is available Bangladesh. Therefore, vegetable waste can be collected from urban and rural areas to produce a large amount of electricity. Besides, cow manure is also efficient in biogas production. Where the cow firm is available, electricity can be produced through biogas generation from cow manure at lowers costs. The demand for Biogas is increasing at a high level coping with the increment of total energy demand. Considerable numbers of biogas plants have already been established in the rural and urban areas by the municipality in Bangladesh, the related data of which are shown in Table 1 and Figure 4. The application of this system will significantly reduce global warming and greenhouse effect.

7. ACKNOWLEDGEMENT

We are heartily grateful to Prof. Dr. Bishwajit Saha coordinator at EEE Department for his valuable support.

REFERENCES

1. Juanga, J., Kuruparan, P. and Visvanathan, C., "Optimizing combined anaerobic digestion process of organic fraction of municipal solid waste (MSW)", ***Proceedings of International Conference on Integrated Solid Waste Management in South Asian Cities***, Siem Reap, Combodia, (5-7 July, 2005), PMID: 17346005. (https://doi.org/10.1177/0734242X07072085).
2. Soupios, P.M., Vallianatos, F., Papadopoulos, I.Th., Makris, J.P. and Marinakis, M., "Surface-geophysical investigation of a landfill in Hania, Crete", ***Proceedings of The International Workshop in Geoenvironment and Geotechnics***, Milos Island, Greece, (2005).
3. Rozdilsky, J.L., "Farm-based anaerobic digestion in Michigan history, current status and future outlook", ***A Report of the Michigan Biomass Energy Program***, (1997).
4. Lowe, E. and Weber, I., "Appendix to manure into gold", ***Framework for Manure Management in Ontario***, (2 March, 2004).
5. Xydis, G., Nanaki, E. and Koroneos, C., "Exergy analysis of biogas production from a municipal solid waste landfill", ***Elsevier, Sustainable Energy Technologies and Assessments***, Vol. 4, (2013), 20-28. (http://doi.org/10.1016/j.seta.2013.08.003).
6. Kumar, S., Mondal, A.N., Gaikwad, S.A., Devotta, S. and Singh, R.N., "Qualitative assessment of methane emission inventory from municipal solid waste disposal sites: A case study", ***Elsevier, Atmospheric Environment***, Vol. 38, No. 29, (2004), 4921-4929. (https://doi.org/10.1016/j.atmosenv.2004.05.052).
7. "Implementation guide for landfill gas recovery reports in the northeast", ***Final Report Policy, Research Center***, Washington, (9 September, 1994).
8. Holm-Nielsen, J.B., Al Seadi, T. and Oleskowicz-Popiel, P., "The future of anaerobic digestion and biogas utilization", ***Elsevier, Bio-Resource Technology***, Vol. 100, No. 22, (2009), 5478-5484. (https://doi.org/10.1016/j.biortech.2008.12.046).
9. Kuo, J. and Dow, J., "Biogas production from anaerobic digestion of food waste and relevant air quality implications", ***Journal of The Air & Waste Management Association***, Vol. 67, No. 9, (Sep. 2017), (Epub: May 2017), 1000-1011. (https://doi.org/10.1080/10962247.2017.1316326).
10. Singh, P., Singh, P. and Gundimeda, H., "Energy and environmental benefits of family biogas plants in India", ***International Journal of Energy Technology and Policy(IJETP)***, Vol. 10, No. 3-4, (2014), 235-264. (RePEc:ids:ijetpo:v:10:y:2014:i:3/4:p:235-264).
11. Arvanitoyannis, I.S., Kassaveti, A. and Stefanatos, S., "Olive oil waste treatment: A comparative and critical presentation of methods, advantages & disadvantages", ***Taylors and Francis, Critical Reviews in Food Science and Nutrition***, Vol. 47, No. 3, (2007), 187-229. (https://doi.org/10.1080/10408390600695300).
12. Sudhakar, K., Ananthakrishnan, R. and Goyal, A., "Biogas production from a mixture of water hyacinth, water chestnut and cow dung", ***International Journal of Science, Engineering and Technology Research (IJSETR)***, Vol. 2, No. 1, (2013).

13. Lindkvist, E., Johansson, M.T. and Rosenqvist, J., "Methodology for analysing energy demand in biogas production pants-A comparative study of two biogas plants", ***Energies***, Vol. 10, No. 11, (2017), 1822. (https://doi.org/10.3390/en10111822).

14. Zhang, L. and Wang, C., "Energy and GHG analysis of rural household biogas systems in China", ***Energies***, Vol. 7, (2014), 767-784. (https://doi.org/10.3390/en7020767).

15. Havukainen, J., Uusitalo, V., Niskanen, A., Kapustina, V. and Horttanainen, M., "Evaluation of methods for estimating energy performance of biogas production", ***Elsevier, Renewable Energy***, Vol. 66, (2014), 232-240. (https://doi.org/10.1016/j.renene.2013.12.011).

16. Zhang, R., El-Mashad, H.M., Hartman, K., Wang, F., Liu, G., Choate, C. and Gamble, P., "Characterization of food waste as feedstock for anaerobic digestion", ***Elsevier, Bioresource Technology***, Vol. 98, No. 4, (2007), 929-935. (https://doi.org/10.1016/j.biortech.2006.02.039).

17. Gunaseelan, V.N., "Biochemical methane potential of fruits and vegetable solid waste feedstocks", ***Elsevier, Biomass and Bioenergy***, Vol. 26, No. 4, (2004), 389-399. (https://doi.org/10.1016/ j.biombioe.2003.08.006).

18. Bond, T. and Templeton, M.R., "History and future of domestic biogas plants in the developing world", ***Elsevier, Energy and Sustainable Development***, Vol. 15, No. 4, (2011), 347-354. (https://doi.org/ 10.1016/j.esd.2011.09.003).

19. Cividino, S.R.S., "Biogas overview of key technologies-benchmarking and potentials", ***Smart-Energy and Network Excellence, Program***, Italy-Austria, (2007-2013).

20. Ghimire, P.C., "SNV supported domestic biogas programmes in Asia and Africa", ***Renewable Energy***, Vol. 49, (2013), 90-94. (https://doi.org/10.1016/j.renene.2012.01.058).

21. Islam, Md.N., Hoque, S.M.N., Mandal, S., Hasan, A. and Nahian, Md.R., "Prospect of rural electrification through biogas in Bangladesh-design & feasibility study of biogas based electricity facility of a poultry farm", ***Proceedings of International Conference on Mechanical, Industrial and Materials Engineering 2017 (ICMIME2017)***, RUET, Rajshahi, Bangladesh, (28-30 December, 2017), Paper ID: ET-281.

22. Monjurul Hasan, A.S.M. and Ammenberg, J., "Biogas potential from municipal and agricultural residual biomass for power generation in Hazaribagh, Bangladesh–A strategy to improve the energy system", ***Elsevier, Renewable Energy Focus***, Vol. 29, (June 2019), 14-23. (https://doi.org/10.1016/j.ref.2019.02.001).

23. Iqbal, S.A., Rahaman, M.Sh. and Yousuf, A., "Present scenario of biogas technology in Bangladesh-prospects, potentials and barriers", ***Proceedings of The 15th Annual Paper Meet (APM 2013)***, Dhaka, Bangladesh, (2014).

24. Bangladesh power development board, (29 Aug., 2018). (http://www.bpdb.gov.bd/bpdb_new/index.php/site/page/5a3f-2fdb-e75f-3cab-e66b-f70d-5408-cbc9-f489-c31c).

25. Nahian, Md.R. and Islam, Md.N., "Prospects and potential of biogas technology in Bangladesh", ***Proceedings of International Conference on Innovations in Science, Engineering and Technology (ICISET)***, Dhaka, Bangladesh, (2016), 1-4. (https://doi.org/10.1109/ ICISET.2016.7856481).

26. Statista, (https://www.statista.com/statistics/760934/bangladesh-share-of-rural-population/).

27. http://biogasworld.com/biogas-calculations/.

Journal of Renewable Energy and Environment

Research Article

Journal Homepage: www.jree.ir

Investigation of the Synergism Effect and Electrocatalytic Activities of Pt and Ru Nanoparticles Supported on the Carbon Aerogel-Carbon Nanotube (CA-CNT) for Methanol Oxidation Reaction (MOR)

Masoumeh Javaheri[a*], Noushin Salman Tabrizi[b], Amir Rafizadeh[b]

[a] *Department of Ceramic, Materials and Energy Research Center (MERC), MeshkinDasht, Alborz, Iran.*
[b] *Department of Energy, Materials and Energy Research Center (MERC), MeshkinDasht, Alborz, Iran.*

PAPER INFO

Paper history:
Received 14 June 2020
Accepted in revised form 17 August 2020

Keywords:
Fuel Cell,
Methanol,
Synergism,
Aerogel,
Nanotube

ABSTRACT

Given that the catalyst and catalyst support properties have a key role to play in the electrochemical activity of fuel cells, in this research, the synergism effect of Pt and Ru nanoparticles reduced on catalyst support [synthesized Carbon Aerogel-Carbon Nanotube (CA-CNT)] was investigated. The catalyst support was synthesized by sol-gel method and the catalyst nanoparticles were reduced on catalyst support using impregnation and hydrothermal method. Different molar ratios of Pt:Ru (i.e., 0:1, 1:0, 3:1, 2:1, 1:1, 1:2, and 1:3) were applied as electrocatalysts for Methanol Oxidation Reaction (MOR). The electrochemical performance of these catalysts was compared with that of commercial Pt/C (20 % wt) for MOR. The physical properties of the synthesized catalyst support (CNT-CA) were studied using FESEM and BET techniques. Moreover, XRD and ICP analyses were employed for investigating each of the synthesized catalyst (Pt/CNT-CA and Ru/CNT-CA). The cyclic voltammetry and chronoamperometry methods were used to conduct electrochemical analysis. Research results indicated that synthesis methods were reliable. Moreover, CNT-CA had a proper performance as the catalyst support and the Pt:Ru with a 3:1 molar ratio was the best catalyst among all the synthesized catalysts for MOR.

https://doi.org/10.30501/jree.2020.234091.1116

1. INTRODUCTION

Recently, fuel cells have been widely considered as a renewable power source. This is a device that produces electrical energy from chemical energy with high efficiency and without pollution. Among all fuel cells, Polymer Exchange Membrane Fuel Cell (PEMFC) and Direct Methanol Fuel Cell (DMFC) have been widespread investigated due to their good commercial abilities. These work at low temperatures. Since DMFCs operate on liquid fuel and do not need complex apparatuses for humidification and heat management, they are considered as a promising choice for energy industrials in the future [1, 2]. However, a significant challenge of commercialization is the intrinsic cost of these fuel cells. Catalyst layer is an important component of the fuel cell because the reactions occur in it. This layer contains catalyst particles and carbon material as catalyst support [3,4]. Considering the specific properties of platinum (Pt) including high catalytic activity, chemical stability, and high exchange current density, it is the best candidate for the catalyst layer. The carbon black Vulcan XC-72 is commonly used as a catalyst support [5].

*Corresponding Author's Email: m.javaheri@merc.ac.ir (M. Javaheri)
URL: http://www.jree.ir/article_112868.html

The main cost of fuel cell is for the catalyst materials. Different approaches have been attempted so far to reduce the cost and enhance the performance of a fuel cell simultaneously. Some approaches can be pointed out that use multi metal as a catalyst and the improved structure of carbon as a catalyst support. Therefore, the researchers concentrate on use of either Pt alloys or catalyst support materials to reinforce the electrocatalytic efficiency of Pt [6-11].

Bimetallic Pt–Ru electrocatalyst is one of the most widespread ones used due to its bifunctional mechanism for Methanol Oxidation Reaction (MOR) [12-17]. However, the best optimal Pt-Ru ratio has not reached wide agreement. Many studies have found that the 1:1 ratio of Pt: Ru was the best [18-21], but some of researchers reported that the other ratio was optimal for enhancing MOR catalytic activity [22, 23].

In recent years, the role of the nanostructure of carbon supports such as Carbon Nanotubes (CNTs), Carbon Nanofibers (CNFs), carbon aerogels, and nano-plates of graphene has received remarkable interest [24,25]. Some characteristics of carbon nanostructure lead to an efficient MOR, which is the main reason for using them as a catalyst support [26].

It is well known that one of the important factors in the catalytic performance of the electrode in fuel cell is the three-phase zone formation and it is dependent upon the interfacial

Please cite this article as: Javaheri, M., Salman Tabrizi, N. and Rafizadeh, A., "Investigation of the synergism effect and electrocatalytic activities of Pt and Ru nanoparticles supported on the carbon aerogel-carbon nanotube (CA-CNT) for methanol oxidation reaction (MOR)", ***Journal of Renewable Energy and Environment (JREE)***, Vol. 7, No. 4, (2020), 50-55. (https://doi.org/10.30501/jree.2020.234091.1116).

among the catalyst (solid), electrolyte (liquid), and reactant (gas). Therefore, surface area, pore size, and electrical conductivity of the catalyst support could be very significant in attaining high electrocatalytic activity [11,27,28]. Since the CA has a unique structure and properties such as high porosity, high surface area, and chemical stability, it can be used as a catalyst support to enhance electrocatalytic activities [29- 33]. The CNT showed high electrical conductivity as the catalyst support and improved the CA conductivity. For this reason, in many research works, good performances were obtained using the above materials [34,35].

According to the mentioned literatures, two points can be observed: 1) each of CNT or CA has been used as a catalyst support separately; 2) Pt/Ru is synthesized as an alloy on carbon particles. The present research attempts to study the effect of using CNT and CA simultaneously (i.e., CNT-CA) as a catalyst support. Moreover, Pt and Ru are deposited on CNT-CA separately; then, an attempt was made to investigate the electrochemical performance of the mixture of the Pt/CNT-CA and Ru/CNT-CA at different ratios of MOR. In this case, the structure of Pt as an effective and important catalyst is maintained; besides, the presence of Ru has positive effect on the performance of the electrode for MOR.

This study investigates the synergism effect of CNT containing Carbon Aerogel (CA) as the catalyst support and the Pt with Ru bimetallic catalyst for DMFC. The goal of this research is to specify the optimal molar ratio of Pt:Ru in the presence of synergism effect of CNT-CA. In addition to Pt/CNT-CA and Ru/CNT-CA, we select different proportions of Pt:Ru as 1:1, 2:1, 3:1, 1:3, and 1:2 to study the catalyst performance for MOR. However, we compared the synthesis catalyst with commercial Pt/C for MOR. The comparison of obtained electrochemical parameters of Pt/CNT-CA and those of commercial Pt/C shows that CNT-CA is a more efficient catalyst support than the carbon Vulcan XCR72. Our results such as EAS and the ratio of forward to backward peak current (I_b/I_f) indicate that the Pt:Ru with 3:1 ratio has the best performance among all the catalysts studied in this research.

2. EXPERIMENTAL

2.1. Materials

Multi-walled carbon nanotubes were supplied from NeutrinoNeunano.Resorcinol($C_6H_4(OH)_2$), formaldehyde (HC HO), sodium carbonate (Na_2CO_3), and solvents were supplied from Merck. In addition, $RuCl_3$. $3H_2O$, H_2PtCl_6. $6H_2O$, and Nafion solution (5 %) were prepared from Aldrich. Ethylene glycol, glycerol, and 2- propanol were prepared from Merck.

The commercial Pt/C (10 wt % Electrochem Inc.) was used to be compared with the synthesized catalyst.

2.2. Catalyst support (CNT- CA) synthesis

The first step is to functionalize the catalyst support. To this end, the adequate amount of synthesized CNT-CA was refluxed in HNO_3 (MERCK) at 80 ^oC for 4 h. In the next step, CNT-CA solid phase was separated using centrifugal (ROTINA 46) and rinsed by distilled water.

The powder was then dried at 80 ^oC for 24 h. Pretreated CNT-CA was divided into 2 parts. One of them was used for Pt/CNT-CA synthesis and the other for Ru/CNT-CA synthesis.

The $RuCl_3$. $3H_2O$ which dissolved in diluted HCl and the H_2PtCl_6. $6H_2O$ which dissolved in ethylene glycol were used as precursors.

To synthesize the Ru/CNT-CA, the catalyst support (CNT-CA) should be vigorously dispersed in 2-propanol and water (3:1 V/V); then, the precise amount of Ru precursor was added to the mixture drop wise and was sonicated for 20 min. In the next step, the mixture was located in the oven at 85 ^oC. Finally, the powder was sintered at 200 ^oC in furnace under H_2 atmosphere for 2 h.

To synthesize the Pt/CNT-CA, the adequate amount of Pt precursor and sodium citrate solution in ethylene glycol were added to the homogenous mixture of CNT-CA and 2-propanol and water (3:1 V/V) drop by drop. The pH was adjusted to 10.5 with addition of KOH solution to ethylene glycol. Then, it was transferred into a Teflon autoclave and conditioned at 130 ^oC for 6 h; in the next step, it was centrifuged, washed, and vacuum dried at 70 ^oC.

2.3. Catalyst layer preparation

As mentioned previously, in this research, different proportions of Pt:Ru were used as electrocatalyst for MOR. Therefore, the desired amount of synthesized Pt/CNT-CA and Ru/CNT-CA was dispersed in mixture of 2-propanol and water (3:1 V/V) and then, Nafion solution (5 % Aldrich) was added. These mixtures were sonicated for 15 min to obtain homogenous catalyst suspensions. Thus, 7 catalysts were prepared and 7 inks containing Pt/CNT-CA, Ru/CNT-CA, and Pt;Ru (1:1, 1:2,1:3,2:1 and 3:1) were prepared. Each of them was put on glassy carbon 5 mm in diameter.

2.4. Physical properties

A scanning electron microscope (Model XL30, Philips co.) and a field emission scanning electron microscope (FESEM model MIRA#TESCAN-XMU) were used for investigating the synthesized catalyst support morphology. To obtain the specific surface area of catalyst support, Barrett-Joyner-Halenda analysis was carried out. Four-point probe was used to determine the CNT-CA electrical resistance.

To obtain XRD pattern, XRD (Philips pw3710 diffractometer with a Cu X-ray source operating at 40 kV and 40 mA) analysis was applied to each of the synthesized catalysts. The amount of reduced Pt and Ru was specified using Inductive Coupled Plasma (ICP) method (ICPOES,Varian Vista-PRO, Australia); for this purpose, 5 mg of each synthesized catalyst was solved in a solution of hydrochloric acid and nitric acid (3/1).

2.5. Electrochemical measurement

For electrochemical analysis, an EG&G Princeton Applied Research Model 2273 instrument was used to specify the electrochemical properties of the catalyst. All electrochemical measurements were carried out in a conventional three-electrode cell. In this cell, the reference electrode (Ag/Agcl) was located near the working electrode (catalyst on glassy carbon with 5mm in diameter) and the applied counter electrode was Pt- plate. Cyclic Voltammetry (CV) was carried out in two conditions, one of which in 0.5 M H_2SO_4 and the other in 0.5 M H_2SO_4 + 2 M CH_3OH; for both of them, Ar was flowing. The chronoamperometry was performed in 0.5 M H_2SO_4 + 2 M CH_3OH. All measurements were carried out at 25 ^oC.

3. RESULTS AND DISCUSSION

3.1. Catalyst support properties

The structure and morphology of the catalyst support was studied by the Field Emission Scanning Electron Microscopy (FESEM).

As shown in Figure 1, the structure of CNT-CA consists of entangled carbon nanotubes surrounded by numerous carbon nanoparticles produced during the pyrolysis process of the organic gel. The dark contrast regions suggest the porous structure. The presence of the pores is further confirmed by BJH analysis. According to the EDS analysis (Fig. 1), the sample was essentially composed of carbon with a small amount of oxygen contained in the surface functional groups. A trace amount of sodium was also detected as impurity.

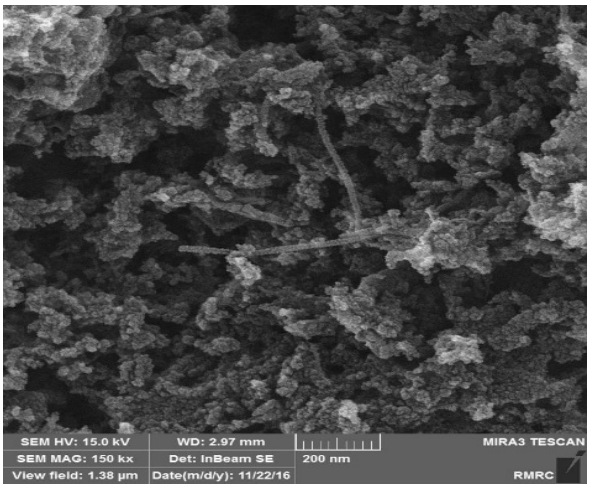

Elt	Line	Int	K	Kr	W%	A %	ZAF
C	Ka	936	0.9932	0.9217	96.71	97.61	0.9516
O	Ka	7.6	0.0040	0.0037	2.83	2.14	0.1321
Na	Ka	13.9	0.0028	0.0026	0.47	0.25	0.5565
			1	0.9280	100	100	

Figure 1. FESEM image of the CNT-C Aerogel, EDS analysis of the CNT-C Aerogel (table)

Nitrogen adsorption/desorption isotherm of the catalyst support at 77 K, which is of IV type, is seen in Figure 2, showing a hysteresis loop of H3 type [37]. This can be due to capillary condensation, indicating the presence of mesopores in the structure. Indeed, BJH analysis showed the existence of both micro and meso pores in the structure with an average pore diameter of 14.97 nm. The measured pore volume was about 1.84 m^3/g and the specific surface area obtained by BET model was 491.7 m^2/g. Density of the sample was measured by a pycnometer to be around 0.2 g/m^3. The chemical inertness and the porous structure with a high surface area fulfill the requirements for the catalyst support. Electrical resistance of the catalyst support was measured by the four-point probe method to be about $14.4x10^{-5}$ ohm.m.

3.2. Catalyst characterization

The XRD patterns of Pt/CNT_CA and Ru/CNT-CA are shown in Figures 3-a and 3-b. In both spectra, the peak centered at about 30° can be ascribed to the CNT_CA.

In Figure 3-a, the peaks at $2\theta = 40°, 47°, 68°$, and 81° are associated with Pt plates (111), (200), (220), and (311), respectively. This result emphasizes that Pt has successfully been reduced on CNT-CA and the broad peaks indicate that the Pt particles are nanosized.

Figure 3-b shows the peaks at $2\theta = 44°$ that emerged from Ru (100) plate. Therefore, Ru particles were successfully reduced and the broad peaks were due to Ru nano-scaled particles.

According to ICP results, the reduced Pt and Ru were 20 % wt and 16 % wt, respectively. Therefore, synthesis method in this research was applied to reducing Pt and Ru on CNT-CA. It needs to be mentioned that since Ru wt% is lower than Pt wt %, the peak observed in the XRD pattern of Ru is less intense than that of Pt.

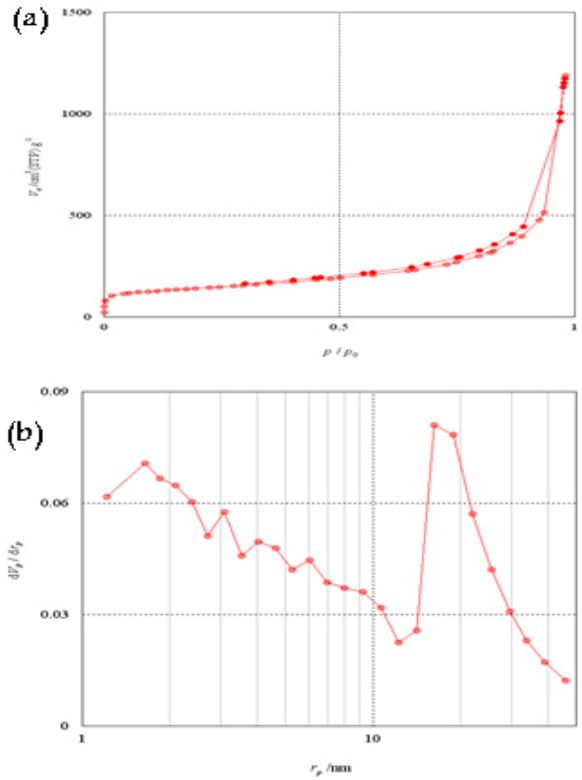

Figure 2. N_2 adsorption/desorption isotherm of the CNT-C/Aerogel (a), BJH plot of pore distribution (b)

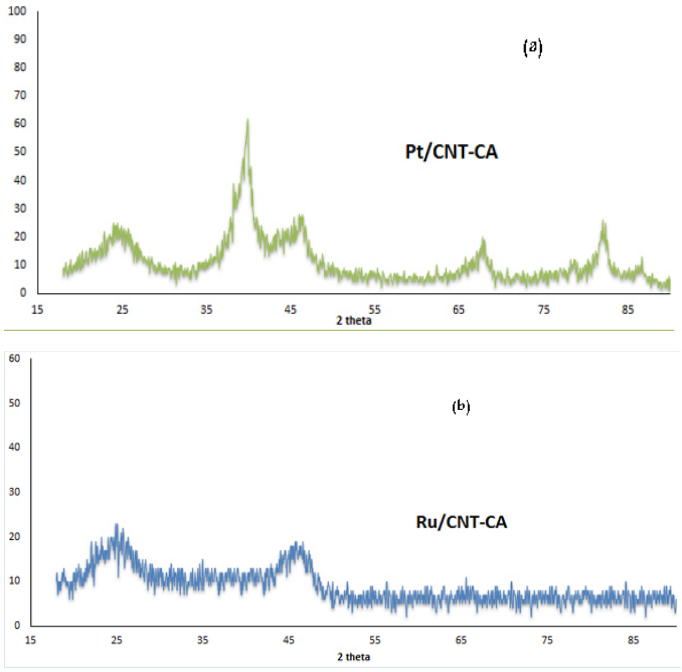

Figure 3. XRD patterns of (a) Pt/CNT-CA and (b) Ru/CNT-CA

3.3. Electrochemical performance of the catalyst

Cyclic Voltammetry (CV) analysis can be used to calculate the electroactive surface area (EAS). Figure 4 shows the CV curve of 7 synthesized catalysts and Pt/C in 0.5 M H_2SO_4 solution. The presence of the hydrogen absorption/desorption peaks in CV curves indicates the catalytic activity of the catalysts. The columbic charge for hydrogen desorption was used to measure the EAS of each catalyst (Table 1) [38]. From the EAS results, it can be concluded that the Pt/ CNT-CA was more active than the commercial Pt/C. This result can be attributed to catalyst support impact. The CNT-CA can enhance the hydrogen desorption on Pt. On the other hand, the simultaneous presence of Ru/CNT-CA and Pt/CNT-CA in the catalyst reinforced the catalytic activity for hydrogen desorption. In Table 1, the catalyst with Pt:Ru of 3:1 ratio has the maximum EAS.

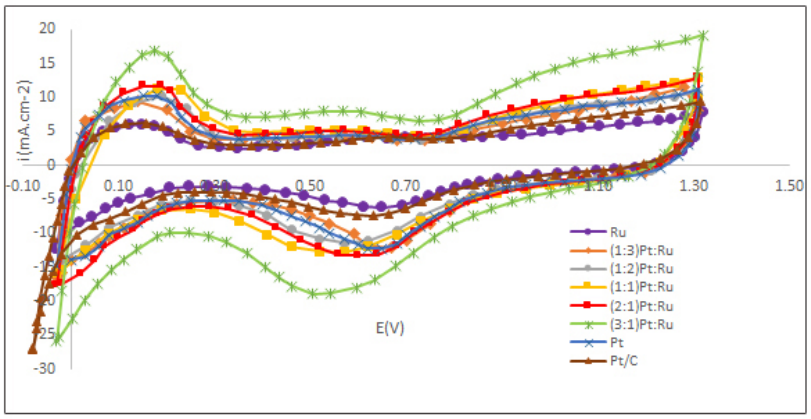

Figure 4. Cyclic voltammetry of synthesized catalysts in 0.5 M H_2SO_4, argon atmosphere, 50 $mV.s^{-1}$ scan rate at 25 °C

Moreover, CV analysis in 0.5 M H_2SO_4 + 2 M CH_3OH solution was used to investigate the electrocatalytic activation for MOR (Fig. 5). The shape of curves is similar. In Figure 5, the forward peaks are located between 0.8 and 0.9 V and the backward peaks are visible between 0.4 and 0.6 V. The forward peak (I_f) is typically attributed to the MOR and the backward peak (I_b) is related to the oxidation of residual intermediate. Note that the current density is related to the reaction rate and the results show that the Pt/ CNT-CA has better behavior than the commercial Pt/C; therefore, the CNT-CA catalyst support could enhance the catalyst performance for MOR. Furthermore, these results emphasize that the Ru particle presence in catalyst has positive effect for MOR kinetic. Comparison of the obtained results (Table 1) reveals that the catalyst with Pt:Ru ratio of 3:1 has the maximum current density among all the catalysts.

One of the important parameters for evaluating the catalyst performance for MOR is the ratio of forward to backward peak current (I_b/I_f). This parameter can be ascribed to the catalyst tolerance so that the higher ratio demonstrates more impressive elimination of the poisoning species on the catalyst surface. Since the catalyst with Pt:Ru ratio of 3:1 has the maximum I_b/I_f ratio, it can be concluded that this is the best catalyst for MOR among all the synthesized catalysts.

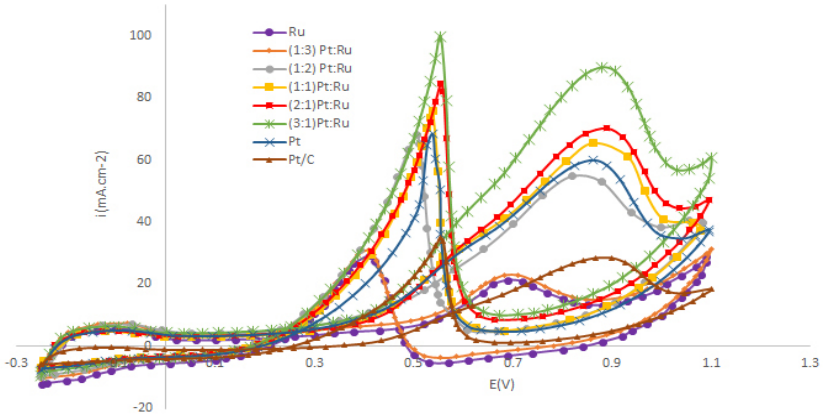

Figure 5. Cyclic voltammetry of synthesized catalysts in 0.5 M H_2SO_4+2 M CH_3OH argon atmosphere, 50 $mV.s^{-1}$ scan rate at 25 °C

Table 1. Electrochemical parameter of synthesized catalyst and commercial catalyst

Catalyst	EAS (m^2/gr)	i_f ($mA.mg_{cat}^{-1}$)	i_b ($mA.mg_{cat}^{-1}$)	i_f ($mA.cm^{-2}$)	i_b ($mA.cm^{-2}$)	(i_f/i_b)
Ru	13.3	53.5	73.25	21.4	29.3	0.73
(1:3) Pt:Ru	19.71	57.52	78	23.01	31.2	0.74
(1:2) Pt:Ru	20.57	138.8	170.25	55.52	68.1	0.81
(1:1) Pt:Ru	25.52	165.75	189.17	66.30	75.67	0.87
(2:1) Pt:Ru	27.3	175.9	211.175	70.36	84.47	0.83
(3:1) Pt:Ru	35.9	225.15	279.17	90.29	99.58	0.91
Pt	23.9	149.85	170.92	59.94	68.37	0.87
Pt/C	18.7	71.47	87.35	28.59	34.94	0.81

Figure 6 shows the chronoamperometry study of the synthesized catalysts. Comparison of the Pt/CNT-CA and commercial Pt/C results (Fig. 6) reveals that the CNT-CA as a catalyst support has a better performance than Vulcan, as expected. Moreover, the results illustrate that the Pt:Ru with 3:1 ratio performs more properly than the other catalyst. The presence of Ru/CNT-CA in catalyst is not only stabilizing the catalyst particle but also enhancing the MOR current.

The obtained results of this research corroborate that the CNT-CA can modify the catalyst performance for MOR. This effect can be ascribed to the high surface area, high electron conductivity, and high porosity of the synthesized CNT-CA. Ru catalyst plays an important role in resisting the CO poisoning of the catalyst during the MOR. This results in the active sites of catalyst to be available for MOR.

Since the Pt particles can readily be poisoned by absorbed CO species, Ru presence helps remove the CO poisoning. In fact, this research used the synergisticm effect of Ru and found that the Pt:Ru with 3:1 ratio as a catalyst had the greatest effect on MOR.

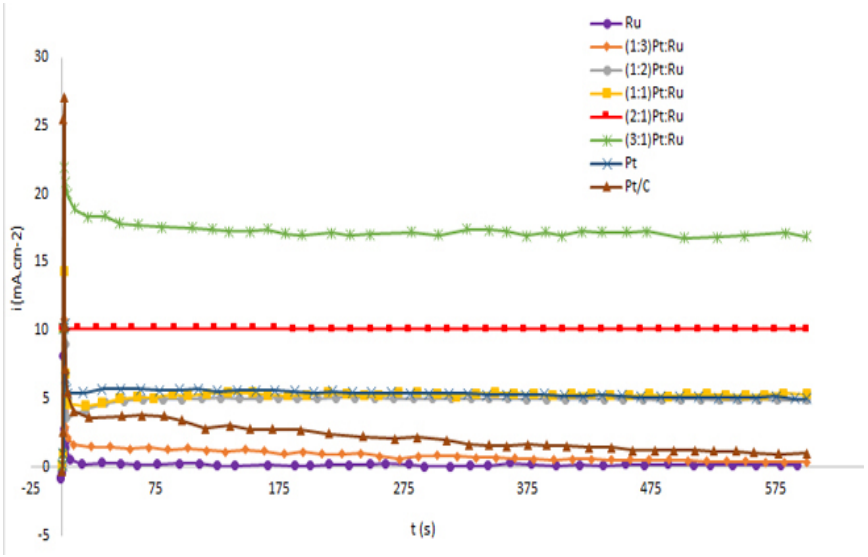

Figure 6. chronoamperemetery of synthesized catalyst in 0.5 M H_2SO_4 + 2 M CH_3OH at 0.6 V and 25°C

4. CONCLUSIONS

In summary, the aim of this research was to investigate not only the effect of simultaneous use of CNT and CA (i.e., CNT-CA) as a catalyst support but also the influence of Ru presence with Pt on the catalyst layer for the MOR reaction. The CNT-CA catalyst support with a high surface area and high electrical conductivity was synthesized by sol-gel method. The catalyst support was distinguished by using SEM, XRD, BET, and four-point probe techniques. Moreover, the catalysts Pt/CNT-CA and Ru/CNT-CA were synthesized by impregnation and hydrothermal methods. Synthesized catalysts were characterized by XRD and ICP technique and the electrochemical activities of the catalysts were studied. Furthermore, the catalysts with different Pt:Ru ratios (1:0,1:1, 2:1, 3:1, 1:2 ,1:3 and 0:1) were studied and their performance was compared with the commercial Pt/C. Research results illustrated that: 1) the synthesis methods were reliable, 2) the CNT-CA showed proper performance as the catalyst support, and 3) the Pt:RU with 3:1 molar ratio was the best catalyst for MOR among all the synthesized catalysts.

It is hoped that in future studies, based on the obtained results in this work which indicated an improvement in the performance of the synthesized catalyst compared to the commercial Pt/C for MOR, the effect of Pt/Ru alloy as well as core-shell structure of these two metals deposited on CNT-CA should be considered. The synthesized catalyst will be used as anode of monocell and studied.

5. ACKNOWLEDGEMENT

This work was supported by Materials and Energy Research Center (MERC).

NOMENCLATURE

EAS	Electro active surface area
CNT	Carbon nanotube
CA	Carbon aerogel
i_f	Forward peak current
i_b	Backwared peak current

REFERENCES

1. Carrette, L., Friedrich, K.A. and Stimming, U., "Fuel cells–fundamentals and applications", ***Fuel Cells***, Vol. 1, No. 1, (2001), 5-39. (https://doi.org/10.1002/1615-6854(200105)1:1<5::AID-FUCE5>3.0.CO;2-G).
2. Ralph, T.R., and Hogarth, M.P., "Catalysis for low temperature fuel cells", ***Platinum Metals Review***, Vol. 46, No. 3, (2002), 117-135. (https://www.technology.matthey.com/article/46/3/117-135/).
3. Figueiredo, J.L. and Pereira, M.F.R., "Synthesis and functionalization of carbon xerogels to be used as supports for fuel cell catalysts", ***Journal of Energy Chemistry***, Vol. 22, No. 2, (2013), 195-201. (https://doi.org/10.1016/S2095-4956(13)60025-X).
4. Tsukagoshi, Y., Ishitobi, H. and Nakagawa, N., "Improved performance of direct methanol fuel cells with the porous catalyst layer using highly-active nanofiber catalyst", ***Carbon Resources Conversion***, Vol. 1, No. 1, (2018), 61-72. (https://doi.org/10.1016/j.crcon.2018.03.001).
5. Uchida, M., Fukuoka, Y., Sugawara, Y., Eda, N. and Ohta, A., "Effects of microstructure of carbon support in the catalyst layer on the performance of polymer-electrolyte fuel cells", ***Journal of The Electrochemical Society***, Vol. 143, No. 7, (1996), 2245. (https://iopscience.iop.org/article/10.1149/1.1836988).
6. Chen, C.-C., Chen, C.F., Hsu, C.-H. and Li, I.-H., "Growth and characteristics of carbon nanotubes on carbon cloth as electrodes", ***Diamond and Related Materials***, Vol. 14, No. 3-7, (2005), 770-773. (https://doi.org/10.1016/j.diamond.2004.12.038).
7. Jaouen, F., Marcotte, S., Dodelet, J.-P. and Lindbergh, G., "Oxygen reduction catalysts for polymer electrolyte fuel cells from the pyrolysis of iron acetate adsorbed on various carbon supports", ***The Journal of***

Physical Chemistry B, Vol. 107, No. 6, (2003), 1376-1386. (https://doi.org/10.1021/jp021634q).

8. Saquing, C.D., Kang, D., Aindow, M. and Erkey, C., "Investigation of the supercritical deposition of platinum nanoparticles into carbon aerogels", ***Microporous and Mesoporous Materials***, Vol. 80, No. 1-3, (2005), 11-23. (https://doi.org/10.1016/j.micromeso.2004.11.019).
9. Abdullah, N., Kamarudin, S.K. and Shyuan, L.K., "Novel anodic catalyst support for direct methanol fuel cell: characterizations and single-cell performances", ***Nanoscale Research Letters***, Vol. 13, No. 1, (2018), 90. (https://link.springer.com/article/10.1186/s11671-018-2498-1).
10. Zhao, X., Yin, M., Ma, L., Liang, L., Liu, C., Liao, J., Lu, T. and Xing, W., "Recent advances in catalysts for direct methanol fuel cells", ***Energy & Environmental Science***, Vol. 4, No. 8, (2011), 2736-2753. (https://doi.org/10.1039/C1EE01307F).
11. Smirnova, A., Dong, X., Hara, H., Vasiliev, A. and Sammes, N., "Novel carbon aerogel-supported catalysts for PEM fuel cell application", ***International Journal of Hydrogen Energy***, Vol. 30, No. 2, (2005), 149-158. (https://doi.org/10.1016/j.ijhydene.2004.04.014).
12. Kim, S., Kwon, Y.H., Jung, Y. and Park, S.J., "Electrochemical behaviors of PtRu/CNTs catalysts prepared by pulse potential plating methods", ***Solid State Phenomena***, Vol. 124-126, (2007), 1039-1042, Trans Tech. Publications Ltd. (https://doi.org/10.4028/www.scientific.net/SSP.124-126.1039).
13. Li, L., and Xing, Y., "Pt−Ru nanoparticles supported on carbon nanotubes as methanol fuel cell catalysts", ***The Journal of Physical Chemistry C***, Vol. 111, No. 6, (2007), 2803-2808. (https://doi.org/10.1021/jp0655470).
14. Liu, Z., Ling, X.Y., Su, X. and Lee, J.Y., "Carbon-supported Pt and PtRu nanoparticles as catalysts for a direct methanol fuel cell", ***The Journal of Physical Chemistry B***, Vol. 108, No. 24, (2004), 8234-8240. (https://doi.org/10.1021/jp049422b).
15. Missiroli, A., Soavi, F. and Mastragostino, M., "Increased performance of electrodeposited PtRu/C-Nafion catalysts for DMFC", ***Electrochemical and Solid-State Letters***, Vol. 8, No. 2, (2005), A110-A114. (https://iopscience.iop.org/article/10.1149/1.1847686).
16. Apanel, G. and Johnson, E., "Direct methanol fuel cells–ready to go commercial?", ***Fuel Cells Bulletin***, Vol. 2004, No. 11, (2004), 12-17. (https://doi.org/10.1016/S1464-2859(04)00410-9).
17. Ramli, Z.A.C. and Kamarudin, S.K., "Platinum-based catalysts on various carbon supports and conducting polymers for direct methanol fuel cell applications: A review", ***Nanoscale Research Letters***, Vol. 13, No. 1, (2018), 410. (https://doi.org/10.1186/s11671-018-2799).
18. Du, H., Li, B., Kang, F., Fu, R. and Zeng, Y., "Carbon aerogel supported Pt–Ru catalysts for using as the anode of direct methanol fuel cells", ***Carbon***, Vol. 45, No. 2, (2007), 429-435. (https://doi.org/10.1016/j.carbon.2006.08.023).
19. Zhu, H., Guo, Z., Zhang, X., Han, K., Guo, Y., Wang, F., Wang, Z. and Wei, Y., "Methanol-tolerant carbon aerogel-supported Pt–Au catalysts for direct methanol fuel cell", ***International Journal of Hydrogen Energy***, Vol. 37, No. 1, (2012), 873-876. (https://doi.org/10.1016/j.ijhydene.2011.04.032).
20. Ren, X., Zelenay, P., Thomas, S., Davey, J. and Gottesfeld, S., "Recent advances in direct methanol fuel cells at Los Alamos National Laboratory", ***Journal of Power Sources***, Vol. 86, No. 1-2, (2000), 111-116. (https://doi.org/10.1016/S0378-7753(99)00407-3).
21. Iwasita, T., Hoster, H., John-Anacker, A., Lin, W.F. and Vielstich, W., "Methanol oxidation on PtRu electrodes, Influence of surface structure and Pt-Ru atom distribution", ***Langmuir***, Vol. 16, No. 2, (2000), 522-529. (https://doi.org/10.1021/la990594n).
22. Dickinson, A.J., Carrette, L.P.L., Collins, J.A., Friedrich, K.A. and Stimming, U., "Performance of methanol oxidation catalysts with varying Pt: Ru ratio as a function of temperature", ***Journal of Applied Electrochemistry***, Vol. 34, No. 10, (2004), 975-980. (https://doi.org/10.1023/B:JACH.0000042668.61391.a4).
23. Shi, M., Zhang, W., Zhao, D. and Chu, Y., "Reduced graphene oxide-supported tungsten carbide modified with ultralow-platinum and ruthenium-loading for methanol oxidation", ***Electrochimica Acta***, Vol. 143, (2014), 222-231. (https://doi.org/10.1016/j.electacta.2014.08.011).
24. Bong, S. and Han, D., "Mesopore-controllable carbon aerogel and their highly loaded PtRu anode electrocatalyst for DMFC applications", ***Electroanalysis***, Vol. 32, No. 1, (2020), 104-111. (https://doi.org/10.1002/elan.201900320).
25. Antolini, E., "Carbon supports for low-temperature fuel cell catalysts", ***Applied Catalysis B: Environmental***, Vol. 88, No. 1-2, (2009), 1-24. (https://doi.org/10.1016/j.apcatb.2008.09.030).
26. Jeng, K.-T., Chien, C.-C., Hsu, N.-Y., Yen, S.-C., Chiou, S.-D., Lin, S.-H. and Huang, W.-M., "Performance of direct methanol fuel cell using carbon nanotube-supported Pt–Ru anode catalyst with controlled composition", ***Journal of Power Sources***, Vol. 160, No. 1, (2006), 97-104. (https://doi.org/10.1016/j.jpowsour.2006.01.057).
27. Wei, S., Wu, D., Shang, X. and Fu, R., "Studies on the structure and electrochemical performance of Pt/carbon aerogel catalyst for direct methanol fuel cells", ***Energy & Fuels***, Vol. 23, No. 2, (2009), 908-911. (https://doi.org/10.1021/ef8006432).
28. Gharibi, H., Javaheri, M., Kheirmand, M. and Abdullah Mirzaie, R., "Optimization of the amount of Nafion in multi-walled carbon nanotube/Nafion composites as Pt supports in gas diffusion electrodes for proton exchange membrane fuel cells", ***International Journal of Hydrogen Energy***, Vol. 36, No. 20, (2011), 13325-13334. (https://doi.org/10.1016/j.ijhydene.2010.09.008).
29. Steigerwalt, E.S., Deluga, G.A., Cliffel, D.E. and Lukehart, C.M., "A Pt−Ru/graphitic carbon nanofiber nanocomposite exhibiting high relative performance as a direct-methanol fuel cell anode catalyst", ***The Journal of Physical Chemistry B***, Vol. 105, No. 34, (2001), 8097-8101. (https://doi.org/10.1021/jp011633i).
30. Bessel, C.A., Laubernds, K., Rodriguez, N.M. and Baker, R.T.K., "Graphite nanofibers as an electrode for fuel cell applications", ***The Journal of Physical Chemistry B***, Vol. 105, No. 6, (2001), 1115-1118. (https://doi.org/10.1021/jp003280d).
31. Maiyalagan, T., Viswanathan, B. and Varadaraju, U.V., "Nitrogen containing carbon nanotubes as supports for Pt–Alternate anodes for fuel cell applications", ***Electrochemistry Communications***, Vol. 7, No. 9, (2005), 905-912. (https://doi.org/10.1016/j.elecom.2005.07.007).
32. Zhang, W.-H., Shi, J.-L., Wang, L.-Z. and Yan, D.-S., "Preparation and characterization of ZnO clusters inside mesoporous silica", ***Chemistry of Materials***, Vol. 12, No. 5, (2000), 1408-1413. (https://doi.org/10.1021/cm990740a).
33. Knupp, S.L., Li, W., Paschos, O., Murray, T.M., Snyder, J. and Haldar, P., "The effect of experimental parameters on the synthesis of carbon nanotube/nanofiber supported platinum by polyol processing techniques", ***Carbon***, Vol. 46, No. 10, (2008), 1276-1284. (https://doi.org/10.1016/j.carbon.2008.05.007).
34. Paust, N., Litterst, C., Metz, T., Zengerle, R. and Koltay, P., "Fully passive degassing and fuel supply in direct methanol fuel cells", ***Proceedings of 2008 IEEE 21st International Conference on Micro Electro Mechanical Systems***, (2008), Wuhan, China, 34-37. (https://doi.org/10.1109/MEMSYS.2008.4443586).
35. Bresciani, F., Rabissi, C., Casalegno, A., Zago, M. and Marchesi, R., "Experimental investigation on DMFC temporary degradation", ***International Journal of Hydrogen Energy***, Vol. 39, No. 36, (2014), 21647-21656. (https://doi.org/10.1016/j.ijhydene.2014.09.072).
36. Tabrizi, N.S. and Yavari, M., "Methylene blue removal by carbon nanotube-based aerogels", ***Chemical Engineering Research and Design***, Vol. 94, (2015), 516-523. (https://doi.org/10.1016/j.cherd.2014.09.011).
37. Yurdakal, S., Garlisi, C., Özcan, L., Bellardita, M. and Palmisano, G., (Photo)catalyst characterization techniques: Adsorption isotherms and BET, SEM, FTIR, UV–Vis, photoluminescence, and electrochemical characterizations, Heterogeneous Photocatalysis, (2019), Elsevier, 87-152. (https://doi.org/10.1016/B978-0-444-64015-4.00004-3).
38. Bockris, J.O'M. and Reddy, A.K.N., Electrochemistry in materials science, Modern electrochemistry 2B: Electrodics in chemistry, engineering, biology, and environmental science, (2000), Springer, 1637-1788. (https://www.springer.com/gp/book/9780306463242).

JREE: Vol. 7, No. 4, (Autumn 2020) 56-66

Journal of Renewable Energy and Environment

Research Article

Journal Homepage: www.jree.ir

Optimization of Small-Scale Trigeneration Systems in Terms of Levelized Total Costs and Carbon Tax Using a Matrix Modeling Approach

Taraneh Taheri[a], Mohammad Behshad Shafii[b*], Sourena Sattari[c], Morteza Khalaji Assadi[d]

[a] *Department of Energy Engineering, Faculty of Natural Resources and Environment, Science and Research Branch, Islamic Azad University, Tehran, Tehran, Iran.*
[b] *Department of Mechanical Engineering, Sharif University of Technology, P. O. Box: 11155-9567, Tehran, Tehran, Iran.*
[c] *Department of Energy Engineering, Sharif University of Technology, Tehran, Tehran, Iran.*
[d] *Department of Fine Arts, Faculty of Architecture, University of Tehran, Tehran, Tehran, Iran.*

PAPER INFO

Paper history:
Received 26 April 2020
Accepted in revised form 12 September 2020

Keywords:
Energy Hub,
Matrix Modeling,
Dispatch Factors,
Economic Analysis,
Optimal Strategy

ABSTRACT

Combined Heat and Power (CHP) systems have increasingly drawn attention in recent years due to their higher efficiency and lower Greenhouse Gas (GHG) emission. Input-output matrix modeling was considered here as one of the efficient approaches for optimizing these energy networks. In this approach, power flow and energy conversion through plant components were modeled by an overall efficiency matrix including dispatch factors and plant component efficiencies. The purpose of this paper is to propose a modification of the objective function presented in some previous studies. This procedure was performed by adding the parameters of plant component lifetime and environmental costs to the objective function. Thus, the optimization problem was formulated by minimizing the total system levelized cost instead of simply hourly energy cost. The study results revealed that producing the electricity by the trigeneration system led to achieving 1256 MWh annual electricity savings that otherwise must be purchased from the grid. The results also showed a significant reduction in annual CO_2 emissions (703.31 tons per year). Furthermore, if the price of purchasing CHP electricity was considered three times more than the current ones, payback times would be less than 5 years.

https://doi.org/10.30501/jree.2020.228287.1108

1. INTRODUCTION

Previous studies demonstrated that when primary energy is converted into electricity, more than half of the energy is lost as waste heat [1]. This amount of energy can be used to meet a portion of demands for heating in residential and commercial buildings. In addition, Transmission and Distribution (T&D) of the electricity from central power plants lead to excess losses of net generation (it is around 9 %) [2]. A significant part of total primary energy is consumed in cities [3]. Distributed generation is one of the strategies to meet the rising energy demand [4]. Locally collected and locally utilized renewable energies can significantly improve the local economy if they are properly planned and implemented [5].

CHP systems with district heating offer an alternative energy production mechanism with higher efficiency and greater energy security than many conventional alternatives [6]. When cooling is generated by waste heat in a CHP plant, a process known either as trigeneration (3 products from one fuel source) or Combined Cooling, Heating and Power (CCHP) can result in higher heat recovery and shorter payback time than comparable cogeneration approaches [7].

*Corresponding Author's Email: behshad@sharif.edu (M.B. Shafii)
URL: http://www.jree.ir/article_113937.html

According to IEA, a significant source of CO_2 emissions is buildings that account for about one-third of global final energy consumption. The International Energy Administration has proposed cogeneration as part of a strategy for reducing GHG emissions [8].

In [9], the effect of micro CHP systems on the GHG emissions in the domestic sector was evaluated. In the optimized case, level of CO_2 emissions was substantially lower than that in the reference case, i.e., with a separate generation of heat and electricity from the grid. In [10], the results demonstrated that the utilization of a CHP system led to the reduction of CO_2, NO_x, and CH_4 emissions in all of the studied buildings.

The concept of cogeneration can be extended to include more outputs. Increase in use of distributed generation technologies has led to the emergence of the terms like "multiple energy carrier systems" [11]. These systems are known as Multi-Source Multi-Product (MSMP) energy systems. The term 'hybrid energy system' is used for introducing an energy system in which its inputs include two or more energy sources. This type of system leads to the improvement of system efficiency [12].

Fossil fuels or renewable energies can be considered as inputs to MSMP systems. The system inputs comprise coal, biomass, natural gas and nuclear, and solar or geothermal

Please cite this article as: Taheri, T., Shafii, M.B., Sattari, S. and Khalaji Assadi, M., "Optimization of small-scale trigeneration systems in terms of levelized total costs and carbon tax using a matrix modeling approach", ***Journal of Renewable Energy and Environment (JREE)***, Vol. 7, No. 4, (2020), 56-66. (https://doi.org/10.30501/jree.2020.228287.1108).

energy. Outputs may also include electricity, heating/cooling power, and so on [13]. In [14], authors studied the chemical conversion, energy utilization, and pollution reductions in Multifunctional Energy Systems (MESs). In [15], an appropriate example was developed to present the advantages of hybrid energy systems in the building sector.

There are several approaches to formulating these types of systems including "the so-called hybrid energy hubs" [16]. Finally, in [17], the term "multi-objective systems" was employed that refers to the energy hub concept. The definitions begin by characterizing the energy hub approach, which can provide an interface among energy producers, consumers, and transportation sectors [8]. In other words, energy hub introduces an interface between the energy networks and loads [19]. In terms of the system, an energy hub represents some functions for conversion and storage of multiple energy carriers. The energy hub approach was developed as part of the project "Vision of Future Energy Networks - VoFEN" at ETH Zurich. VoFEN project aimed to organize the optimum configuration of energy systems in the future [20]. An energy hub is considered as a unit for conversion and, sometimes, it represents storage of multiple energy carriers [21].

The energy hub is defined by its conversion matrix. Indeed, it is a matrix that represents the conversion efficiency of one input into one output. In [22], an operational analysis was conducted for multifunctional energy systems at a district level. The analysis consists of electricity, heat, and gas distribution networks. In this case, an efficiency matrix was utilized to model their interrelationships.

In [23], the matrix modeling method was formulated based on the energy hub concept. The authors modeled energy flows among trigeneration components through construction of the overall efficiency matrix, which represents the whole plant. This matrix formulation suggests an appropriate model for optimizing the operational cogeneration problems. An optimal strategy was determined for a case study and its objective function was to minimize the hourly energy cost. The achieved results demonstrate the effectiveness of the proposed matrix formulation.

In the optimization approach proposed by [23], the minimization of hourly energy costs was an operational optimization criterion. However, the investment costs were not considered for the equipment in the objective function. This simplification leads to less accurate solutions, especially in the case of hybrid networks. Given that energy costs of renewable energies such as solar and wind are zero, ignoring their convertor investment costs will make them the optimum choice among other forms of energies. The innovation of this paper is to propose a modification to the objective function presented in some previous studies. In this paper, the minimization problem was redefined by adding the investment costs of subsystems and applying levelized cost analysis. This procedure leads to the improvement of accuracy, which is necessary to see the coupling between the initial costs of equipment and long-term economic performance and quantify long-term outlook. Finally, environmental cost was added to the total cost by assigning the carbon tax to the GHG emissions. It was accomplished to quantify the benefits of reducing GHG emission, reached by applying the trigeneration system. Thus, the optimization problem was formulated by minimizing the total system levelized cost instead of simply hourly energy cost. Applying the optimal strategy determines which components to use per hour and how much each of these components is used to supply electricity, heating, and cooling.

2. METHOD

2.1. Matrix modeling procedure in trigeneration systems

A detailed technical, economic, and environmental evaluation is required for successful implementation of cogeneration projects [24].

In the MSMP energy system, matrix modeling defines the system using an overall efficiency matrix, which is composed of the conversion efficiencies of the inputs to outputs. Inputs and outputs were presented for the system in the matrix form. All of the elements in the input and output matrices are considered with the same order. In this study, energy vectors include fuel (F, input), electricity (E, both input from the grid and output to the load), heat (Q, output), and cooling (C, output). Then, the input and output vectors are considered as follows:

$$\mathbf{V_i} = [F_i, E_i, Q_i, C_i]^T \quad (1)$$

$$\mathbf{V_o} = [F_o, E_o, Q_o, C_o]^T \quad (2)$$

Similar to the study presented in [23], a trigeneration system was considered with the following specifications: 3 micro gas turbines as the prime mover, 6 auxiliary boiler units fueled by natural gas and sized to the maximum heating load, 2 water absorption units, and 2 compression electric chiller units. Figure 1 shows the links between the system components:

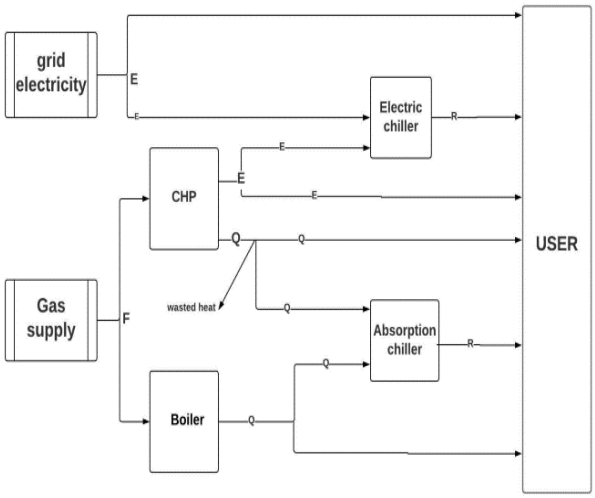

Figure 1. Input-output diagram of the case study trigeneration system

First, an efficiency matrix is individually constructed for each converter [23]. Afterward, the interconnection matrices are built and dispatch factors are also considered. Dispatch factors are used when an input goes to more than one component. Dispatch factor can take a value between 0 and 1 [4].

In this study, the interconnection matrix is a diagonal 4×4 matrix that represents the connections between the plant components including inputs and outputs. For example, the $T^{M, N}$ interconnection matrix defines the direct connection between component M and component N. In the interconnection matrix, the elements in the main diagonal are

either unity or dispatch factors. This is dependent on the ratio of the input energy for a given component. For the understudied system, the elements in the main diagonal of the interconnection matrix are denoted by D as follows:

$$\mathbf{D}^{O,B} = [0, 0, \alpha_{QQ}^{B}, 0] \quad (3)$$

$$\mathbf{D}^{O,GT} = [0, \alpha_{EE}^{GT}, \alpha_{QQ}^{GT}, 0] \quad (4)$$

$$\mathbf{D}^{O,ECh} = [0, 0, 0, 1] \quad (5)$$

$$\mathbf{D}^{O,ACh} = [0, 0, 0, 1] \quad (6)$$

$$\mathbf{D}^{O,GE} = [0, \alpha_{EE}^{GE}, 0, 0] \quad (7)$$

$$\mathbf{D}^{B,I} = [1- \alpha_{YF}^{GS}, 0, 0, 0] \quad (8)$$

$$\mathbf{D}^{GT,I} = [\alpha_{YF}^{GS}, 0, 0, 0] \quad (9)$$

$$\mathbf{D}^{ECh,GT} = [0, 1- \alpha_{EE}^{GT}, 0, 0] \quad (10)$$

$$\mathbf{D}^{ECh,I} = [0, 1- \alpha_{EE}^{GE}, 0, 0] \quad (11)$$

$$\mathbf{D}^{ACh,B} = [0, 0, 1- \alpha_{QQ}^{B}, 0] \quad (12)$$

$$\mathbf{D}^{ACh,\ GT} = [0, 0, \alpha_{CQ}^{GT}, 0] \quad (13)$$

The general approach to constructing the overall efficiency matrix is as follows: there is a backward movement from the outputs to the inputs. This process initiates by the first output and moves backward to the input. We should follow the path by multiplying each individual component efficiency matrix by its relevant interconnection matrix. There are subdivisions and junctions on the path. In a subdivision, the input from one component is split into two or more components or loads. In a junction, the input energy to one component stems from multiple components. If a junction is found in an output toward input path, we should summate the terms found in the paths from the junction point to the inputs. By getting at the input, the scanning procedure will restart from the last saved junction point. When all of the junctions are traced, the procedure is completed.

In the above procedure, the final expression will be configured for the overall efficiency matrix of the system as follows:

$$\mathbf{R} = \mathbf{T}^{O,i}\mathbf{I} + \mathbf{T}^{O,B}\mathbf{R}^{B}\mathbf{T}^{B,i}\mathbf{I} + \mathbf{T}^{O,GT}\mathbf{R}^{GT}\mathbf{T}^{GT,i}\mathbf{I} + \mathbf{T}^{O,ECh}\mathbf{R}^{ECh}(\mathbf{T}^{ECh,i}\mathbf{I} + \mathbf{T}^{ECh,GT}\mathbf{R}^{GT}\mathbf{T}^{GT,i}\mathbf{I}) + \mathbf{T}^{O,ACh}\mathbf{R}^{Ach}(\mathbf{T}^{ACh,B}\mathbf{R}^{B}\mathbf{T}^{B,i}\mathbf{I} + \mathbf{T}^{ACh,GT}\mathbf{R}^{GT}\mathbf{T}^{GT,i}\mathbf{I}) \quad (14)$$

In this trigeneration system, the efficiency entries are assumed to be constant for each component (its rated values) [23].

2.2. Formulation of trigeneration optimization problem

Overall trigeneration system optimization is involved in optimizing dispatch factors, energy sources, and components capacities. To minimize the total costs, the outcome would be to meet the building energy demands by purchasing a rational amount of electricity and fuel to run the trigeneration system.

The energy demand vector (V_d), the amounts of input energies, and the share of energy flows correspond to different ratios of dispatch factors. When these dispatch factors are multiplied by the component efficiencies, the elements will be constructed for the overall efficiency matrix. Given that the dispatch factors are dependent variables, they can be reduced to independent ones. The obtained degrees of freedom provide the basis for developing a nonlinear optimization problem. Thus, the independent dispatch factor vector is presented as follows:

$$\boldsymbol{\alpha} = [\alpha_{EE}^{GE}, \alpha_{YF}^{GS}, \alpha_{EE}^{GT}, \alpha_{QQ}^{GT}, \alpha_{CQ}^{GT}, \alpha_{QQ}^{B}]^{T} \quad (15)$$

2.2.1. Objective function

To evaluate an energy system, the most important issues comprise energy demands, total cost, and GHG emissions [25]. Environmental costs can be considered as a cost category [26]. GHG emissions are estimated by multiplying either the fuel consumption or landfill gas potential by the GHG emission factor. In some jurisdictions, GHG emission factors might be calculated for electricity generation through an aggregate basis to facilitate the preparation of GHG calculations. This value is multiplied by T&D losses (%) and GHG emission factor for the base case electricity system. It is performed to calculate the GHG emissions associated with the T&D losses for the proposed case power system [27].

Here, emission costs of natural gas and the central electricity mix are estimated through the following Equation [27]:

$$C_{emiss} = (GEF_F\ F + GEF_E\ E)\ Ctx \quad (16)$$

Finally the objective function can be rewritten as follows:

$$\text{Total cost} = C_{inv}^{GT} + C_{inv}^{B} + C_{inv}^{ACh} + C_{inv}^{ECh} + C_{O\&M}^{GT} + C_{O\&M}^{B} + C_{O\&M}^{ACh} + C_{O\&M}^{ECh} + C_{F}^{GS}Fi + C_{Ei}^{GE}Ei\_C_{Eo}^{GE}(Ei\_Eo) + C_{emiss} \quad (17)$$

where $C_{inv}^{GT}, C_{inv}^{B}, C_{inv}^{ACh}$, and C_{inv}^{ECh} are the hourly equivalent investment costs for each sub-system of producers, primary converters, and secondary converters, respectively. $C_{O\&M}^{GT}, C_{O\&M}^{B}, C_{O\&M}^{ACh}$, and $C_{O\&M}^{ECh}$ are the hourly equivalent operation and maintenance costs for each sub-system that regularly occur and they are considered for preserving the mentioned sub-system. C_{F}^{GS} and C_{Ei}^{GE} are the hourly prices of purchasing input energies (natural gas and grid electricity). C_{Eo}^{GE} is the hourly price of selling the surplus electricity to the grid. Cemiss is GHG emission cost of consuming input energies. Here, this study has addressed the impact of such tax on the economics of the studied trigeneration system.

As the series of costs are not uniform, the levelized value should be computed. Therefore, it is essential to apply the capital recovery factor to estimate all of the costs for each year throughout the entire economic life of the plant. It is assumed that all prices are escalated at the same rate throughout the project life cycle. The hourly capital recovery factor can be calculated through the following equation [28]:

$$CRF = \frac{1}{8760}\left(\frac{I(1+I)^{n}}{(1+I)^{n}-1}\right) \quad (18)$$

where I is the interest rate and n is the lifetime (Yr) of each sub-system.

Table 1 summarizes the rated capacities of the used relevant equipment as well as their investment and operation costs. Similar to [23], the current trigeneration system consists of three micro gas turbines of 100 kW_E and six auxiliary boilers of 150 kWt capacity. Two chillers are also sized to the cooling load peak.

Table 1. The rated capacities of the used relevant equipment

Equipment	Capacity (kW)	Efficiency (%)	Investment Cost (€/kW)	Annual cost (€/kWh)	Life cycle (yr)
Trigeneration system (3 micro-turbines)	300 (electrical) 450 (thermal)	$\eta_E = 0.3$ $\eta_Q = 0.45$	2000	0.02	15
Boiler (6 units)	900	$\eta_t = 0.8$	200	0.01	25
Electric Chiller (2 units)	400	$COP_{ECh}=3$	400	0.04	25
Absorption Chiller (2 units)	400	$COP_{ACh} = 0.7$	250	0.02	15

2.2.2. Constraints

The equality constraints express energy balances for each energy carrier at the inputs and outputs of plant components and the whole system. Therefore, we have:

$$\mathbf{R}^X\mathbf{V}_i^X - \mathbf{V}_o^X = 0 \quad \text{for } X \in \mathbf{X} \tag{19}$$

$$\mathbf{R}\mathbf{V}_i - \mathbf{V}_o = \mathbf{0} \tag{20}$$

$$E_i \,.\, (E_o - E_d) = 0 \tag{21}$$

Eq. (21) suggests a condition in which electricity is either sold to or bought from the grid. It is associated with the inequality constraint Ed≤ Eo. When one energy carrier is split into a number of components at a subdivision, the input energy of each component represents the ratio of total energy flow. Thus, dispatch factors should be greater than or equal to zero and no more than one (Eqs. 22 and 23). The sum of all the divided energy carriers must be identical to the initial energy carrier. Furthermore, input fuel, purchased electricity from the grid, and electricity sold back to the grid must be positive.

$$-\boldsymbol{\alpha} \leq 0 \tag{22}$$

$$\boldsymbol{\alpha} - 1 \leq 0 \tag{23}$$

$$-E_i \leq 0 \tag{24}$$

$$-F_i \leq 0 \tag{25}$$

Each plant convertor may have thresholds such that the convertor would be cut down for outputs below a certain threshold. The lower bounds are set to zero for boilers, electric chillers, and absorption chillers. For the micro gas turbine, the technical lower limit is equal to 50 % of its rated output. The GT is switched off below this threshold. The maximum limits of the equipment are equal to the rated capacities of them.

According to the output upper and lower bounds for the components, we can have the corresponding inequality constraints as follows:

$$\mathbf{R}\mathbf{V}_i^X - \bar{\mathbf{V}}^X \leq 0 \quad \text{for } X \in \mathbf{X} \tag{26}$$

$$\underline{\mathbf{V}}^X - \mathbf{R}^X\mathbf{V}_i^X \leq 0 \quad \text{for } X \in \mathbf{X} \tag{27}$$

2.2.3. Optimization algorithm

These types of optimization problems can be solved by applying several methods such as penalty and barrier functions, gradient projection algorithm, sequential quadratic programming, and Genetic algorithm [19].

The optimization function chosen here is fmincon.m, in MATLAB, whose algorithm is set to be ‘sqp’ (sequential quadratic programming).

2.3. Case study

First, the optimization was run with respect to the same input datasets as those used in Gianfranco Chicco and Pierluigi Mancarella [23]. This procedure was employed to validate the results. For example, the gas price was set to 20 €/MWh_t and it was assumed that this price would remain constant throughout the analysis. For the sake of simplicity, buying and selling electricity prices were assumed to be the same. Second, the optimization problem was solved by setting the equipment investment and O&M costs to zero and ignoring the greenhouse gas emissions. Therefore, the required conditions presented in [23] were stimulated. Figure 2 shows the results.

The simulation results are consistent with the results obtained in [23]. There was no significant difference between the results. The errors were associated with digitizing the diagrams of load patterns to obtain the load data of the mentioned paper.

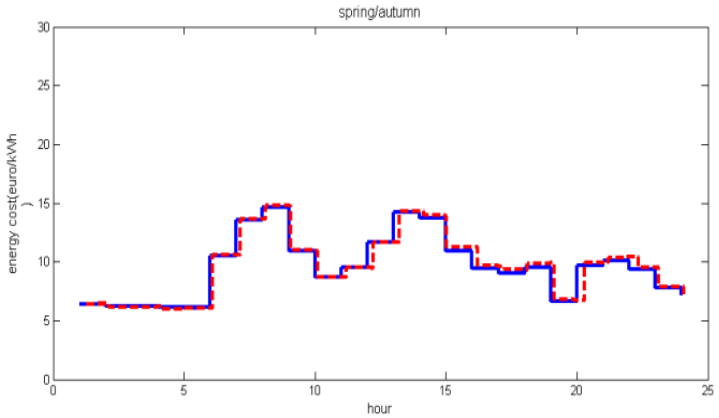

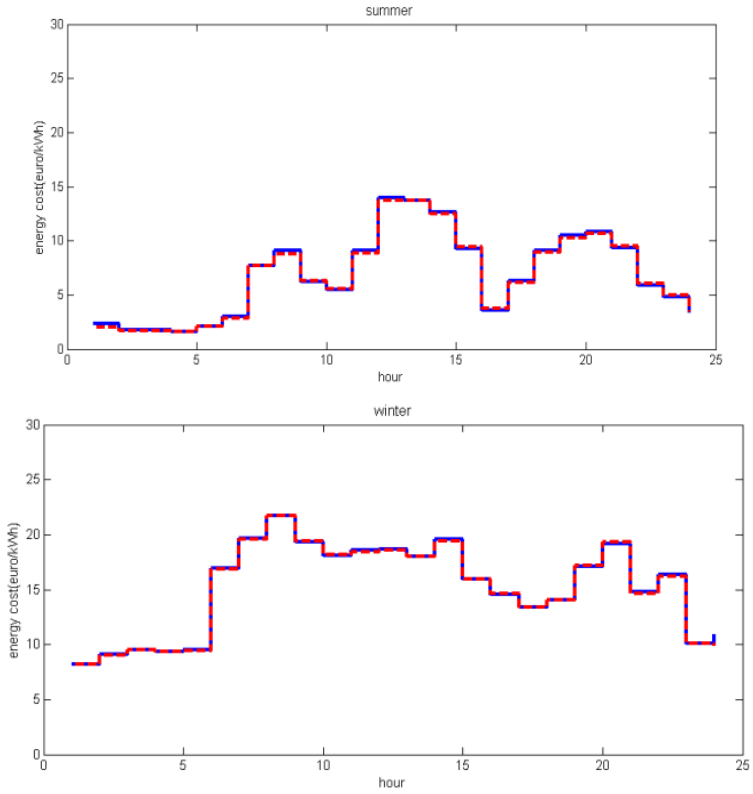

Figure 2. Verification of the written optimization code by simulating the conditions of Mancarella et al. [23]. The results achieved with minimum hourly energy cost over the 3 seasonal days (blue) show good consistency with those of the mentioned study (red)

3. RESULTS AND DISCUSSION

The true value of CHP over its lifetime was reached by analyzing several items including capital and maintenance costs and financial and environmental benefits. To this end, the optimization was repeated by considering the levelized costs of plant components and evaluating the environmental costs due to the electricity generated and fuel consumption. Figure 3 shows the optimal total cost in comparison with the energy cost on three seasonal days.

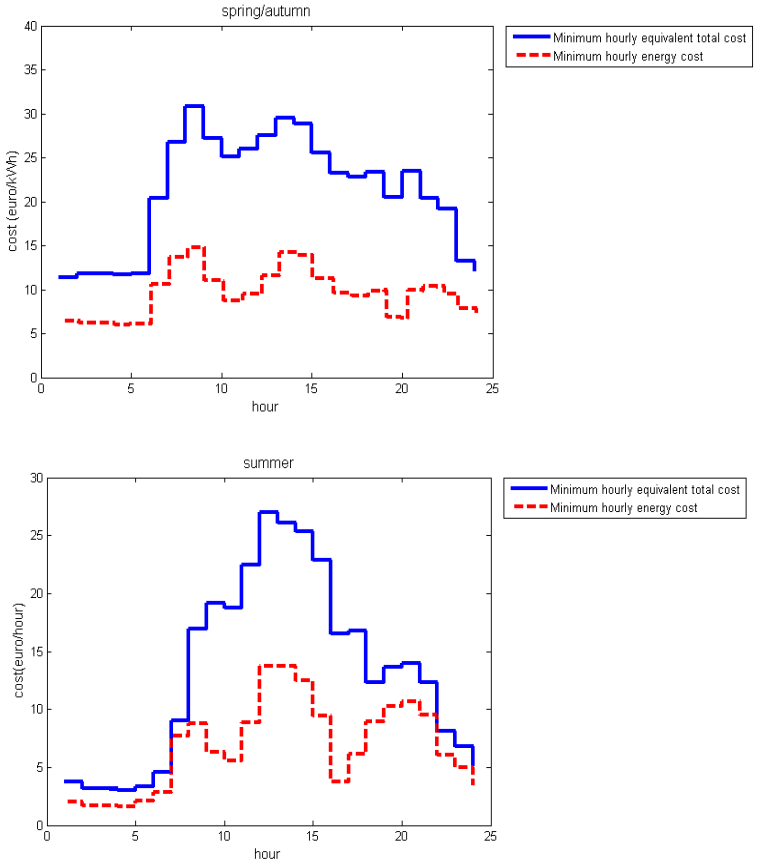

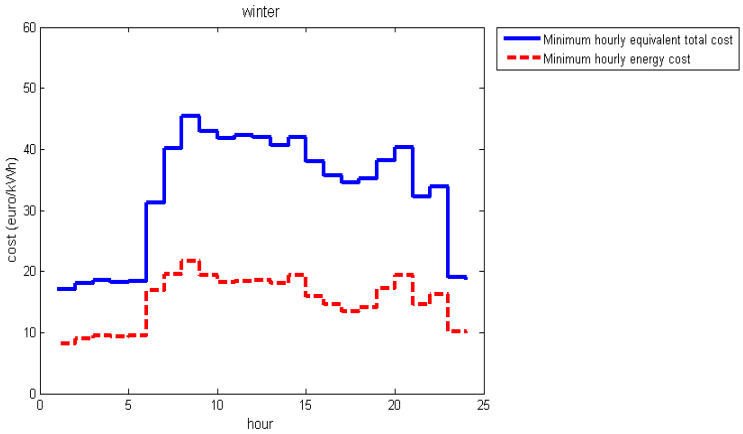

Figure 3. Minimum hourly equivalent levelized total cost (blue) compared to minimum hourly energy cost on the 3 seasonal days

The blue line represents the total costs of the studied trigeneration system. These costs are included in investment costs, energy costs, operation and maintenance costs, and GHG emission taxes on the fuel consumption and grid electricity generation. The total costs are plotted against the hourly energy costs. The minimum differences between the two lines were observed during the first hours of the summer, because the electricity demand in the optimum case was totally supplied through grid electricity during these hours. Thus, the cost of the micro turbines has no contribution to the total cost in these hours. Therefore, GHG emission costs were added only to the base case. It should be mentioned that the equipment investment costs are converted to equivalent levelized costs. Then, the costs were calculated according to the hours, resulting in the optimum case. Thus, the levelized equipment cost was set to zero during non-use hours.

Relevant power flows corresponding to the minimum total levelized cost are shown in Figs. 4, 5, and 6.

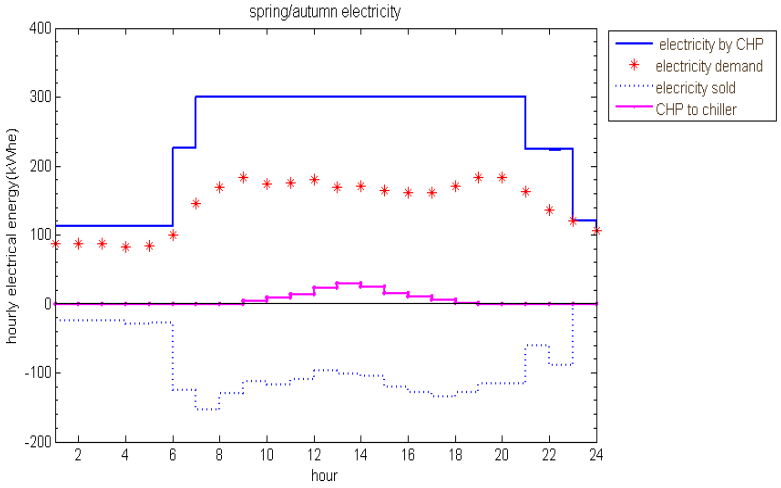

a) Spring/Autumn electricity

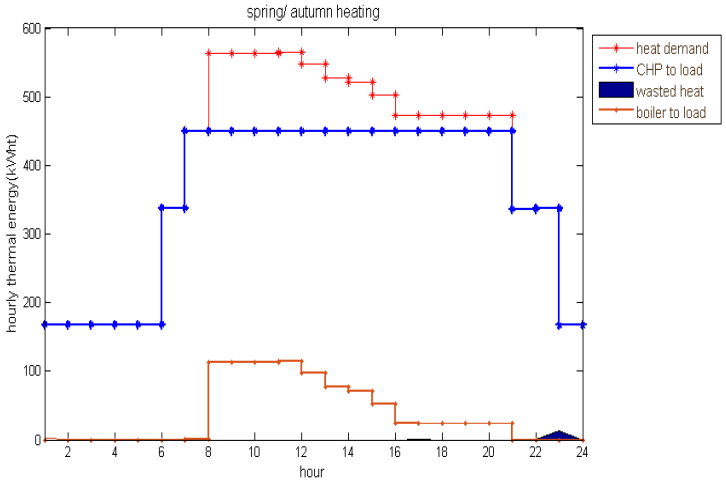

b) Spring/Autumn heating

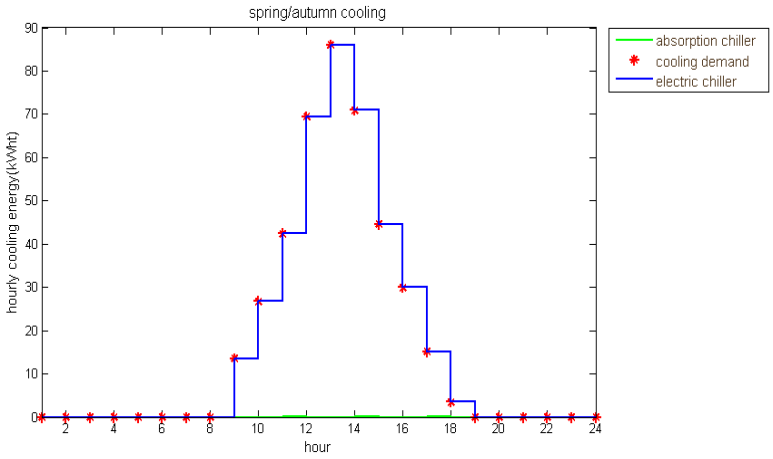

c) Spring/Autumn cooling

Figure 4. Hourly energy flows on a typical day in an intermediate (spring or autumn) season for the optimal operational strategy; a) electricity, b) heating, and c) cooling

Figure 4a shows that the entire electricity demand is supplied by the CHP during a typical day of an intermediate (spring/autumn) season. Thus, no electricity is purchased from the grid. A part of the electricity generated by CHP goes to the electric chiller. From 7 to 21, the CHP system (3 micro-turbines) operates at its rated capacity (300 kW_E). The surplus electricity is sold to the grid, as shown by the dotted line in Figure 4a. The heat generated by CHP can meet the whole heating demand for the intermediate season, from 21 to 8, except during 8 to 21, although it operates at its rated heating capacity (450 kW_Q), it cannot meet the entire heating demand. Accordingly, the remaining demand is supplied through operation of auxiliary boiler (Figure 4b). The entire cooling demand is met by the electric chiller during a day in the intermediate season. It operates with power supply from the CHP (Figure 4c).

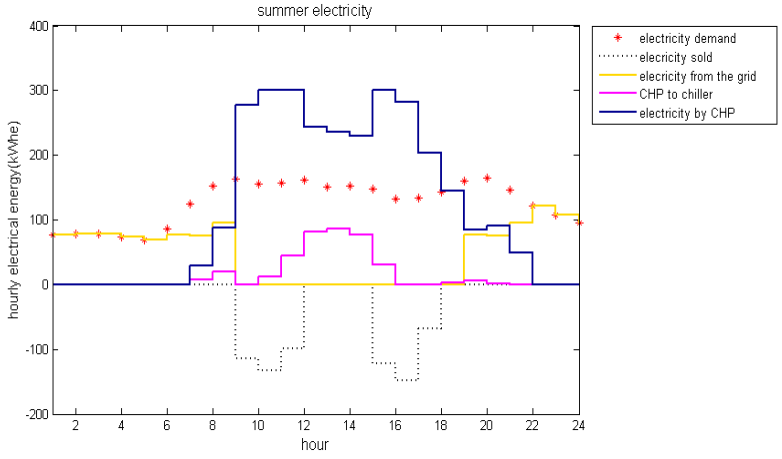

a) Summer electricity

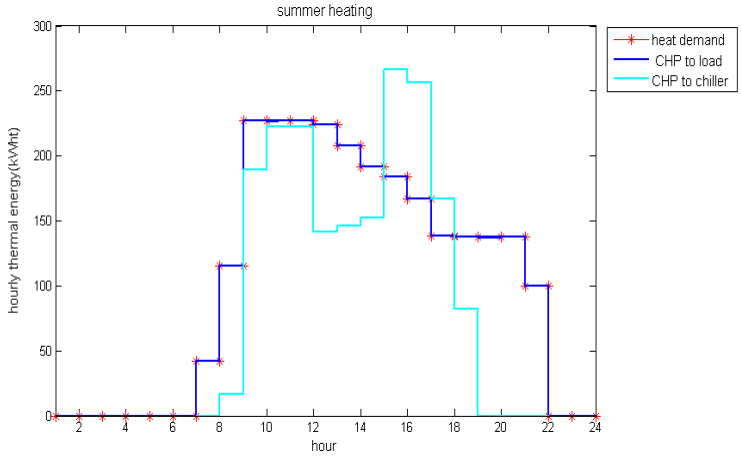

b) Summer heating

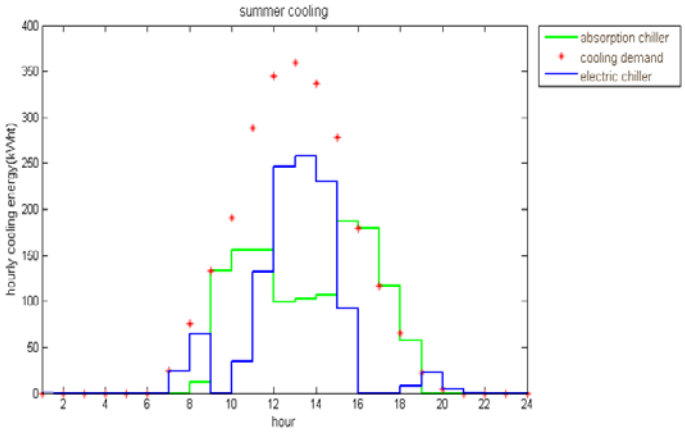

c) Summer cooling

Figure 5. Hourly energy flows on a typical day in summer season for the optimal operational strategy; a) electricity, b) heating, and c) cooling

On a summer day, due to the increased power demand, applying CHP leads to much more heat. Thus, regarding low heating demand during the night, the CHP is switched off from 22 to 7 in the optimal strategy. Furthermore, selling the surplus of generated electricity to the grid is not profitable during the interval of time. Therefore, the electricity is bought from the grid. From 19 to 22, about half of the electricity demand is supplied by the CHP and the remaining electricity comes from the grid. From 7 to 20, the produced electricity on a summer day can be used to power compressors for the cooling system. The excess electricity is sold to the grid during the interval of time (Figure 5a). From 7 to 22, the entire heating demand is met by the CHP, while the excess heat is used to run the absorption chiller (Figure 5b). The cooling demand on a summer day is covered by both the absorption and electric chillers whose supplies come from the CHP (Figure 5c).

The electricity generated by CHP is sold during the entire winter day. In the optimal strategy, the CHP system (3 micro-turbines) operates at its rated capacity from 6 to 23 (Figure 6a). Although the CHP operates at its rated capacity in these hours, it cannot cover the whole thermal demand. In this case (from 6 to 23), the remaining heating load is provided by the auxiliary boiler. On a winter day, the CHP supplies the total heating demand from 23 to 6. As there is no cooling demand, no energy goes to chillers (Figure 6b).

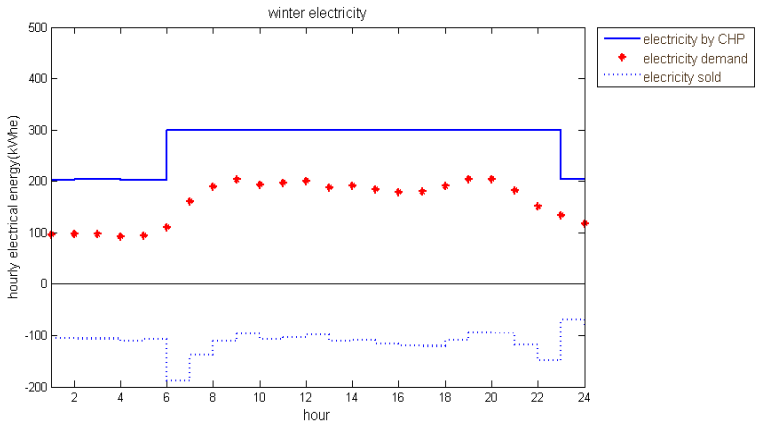

a) Winter electricity

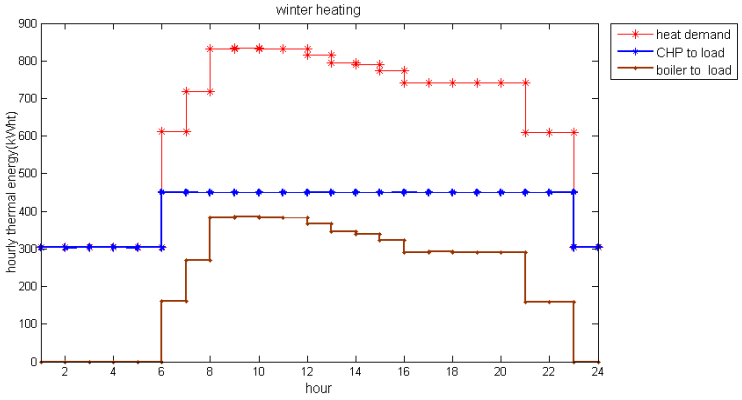

b) Winter heating

Figure 6. Hourly energy flows on a typical day in winter season for the optimal operational strategy; a) electricity, b) heating

As it can be seen, despite the added cost of the equipment, the optimal strategy offers the CHP to be switched on for most of the time instead of buying electricity from the grid. One reason is that the hourly equivalent equipment cost is negligible for the CHP system components throughout the lifetime of the plant. This situation makes it still profitable in comparison with the buying electricity from the grid. The second reason is that less carbon tax is levelized on the power generated by the CHP. Since CHP cogenerates electricity and heat, the application of CHP instead of using grid electricity and boiler separately for producing the same amount of electricity and heat reduces GHG emissions.

3.1. Payback time

The current utilization of cogeneration systems is extremely low in the United State residential sector. It is mainly due to their high costs in comparison with conventional energy systems [29]. Therefore, utilization of these types of technologies in the domestic sector requires comprehensive technical and economic analysis and it may also be able to acquire government grants [30].

In the studied system, electricity can be either purchased from or sold to the grid. It is implemented by considering the corresponding electricity prices. In this case study, it was assumed that the remaining electricity was sold back to the grid at the same price with purchasing electricity from the grid. Therefore, the annual profits could not recoup the investment costs as well as annual O&M and energy costs. To make the CHP option profitable, it is essential to sell the surplus electricity of CHP at higher prices.

Therefore, the optimization was [16] performed first with respect to the assumption that the entire electricity demand would be met by the CHP system and no electricity was bought from the grid. The hourly profit was calculated for selling surplus electricity in 3 typical days corresponding to 3 spring/autumn, summer, and winter seasons.

The optimization was repeated with respect to different selling/purchasing electricity rates to/from the grid prices ratios. Based on the achieved results, Figure 7 depicts that payback time decreases by increasing the purchasing price for the electricity generated by the CHP system. If the price of purchasing CHP electricity is considered three times more than the current ones, payback times below 5 years can be achieved.

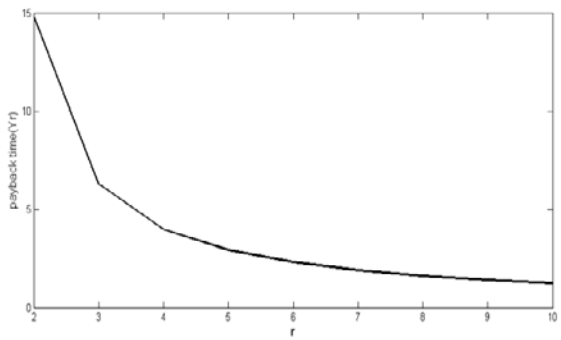

Figure 7. The range of payback periods of the studied CCHP system, calculated for different selling to purchasing electricity prices ratios (r)

4. CONCLUSIONS

In the studied system, application of CCHP led to saving in the electricity bought from the grid. These savings were computed and the emissions from the fuel consumption were evaluated. Electricity generation by CCHP led to achieving 1256 MWh annual electricity savings that otherwise must be purchased from the grid. The results also showed a significant reduction in annual CO_2 emissions (703.3 tons per year). The environmental impact of this project was assessed by GHG emission analysis. The results showed that applying the trigeneration system reduced CO_2 emission by 10550 tons during the system lifetime (15 Years). If the carbon tax was assigned to GHG emissions, the advantages of GHG emission reduction would be quantified (prices varying from 1 to 100 €/ton of CO_2; an average cost of 30 €/ton CO_2 was set [31]). This process led to 21099 € savings annually.

Increase in purchasing price of the electricity generated by these technologies can be considered as one of the supportive policies to promote the renewable energies as well as CHP systems. The attained results showed that this strategy would make cogeneration energy systems profitable and improve the contribution of these systems for supplying electrical and thermal demands in residential buildings.

5. ACKNOWLEDGEMENT

We appreciate all the assistance and guidance of relevant researchers during the course of this research.

NOMENCLATURE

ACh	Absorption chiller
B	Boiler
C	Cooling (kWh)
C	Cost (€)
Ctx	Carbon tax
D	Main diagonal of the interconnection matrix
d	Demand
E	Electricity(kWh_E)
ECh	Electrical chiller
Emiss	Emission
F	Fuel (kWh_t)
GE	Grid electricity
GEF	Greenhouse gasses emission factor (tons of CO_2 per kWh)
GS	Gas supply
GT	Micro gas turbine
i	Input
I	Interest rate
inv	Investment
M	Number of energy vectors
n	Lifetime
o	Output
Q	Heat (kWh_t)
R	Efficiency matrix
T	Interconnection matrix
v	Array of energy vectors
X	Plant components
Y	Cogenerator
Greek letters	
α	Dispatch factor
η	Efficiency
Abbreviations	
CCHP	Combined cooling, heat and power
COP	Coefficient of performance
CRF	Capital recovery facor
GHG	Greenhouse gasses
IEA	International energy agency
MESs	Multifunctional energy systems
MSMP	Multi-source multi-product
O&M	Operation and maintenance

sqp	Sequential quadratic programming	**Superscript**	
T&D	Transmission and distribution	T	Array or matrix transposition operator
Subscripts			
t	Thermal		

APPENDICES

Appendix A. Hourly electricity, heat and cooling loads for the 3 typical seasonal days used in the case study [23]

Hour	Spring/Autumn load (kWh)			Summer load (kWh)			Winter load (kWh)		
	Electricity	Heating	Cooling	Electricity	Heating	Cooling	Electricity	Heating	Cooling
1.00	87.00	168.00	0.00	77.34	0.00	0.00	96.67	303.39	0.00
2.00	87.00	168.00	0.00	78.32	0.00	0.00	97.48	304.87	0.00
3.00	87.00	168.00	0.00	78.32	0.00	0.00	97.08	304.87	0.00
4.00	83.00	168.00	0.00	74.05	0.00	0.00	92.21	303.39	0.00
5.00	85.00	168.00	0.00	69.79	0.00	0.00	94.64	303.39	0.00
6.00	100.00	338.17	0.00	86.85	0.00	0.00	111.27	610.99	0.00
7.00	146.00	450.43	0.00	125.25	41.70	24.46	161.54	718.95	0.00
8.00	170.00	563.73	0.00	152.82	115.29	76.06	189.92	832.83	0.00
9.00	183.00	563.73	13.57	162.66	226.77	132.73	203.30	834.30	0.00
10.00	174.00	563.73	26.70	155.44	227.40	190.25	193.57	832.83	0.00
11.00	176.00	564.78	42.36	157.09	227.39	288.36	196.81	832.83	0.00
12.00	180.00	547.99	69.39	161.68	224.02	345.04	201.27	816.56	0.00
13.00	170.00	527.01	86.06	150.52	208.14	359.42	188.30	795.85	0.00
14.00	171.00	520.72	70.91	152.82	191.82	336.58	191.54	789.94	0.00
15.00	165.00	502.88	44.64	147.24	183.92	278.21	184.24	773.67	0.00
16.00	161.00	473.51	29.99	133.13	166.99	179.25	179.38	741.14	0.00
17.00	161.00	473.51	15.08	134.44	138.20	116.66	179.78	742.61	0.00
18.00	171.00	473.51	3.46	143.63	137.58	65.06	190.73	741.14	0.00
19.00	184.00	473.51	0.00	160.70	137.58	21.92	204.52	741.14	0.00
20.00	184.00	473.51	0.00	164.96	137.58	5.01	204.52	741.14	0.00
21.00	163.00	336.08	0.00	145.60	99.60	0.00	182.22	609.52	0.00
22.00	136.00	337.12	0.00	121.64	0.00	0.00	151.00	609.52	0.00
23.00	120.00	167.17	0.00	107.20	0.00	0.00	133.97	304.87	0.00
24.00	106.00	167.17	0.00	95.39	0.00	0.00	118.16	304.87	0.00

Appendix B. Hourly grid electricity prices on the 3 seasonal days of the case study [23]

Electricity price (€/MWh)			
Hour	Spring/Autumn	Summer	Winter
1	40	30	50
2	20	20	40
3	20	20	40
4	20	20	40
5	20	30	40
6	40	40	40
7	40	50	50
8	60	70	70
9	110	100	110
10	120	110	110
11	120	110	110
12	110	80	110
13	80	70	100
14	80	80	80
15	90	80	100
16	90	100	110
17	90	80	120
18	90	70	120
19	120	60	110
20	90	60	80
21	70	60	80
22	60	50	50
23	40	50	50
24	40	40	40

REFERENCES

1. Metz, B., Davidson, O.R., Bosch, P.R., Dave, R. and Meyer, L.A. (eds), Fourth assessment report of the IPCC (Climate change 2007), IPCC, Cambridge University Press, (2007). (https://ipcc.ch/report/ar4/wg3).
2. International Energy Agency, Why CHP/DHC?, (2018). (https://www.iea.org/chp/whychpdhc).
3. Keirstead, J., "The impact of CHP (combined heat and power) planning restrictions on the efficiency of urban energy systems", ***Energy***, Vol. 41, No. 1, (2012), 93-103. (https://doi.org/10.1016/j.energy.2011.06.011).
4. Schulze, M., Friedrich, L. and Gautschi, M., "Modeling and optimization of renewables: Applying the energy hub approach", ***Proceedings of 2008 IEEE International Conference on Sustainable Energy Technologies***, Singapore, (2008). (https://doi.org/10.1109/ICSET.2008.4746977).
5. Bandyopadhyay, S., "The first step towards energy revolution", ***Clean Technologies and Environmental Policy,*** Vol. 21, No. 2, (2019), 227-228. (https://doi.org/10.1007/s10098-019-01674-4).
6. Kellya, S. and Pollittb, M., "An assessment of the present and future opportunities for combined heat and power with district heating (CHP-DH) in the United Kingdom", ***Energy Policy***, Vol. 38, No.11, (2010), 6936-6945. (https://doi.org/10.1016/j.enpol.2010.07.010).
7. Meckler, M., Sustainable on-site CHP systems, design, construction, and operations, McGraw-Hill, (2010), ISBN 978-0-07-160317-1.
8. International energy agency, Combined heat and power, evaluating the benefits of greater global investment, (2010). (http://www.iea.org/Papers/2008/chp_report.pdf).
9. Merkel, E., McKenna, R. and Fichtner, W., "Optimization of the capacity and the dispatch of decentralized micro-CHP systems: A case study for the UK", ***Appied Energy***, Vol. 140, (2015), 120-134. (https://doi.org/10.1016/j.apenergy.2014.11.036).
10. Mago, P.J. and Smith, A.D., "Evaluation of the potential emissions reductions from the use of CHP systems in different commercial buildings", ***Building and Environment***, Vol. 53, (2012), 74-82. (https://doi.org/10.1016/j.buildenv.2012.01.006).
11. Bakken, B., Haugstad, A., Hornnes, K. S. and Vist, S., "Simulation and optimization of systems with multiple energy carriers", ***Proceedings of the Scandinavian Conference on Simulation and Modeling***, Linköping, Sweden, (1999). (http://citeseerx.ist.psu.edu/viewdoc/download?doi=10.1.1.414.5376&rep=rep1&type=pdf).
12. Paska, J.B., "Hybrid power systems-An effective way of utilizing primary energy sources", ***Renewable Energy***, Vol. 34, No. 11, (2009), 2414-2421. (https://doi.org/10.1016/j.renene.2009.02.018).
13. International Energy Agency, Technology roadmap energy-efficient buildings: Heating and cooling equipment, IEA, Paris, (2011). (https://www.iea.org/reports/technology-roadmap-energy-efficient-buildings-heating-and-cooling-equipment).
14. Cai, R., Jin, H., Gao, L. and Hong, H., "Development of multifunctional energy systems (MESs)", ***Energy***, Vol. 35, No. 11, (2010), 4375-4382. (https://doi.org/10.1016/j.energy.2008.12.016).
15. Colella, F.U., "Desalted water provided by a poligeneration scheme for the tourist sector", ***Desalination***, Vol. 205, No. 1-3, (2007), 279-297. (https://doi.org/10.1016/j.desal.2006.02.057).
16. Bahrami, S. and Safe, F., "A financial approach to evaluate an optimized combined cooling, heat and power system", ***Energy and Power Engineering,*** Vol. 5 No. 5, (2013), 352-362. (https://doi.org/10.4236/epe.2013.55036).
17. Nazara, M.H., "Multiobjective electric distribution system expansion planning using hybrid energy hub concept", ***Electric Power Systems Research***, Vol. 79, No. 6, (2009), 899-911. (https://doi.org/10.1016/j.epsr.2008.12.002).
18. Kienzle, F., Favre-Perrod, P., Arnold, M. and Andersson, G., "Multi energy delivery infrastructures for the future", ***Proceedings of First International Conference on Infrastructure Systems and Services: Building Networks for a Brighter Future (INFRA)***, Rotterdam, (2008), 1-5. (https://doi.org/10.1109/INFRA.2008.5439681).
19. Geidl, M., "Integrated modeling and optimization of multi-carrier energy systems", Dissertation for the Doctoral Degree, Eidgenossische Technische Hochschule (ETH), Zurich, Nr. 17141, (2007). (https://pdfs.semanticscholar.org/163e/46095eb5af05b908745a8ab61c4820ea8bcb.pdf).
20. Kraus, T., "Maximizing exergy efficiency in multi-carrier energy systems", ***Proceedings of Power and Energy Society General Meeting, 2010 IEEE***, (2010). (https://doi.org/10.1109/PES.2010.5589999).
21. Geidl, M., Koeppel, G., Favre-Perrod, P., Klockl, B., Andersson, G. and Frohlich, K., "Energy hubs for the future", ***Power and Energy Magazine,*** IEEE, Vol. 5, No. 1, (2007), 24-30. (http://doi.org/10.1109/MPAE.2007.264850).
22. Liu, X. and Mancarella, P., "Modelling, assessment and Sankey diagrams of integrated electricity-heat-gas networks in multi-vector district energy systems", ***Applied Energy***, Vol. 167, (2016), 336-352. (https://doi.org/10.1016/j.apenergy.2015.08.089).
23. Mancarella, M. and Chicco, G., "Matrix modeling of small-scale trigeneration systems and application to operational optimization", ***Energy***, Vol. 34, (2009), 261-273. (https://doi.org/10.1016/j.energy.2008.09.011).
24. Amber, K.P., "Development of a combined heat and power sizing model for higher education buildings in the United Kingdom", ***Energy and Buildings***, Vol. 172, (2018), 537-553. (https://doi.org/10.1016/j.enbuild.2018.02.027).
25. Liu, M., Shi, Y. and Fang, F., "Combined cooling, heating and power systems: A survey", ***Renewable and Sustainable Energy Reviews***, Vol. 35, (2014), 1-22. (https://doi.org/10.1016/j.rser.2014.03.054).
26. Carvalho, M., Lozano, M.A., Serra, L.M. and Wohlgemuth, V., "Modeling simple tri-generation systems for the distribution of environmental loads", ***Environmental Modelling & Software***, Vol. 30, (2012), 71-80. (https://doi.org/10.1016/j.envsoft.2011.11.005).
27. The RETScreen clean energy project analysis software, Natural resources Canada–Canmet ENERGY, Ontario, Canada. (https://www.nrcan.gc.ca/energy/software-tools/7465).
28. Sorrels, J.L. and Walton, T.G., Cost estimation: Concepts and methodology, U.S. Environmental Protection Agency, (2017). (https://www.epa.gov/sites/production/files/2017-12/documents/epaccmcostestimationmethodchapter_7thedition_2017.pdf).
29. Vishwanathan, G., "Techno-economic analysis of high-efficiency natural-gas generators for residential combined heat and power", ***Applied Energy***, Vol. 226, (2018), 1064-1075. (https://doi.org/10.1016/j.apenergy.2018.06.013).
30. Hoseinzadeh, S., Zakeri, M.H., Shirkhani A. and Chamkha, A.J., "Analysis of energy consumption improvements of a zero-energy building in a humid mountainous area", ***Journal of Renewable and Sustainable Energy***, Vol. 11, No. 1, (2019), 015103. (https://doi.org/10.1063/1.5046512).
31. Postic, S. and Clément, M., Global carbon account 2019, Paris, (2019). (https://www.i4ce.org/wp-core/wp-content/uploads/2019/05/i4ce-PrixCarbon-VA.pdf).

ABSTRACTS

Ex-Situ CO_2 Capture and Utilization Over the Bauxite Residue: Lifecycle and Economic Recovery Assessment

Kazem Kashefi[a*], Alireza Pardakhti[a], Majid Shafiepour[a], Azadeh Hemmati[b]

[a] *Department of Environmental Engineering, School of Environment, College of Engineering, University of Tehran, P. O. Box: 11155-4563, Tehran, Tehran, Iran.*
[b] *Department of Petroleum and Chemical Engineering, Science and Research Branch, Islamic Azad University, P. O. Box: 14515-775, Tehran, Tehran, Iran.*

PAPER INFO

Paper history:
Received 09 April 2020
Accepted in revised form 14 July 2020

Keywords:
Carbon Capture and Utilization,
Life Cycle Assessment,
Carbon Footprint,
Greenhouse Gas Emission

ABSTRACT

Carbon-dioxide Capture and Utilization (CCU) technology is an efficient process in the portfolio of greenhouse gas reduction approaches and is programmed to mitigate global warming. Given that the prime intention of CCU technologies is to prevent CO_2 emissions into the atmosphere, it remains to be seen if these approaches cause other environmental impacts and consequences. Therefore, the Life Cycle Assessment (LCA) approach was considered to account for all environmental aspects, in addition to the emission of greenhouse gases. In this study, the Life Cycle Inventory (LCI) methodology was employed to quantify the environmental impacts of indirect carbonation of Red Mud (RM), a waste byproduct of alumina production line in Jajarm Alumina Plant, Iran by CO_2 exhausted from the plant stacks based on International Organization for Standardizations (ISO) of ISO 14040 and ISO 14044. The results confirmed the reduction of CO_2 emission by 82 %. The study of carbon footprint based on ISO 14064 under the criterion of PAS 2050 revealed CO_2 emission equivalent to 2.33 kg/ ton RM, proving that CCU managed to mitigate the CO_2 emission by 93 % compared to the conventional technology employed in Jajarm Plant, which produced around 34 kg CO_2 per 1 ton RM. Furthermore, the economic evaluation of the process brought about 243 $/ton RM in profit via the sales of products including silica, aluminum, hematite, and calcium carbonate. The outcomes of the present study highlight that the intended CCU technology is a practicable approach for large-scale applications.

https://doi.org/10.30501/jree.2020.225900.1097

چکیده

تکنولوژی به‌دام اندازی و بهره‌برداری کربن‌دی‌اکسید (CCU) یک روش مفید در جهت کاهش گازهای گلخانه‌ای به‌منظور کاهش گرمایش جهانی می‌باشد. اگرچه مقصود اصلی تکنولوژی‌های CCU جلوگیری از انتشار گاز CO_2 به اتمسفر می‌باشد، اما باید این اطمینان حاصل گردد که این روش اثرات و پیامدهای زیست‌محیطی دیگری را در پی نداشته‌باشند. باتوجه به این مطلب، دستاورد ارزیابی چرخه‌ی حیات با هدف احتساب تمامی پیامدهای زیست‌محیطی افزون بر انتشار گازهای گلخانه‌ای در نظر گرفته شد. در این مطالعه، روش‌شناسی فهرست چرخه‌ی حیات بر اساس استانداردهای ISO 14040 و ISO 14044 به منظور محاسبه‌ی اثرات محیط‌زیستی کربناسیون غیرمستقیم گل قرمز، پسماند کارخانه‌ی تولید آلومینای جاجرم، توسط گاز CO_2 خروجی از دودکش‌های کارخانه مورد بررسی قرار گرفت. نتایج، کاهش ۸۲ ٪ انتشار معادل CO_2 را نشان داد. نتایج به‌دست آمده بر اساس استاندارد ISO 14064 طبق معیار PAS ۲۰۵۰، که چارچوب مطالعه‌شده برای بررسی رد پای کربن در این مطالعه است، انتشار معادل CO_2 به میزان kg ۲/۳۳ به‌ازای ۱ تن گل قرمز را نشان داد که بیانگر کاهش ۹۳ ٪ انتشار معادل CO_2 در مقایسه با تکنولوژی متداول کارخانه‌ی جاجرم که انتشار معادل CO_2 حدود kg ۳۴ به ازای ۱ تن گل قرمز را دارد، می‌باشد. علاوه‌براین، ارزیابی اقتصادی فرآیند حاکی از سود معادل ۲۳۴ دلار به ازای ۱ تن گل قرمز دارد که ناشی از فروش محصولات از جمله سیلیکا، آلومینیوم، هماتیت و کربنات کلسیم می‌باشد. نتایج این تحقیق نشان داد که تکنولوژی CCU یک دستاورد قابل اجرا برای کاربرد در مقیاس بزرگ است.

Feasibility Study of Powering Desiccant Evaporative Cooling Systems with Photovoltaic Solar Panels for Hot and Humid Climates of Iran

Ahmad Naderi Nobandegani, Mohammad Ahmadzadehtalatapeh*

Department of Mechanical & Marine Engineering, Chabahar Maritime University, P. O. Box: 99717-56499, Chabahar, Sistan and Baluchestan, Iran.

P A P E R I N F O

Paper history:
Received 14 April 2020
Accepted in revised form 27 July 2020

Keywords:
Buildings,
Energy Consumption,
Desiccant Evaporative Cooling System (DECS),
Indoor Air,
TRNSYS

A B S T R A C T

In the present study, the performance of a Desiccant Evaporative Cooling System (DECS) under eight different designs to provide the desired indoor air conditions for administration buildings was explored via TRNSYS software. An administration building in Chabahar, Iran as a region with a high cooling load demand was considered for the study. The simulation results indicated that the two-stage desiccant cooling system (Des. H) was the most suitable design, and it enjoyed the potential to keep the indoor air conditions within the standard recommendations. It was also shown that Des. H is the superior design in terms of energy performance and can meet the space cooling load requirements. The study showed that Des. H had the highest COP value with 2.83. The possible application of solar energy to the regeneration process of the Des. H was also studied. The simulations revealed that Des. H with and without the solar panels had less energy consumption than the existing system. The study showed that the application of Des. H could ensure 26.97 % saving in power per year in comparison to the existing system. Moreover, it was demonstrated that the addition of PVT panels to Des. H could increase the rate of annual power saving to about 68.03 %.

https://doi.org/10.30501/jree.2020.225286.1096

چکیده

در این مطالعه، عملکرد یک سیستم خنک‌کننده دسیکنت تبخیری (DECS) تحت هشت طرح مختلف به منظور تأمین هوای مطلوب برای یک ساختمان اداری با بکارگیری نرم افزار TRNSYS مورد ارزیابی قرار گرفته است. به این منظور یک ساختمان اداری در چابهار، ایران به عنوان یک منطقه با نیاز بار سرمایشی بالا مورد مطالعه قرار گرفته است. نتایج شبیه‌سازی نشان می‌دهد که طرح خنک‌کننده دسیکنت دو مرحله‌ای (Des. H) جهت تأمین هوای مطلوب ساختمان نسبت به دیگر طرح‌ها مناسب‌تر بوده و این پتانسیل را دارد که شرایط هوای داخل ساختمان را در محدوده استاندارد نگه دارد. همچنین نشان داده شد که طرح Des. H از نظر عملکرد انرژی از شرایط مناسب‌تری برخوردار بوده و می‌تواند بار سرمایشی مورد نیاز فضا را تأمین نماید. نتایج مطالعه نشان می‌دهد طرح خنک کننده دسیکنت دو مرحله‌ای بالاترین مقدار COP را به مقدار ۲/۸۳ در بین طرح‌های مطالعه شده دارد. در ادامه امکان بکارگیری انرژی خورشیدی در مرحله بازیابی سیستم دسیکنت طرح Des. H مورد مطالعه قرار گرفت. نتایج شبیه‌سازی نشان داد که سیستم DECS تحت طرح Des. H مصرف سالیانه انرژی را به میزان ۲۶/۹۷ ٪ در مقایسه با سیستم موجود کاهش می‌دهد. به علاوه مطالعه نشان می‌دهد در صورت بکارگیری طرح Des. H به همراه PVT, کاهش مصرف سالیانه به میزان ۶۸/۰۳ ٪ افزایش می‌یابد.

Feasibility Study of Using Renewable Energies in the Water and Wastewater Industry (Case Study: Tehran Water and Wastewater Company)

Ensieh Ozgoli[a], Younes Noorollahi[b*], Reza Arjmandi[a], Ali Mohammadi[a]

[a] *Department of Environment Management, Faculty of Natural Resources and Environment, Science and Research Branch, Islamic Azad University, P. O. Box: 1477893855, Tehran, Tehran, Iran.*
[b] *Department of Renewable Energy and Environmental Engineering, Faculty of New Sciences and Technologies, University of Tehran, Tehran, Tehran, Iran.*

PAPER INFO

Paper history:
Received 12 April 2020
Accepted in revised form 28 July 2020

Keywords:
Greenhouse Gases,
Prediction Model,
Electricity Consumption,
Renewable Energy,
Carbon Tax

ABSTRACT

Climate change refers to any significant and long-term alterations in global or regional weather conditions. The impact of climate change on the industrial plans is enormous, while the water supply sector has been challenged to examine how it could continuously operate in the current situation. Optimization of energy consumption and reduction of Greenhouse Gases (GHG) emissions are some of the priorities of water companies. The objective of the study is to propose a novel evaluation approach to the feasibility of using renewable energies (solar, wind, and biomass) in the water and wastewater industry. Tehran Water and Wastewater Company consists of six regional districts and forecasting of its energy consumption, power costs, and carbon tax rates for the next ten years was done by using the regression model. The results indicated that increase in water supply and electricity consumption was evidenced by the increase in Tehran's annual population. GHG emissions were calculated in two scenarios, the first of which is based on the total supply of required electricity from conventional power plants and the second is on the generation of approximately one-third by renewable energies. In addition to the higher emissions of carbon dioxide (CO_2) from diesel and oil power plants than the natural gas-fueled plants, by increasing the carbon tax to more than 30 USD per tonne of CO_2, it is expected that the emissions will be reduced by 30 % in all fossil-fueled power plant types. Results showed that a small amount of tax was not effective in reducing GHG emissions.

https://doi.org/10.30501/jree.2020.226666.1099

چکیده

تغییرات آب و هوا به هرگونه تغییر و تحولات مهم و بلندمدت در شرایط آب و هوایی جهانی یـا منطقـه‌ای اشـاره دارد. تـأثیر تغییـرات آب و هـوا در برنامه‌ریزی‌های صنعتی بسیار زیاد است، بطوریکه که بخش تأمین آب شرب برای بررسی چگونگی فعالیت پایدار در شرایط حاضر، به چالش کشـیده شده است. بهینه‌سازی مصرف انرژی و کاهش انتشار گازهای گلخانه ای (GHG) از اولویت‌های شرکت‌های آب است. هدف از این مطالعه، ارائه یـک روش ارزیابی جدید برای امکان‌سنجی استفاده از انرژی‌های تجدیدپذیر (خورشیدی، باد و زیست‌توده) در صنعت آب و فاضلاب اسـت. شـرکت آب و فاضلاب تهران از شش منطقه تشکیل شده است و پیش‌بینی مصرف انرژی، هزینه‌های انرژی و نرخ مالیات کربن برای ده سال آینده آن با استفاده از مدل رگرسیون پیش‌بینی شده است. نتایج نشان داد که افزایش مشهود آبرسانی و مصرف برق، ناشی از افـزایش جمعیـت سـالانه تهـران مـی‌باشـد. محاسبه انتشار GHG در قالب دو سناریو انجام شده است، سناریو اول مبتنی بر تأمین کل الکتریسیته موردنیاز از نیروگاه‌های رایج و دومی براساس تولید حدود یک سوم آن از انرژی‌های تجدیدپذیر است. علاوه بر انتشار دی اکسید کربن (CO_2) بالاتر از نیروگاه‌های با سوخت دیزل و نفت نسـبت به نیروگاه‌هایی که با گاز طبیعی کار می‌کنند، با در نظر گرفتن مالیات کربن به بیش از ۳۰ دلار در هر تن انتشار CO_2، پیش‌بینی می‌شود که میزان انتشار آن تا میزان ۳۰ ٪ برای همه انواع نیروگاه‌های سوخت فسیلی، کاهش یابد. همچنین، نتایج نشان داد که مقدار کـم مالیـات در کـاهش انتشـار GHG مؤثر نیست.

Adaptive Robust Control Design to Maximize the Harvested Power in a Wind Turbine with Input Constraint

Hossein Dastres, Ali Mohammadi, Behrooz Rezaie*

Department of Electrical and Computer Engineering, Babol Noshirvni University of Technology, P. O. Box: 47148-71167, Babol, Mazandaran, Iran.

PAPER INFO

Paper history:
Received 17 April 2020
Accepted in revised form 02 August 2020

Keywords:
Second-Order Sliding Mode Control,
Fast Integral Terminal Sliding Mode Control,
Input Saturation,
Maximum Power Point Tracking

ABSTRACT

This paper deals with the problem of maximizing the extracted power from a wind turbine in the presence of model uncertainties and input saturation. An adaptive second-order integral terminal sliding mode speed control method is utilized to address this problem. The presented method benefits from the advantages of several control techniques, i.e., adaptability, robustness, finite-time convergence, and the capability of coping with the input saturation. The robust nature of the designed controller causes its high performance in facing the uncertainties in the wind turbine model. In this paper, to compensate for the effect of input saturation, an auxiliary dynamic variable is added to the tracking error and also an adaptation law is designed so that the finite-time convergence of the closed-loop system can be achieved. Moreover, to reduce the mechanical stresses which are the result of the chattering phenomenon, a second-order sliding surface is employed. The finite-time convergence of the designed controller has been proven by the Lyapunov stability theorem in which the finite-time convergence of the tracking error to zero is guaranteed. Finally, to illustrate the effectiveness and satisfactory performance of the proposed controller, two comparative simulations are carried out. The results of this comparison show that the proposed controller has less error to track the optimal speed and when the model uncertainties and input saturation occur in the wind turbine system, the proposed controller is almost 3 % more efficient than the existing controllers.

https://doi.org/10.30501/jree.2020.224180.1093

چکیده

این مقاله مسئله حداکثرکردن توان استخراج شده از یک توربین بادی در حضور عدم قطعیت‌های مدل و اشباع ورودی را بررسی می‌کند. به این منظور، از یک روش کنترل سرعت مد لغزشی ترمینال مرتبه دوم تطبیقی بهره گرفته می‌شود. روش پیشنهادی مزایای چندین تکنیک کنترلی از قبیل قابلیت تطبیق، مقاوم بودن، همگرایی زمان محدود و توانایی مقابله با اشباع ورودی را دارا می‌باشد. طبیعت مقاوم کنترل‌کننده طراحی شده باعث عملکرد بالای آن در مواجهه با نامعینی‌های موجود در مدل توربین بادی می‌گردد. در این مقاله جهت جبران اثر اشباع ورودی، یک متغیر دینامیکی کمکی به خطای ردیابی اضافه شده است و همچنین یک قانون تطبیق به گونه‌ای طراحی شده است که همگرایی زمان محدود سیستم حلقه بسته حاصل گردد. به علاوه، جهت کاهش تنش‌های مکانیکی حاصل از پدیده چترینگ، یک سطح لغزش مرتبه دوم به کار برده شده است. همگرایی زمان- محدود کنترل‌کننده طراحی شده با استفاده از قضیه پایداری لیاپانف ثابت می‌گردد که در آن تضمین می‌شود که خطای دنبال‌یابی در زمان- محدود به صفر همگرا می‌گردد. در نهایت، عملکرد مؤثر و رضایت‌بخش کنترل‌کننده پیشنهادی با انجام دو شبیه‌سازی مقایسه‌ای نشان داده می‌شود و برتری روش پیشنهادی مشخص می‌گردد. نتایج این مقایسه نشان می‌دهد که کنترل‌کننده پیشنهادی خطای کمتری در دنبال‌یابی سرعت بهینه دارد و هنگامی که عدم قطعیت‌های مدل و اشباع ورودی در سیستم توربین بادی رخ می دهد، نسبت به کنترل‌کننده‌های موجود تقریباً ۳ ٪ راندمان بیشتری دارد.

Biogas Potentiality Through Waste Management in Bangladesh

Parvez Mosharraf[a], Md. Saroyar Zahan[a], Dilip Kumar Das[b], Suman Chowdhury[a*]

[a] *Department of Electrical and Electronic Engineering, International University of Business Agriculture and Technology, Uttara Model Town, Dhaka 1230, Bangladeh.*
[b] *Department of Mathematics, International University of Business Agriculture and Technology, Uttara Model Town, Dhaka 1230, Bangladeh.*

PAPER INFO

Paper history:
Received 12 March 2020
Accepted in revised form 09 August 2020

Keywords:
Anaerobic Digestion,
Biogas,
Landfill,
Waste,
Power

ABSTRACT

This study offers an effective solution to meet the growing demands of biogas plants for energy. This paper presents a model and simulates the digestion process of biogas production from the organic and food processing waste that contains high moisture. Biogas is produced by bacteria through the bio-degradation of organic material under anaerobic conditions. According to the findings, in case of biogas production, the broiler chicken manure is approximately 88 %. From the analysis, it is observed that the chicken broiler waste is approximately 88 % more efficient than the unsorted waste. In addition, in the case of digestate, the cow manure is approximately 6.25 % more efficient than the garden waste. The present study aims to investigate the performance of different types of wastes regarding biogas production. To this end, different types of waste were considered in data analysis. According to the data analysis, biogas production is highly affected by the type of waste.

https://doi.org/10.30501/jree.2020.222856.1089

چکیده

این مطالعه یک راه حل مؤثر برای رفع نیازهای رو به رشد واحدهای بیوگاز برای انرژی ارائه می‌دهد. مدل ارائه شده در این مقاله به شبیه‌سازی فرآیند هضم تولید بیوگاز از زباله‌های فرآوری مواد آلی و مواد غذایی که حاوی رطوبت زیادی هستند، می‌پردازد. بیوگاز توسط باکتری‌ها و از راه تجزیه بیولوژیکی مواد آلی، تحت شرایط بی‌هوازی تولید می‌شود. با توجه به یافته‌های بدست آمده، در موارد تولید بیوگاز حاصل از تجزیه و تحلیل ضایعات مرغی، مشاهده می‌شود که ضایعات مرغ‌های گوشتی دسته‌بندی شده در مقایسه با ضایعات مرغی دسته‌بندی نشده که به طور تقریبی ۸۸ ٪ است، کارآمدتر هستند. هم‌چنین، به شکل کلی، هضم هوازی کود گاو تقریباً ۶/۲۵ ٪ از زباله های باغی کارآمدتر است. مطالعه حاضر با هدف بررسی عملکرد انواع مختلفی از پسماندهای تولید بیوگاز انجام شده است. برای این منظور، انواع مختلفی از پسماندها در آنالیز داده‌ها مورد بررسی قرار گرفت. با توجه تجزیه و تحلیل داده‌ها، تولید بیوگاز به شدت تحت تأثیر نوع مواد زائد است.

Investigation of the Synergism Effect and Electrocatalytic Activities of Pt and Ru Nanoparticles Supported on the Carbon Aerogel-Carbon Nanotube (CA-CNT) for Methanol Oxidation Reaction (MOR)

Masoumeh Javaheri[a*], Noushin Salman Tabrizi[b], Amir Rafizadeh[b]

[a] *Department of Ceramic, Materials and Energy Research Center (MERC), MeshkinDasht, Alborz, Iran.*
[b] *Department of Energy, Materials and Energy Research Center (MERC), MeshkinDasht, Alborz, Iran.*

P A P E R I N F O

Paper history:
Received 14 June 2020
Accepted in revised form 17 August 2020

Keywords:
Fuel Cell,
Methanol,
Synergism,
Aerogel,
Nanotube

A B S T R A C T

Given that the catalyst and catalyst support properties have a key role to play in the electrochemical activity of fuel cells, in this research, the synergism effect of Pt and Ru nanoparticles reduced on catalyst support [synthesized Carbon Aerogel-Carbon Nanotube (CA-CNT)] was investigated. The catalyst support was synthesized by sol-gel method and the catalyst nanoparticles were reduced on catalyst support using impregnation and hydrothermal method. Different molar ratios of Pt:Ru (i.e., 0:1, 1:0, 3:1, 2:1, 1:1, 1:2, and 1:3) were applied as electrocatalysts for Methanol Oxidation Reaction (MOR). The electrochemical performance of these catalysts was compared with that of commercial Pt/C (20 % wt) for MOR. The physical properties of the synthesized catalyst support (CNT-CA) were studied using FESEM and BET techniques. Moreover, XRD and ICP analyses were employed for investigating each of the synthesized catalyst (Pt/CNT-CA and Ru/CNT-CA). The cyclic voltammetry and chronoamperometry methods were used to conduct electrochemical analysis. Research results indicated that synthesis methods were reliable. Moreover, CNT-CA had a proper performance as the catalyst support and the Pt:Ru with a 3:1 molar ratio was the best catalyst among all the synthesized catalysts for MOR.

https://doi.org/10.30501/jree.2020.234091.1116

چکیده

از آنجا که خواص کاتالیست و پایه کاتالیست در فعالیت الکتروشیمیایی پیل‌های سوختی نقش کلیدی ایفا می‌کند، در این تحقیق اثر هم‌افزایی نانوذرات Pt و Ru احیاء شده بر روی کربن آیروژل-کربن نانوتیوب (CA-CNT) بررسی شده است. پایه کاتالیست با روش سل- ژل سنتز شده و نانوذرات کاتالیست با روش غوطه وری و هیدروترمال بر روی پایه کاتالیست احیاء شده است. به عنوان الکتروکاتالیست نسبتهای مولی متفاوتی از Pt:Ru (۱:۳ و ۱:۲، ۱:۱، ۲:۱، ۳:۱، ۱:۰، ۰:۱) برای واکنش اکسایش متانول به‌کار رفته است. فعالیت الکتروکاتالیستی این کاتالیستها با Pt/C تجاری مقایسه شده است. ویژگیهای فیزیکی پایه کاتالیست سنتز شده با استفاده از تکنیکهای BET و FESCM بررسی شدند. همچنین XRD و ICP برای شناسایی کاتالیستهای سنتز شده استفاده شدند. برای بررسیهای الکتروشیمیایی از تکنیکهای ولتامتری چرخه‌ای (CV) و کرونوآمپرومتری استفاده شد. نتایج نشان دادند که روشهای به‌کار رفته برای سنتز معتبر است، همچنین CA-CNT کارآیی مناسبی به عنوان پایه کاتالیست دارد و از بین تمام کاتالیستهای سنتز شده، Pt:Ru با نسبت مولی ۳:۱ بهترین کاتالیست برای MOR است.

Optimization of Small-Scale Trigeneration Systems in Terms of Levelized Total Costs and Carbon Tax Using a Matrix Modeling Approach

Taraneh Taheri[a], Mohammad Behshad Shafii[b*], Sourena Sattari[c], Morteza Khalaji Assadi[d]

[a] *Department of Energy Engineering, Faculty of Natural Resources and Environment, Science and Research Branch, Islamic Azad University, Tehran, Tehran, Iran.*
[b] *Department of Mechanical Engineering, Sharif University of Technology, P. O. Box: 11155-9567, Tehran, Tehran, Iran.*
[c] *Department of Energy Engineering, Sharif University of Technology, Tehran, Tehran, Iran.*
[d] *Department of Fine Arts, Faculty of Architecture, University of Tehran, Tehran, Tehran, Iran.*

PAPER INFO

Paper history:
Received 26 April 2020
Accepted in revised form 12 September 2020

Keywords:
Energy Hub,
Matrix Modeling,
Dispatch Factors,
Economic Analysis,
Optimal Strategy

ABSTRACT

Combined Heat and Power (CHP) systems have increasingly drawn attention in recent years due to their higher efficiency and lower Greenhouse Gas (GHG) emission. Input-output matrix modeling was considered here as one of the efficient approaches for optimizing these energy networks. In this approach, power flow and energy conversion through plant components were modeled by an overall efficiency matrix including dispatch factors and plant component efficiencies. The purpose of this paper is to propose a modification of the objective function presented in some previous studies. This procedure was performed by adding the parameters of plant component lifetime and environmental costs to the objective function. Thus, the optimization problem was formulated by minimizing the total system levelized cost instead of simply hourly energy cost. The study results revealed that producing the electricity by the trigeneration system led to achieving 1256 MWh annual electricity savings that otherwise must be purchased from the grid. The results also showed a significant reduction in annual CO_2 emissions (703.31 tons per year). Furthermore, if the price of purchasing CHP electricity was considered three times more than the current ones, payback times would be less than 5 years.

https://doi.org/10.30501/jree.2020.228287.1108

چکیده

سیستمهای تولید ترکیبی توان و گرما به سبب بازده بالاتر و انتشار گازهای گلخانه ای کمتر، در سالهای اخیر توجه روزافزونی را به خود جلب کرده اند. یکی از روشهای بهینه‌سازی این شبکه های انرژی مدل‌سازی ورودی- خروجی است. در این روش، ابتدا ماتریسهای بازده برای تک تک اجزای نیروگاه تعریف می‌شود. جریان انرژی و تبدیلهای انرژی موجود در مسیر به شکل درختی و در مسیری رو به عقب از خروجی تا ورودی دنبال می‌شود. در نهایت جریان انرژی و تبدیلات آن از میان اجزای نیروگاه با ماتریس بازده کل، مدل‌سازی می‌شود. تابع هدفی که برای بهینه‌سازی در این مقاله معرفی می‌شود، پارامترهایی را منظور می‌کند که در پژوهشهای قبلی این نوع مدل‌سازی درنظر گرفته نشده بودند؛ از جمله هزینه سرمایه گذاری تجهیزات، و هزینه‌های زیست‌محیطی و سپس فرمول‌سازی مسأله‌ی بهینه‌سازی کمینه کردن کل هزینه تراز شده سیستم در طول عمر صورت می‌گیرد. نتایج حاصل نشان داد که تولید برق از طریق سیستم تولید سه‌گانه به صرفه‌جویی ۱۲۵۶ مگاوات ساعت الکتریسیته در سال انجامید که درغیر این صورت می‌بایست از شبکه خریداری می‌شد. نتایج همچنین کاهش سالانهٔ حدود ۷۰۰ تن معادل گاز کربن دی اکسید را نشان داد. افزون بر این، بررسی حاصل حاکی از آن بود که درصورت ۳ برابر شدن قیمت فروش برق حاصل از سیستم تولید سه‌گانه نسبت به قیمت خرید برق از شبکه، زمان بازگشت سرمایه به کمتر از ۵ سال کاهش می‌یابد.

CONTENTS

Journal Homepage: www.jree.ir